UCLouvain

École polytechnique de Louvain

Study of the dynamic behaviour of large scale PEM electrolysers in a fast demand response perspective

Author: **Martin PASTURE**
Supervisor: **Emmanuel DE JAEGER**
Readers: **Cyril COUSEIN, Joris PROOST**
Academic year 2021–2022
Master [120] in Electrical Engineering

Acknowledgments

I am honoured to have received the guidance of Prof. Emmanuel De Jaeger throughout the year. I thank him for the time spent with me, his guidance and valuable feedback during the work.
Secondly, I would like to thank Cyril Cousein for his time and support, and also for the decisive inputs about the model and the data he provided to me.
I am captivated by societal implication of the grid and I am grateful for the opportunity to learn and also to contribute, in a modest manner, to ongoing related researches.
I also would like to thank Prof. Joris Proost for agreeing to be the reader of this master thesis and taking time to evaluate my work.
Finally, I wish to express my sincere gratitude to all those who supported me during my research, most notably, my parents for their proofreading and advice.

Abstract

In the energy decarbonisation context that we are facing, hydrogen and electrolysers seem to be solutions to many different problems. In this master thesis, we are looking specifically to use electrolysers to help the stability of the electrical power grid. Indeed, this stability depends on the instantaneous balance between the consumed and the produced electrical power. It is therefore necessary to set up devices able to adapt dynamically the electrical power.

More precisely, this work studies the possibility of utilizing electrolyser to provide FCR (frequency containment reserve) services. It requires that the electrolyser adapts its power consumption to contribute to the grid balance. It is putting high requirements on the electrolyser dynamic behaviour, which is the capacity to react quickly.

The thesis starts by using the scientific literature to build a model representing the electrolyser. To achieve this, a theoretical model for each subsystem is provided and described in detail.

The model is then made available for computer simulation of real grid conditions. This is achieved by adapting the recently released MatLab model to the research questions studied. Modifications are made to the electrical supply integrating the electrical dynamic behaviour of the electrolyser, the voltage model modifications, a scale up of the model to reach 1MW and other minor modifications. The resulting model is then validated using several empirical data found in the literature. Time constants are provided for all key aspects of the modeled electrolyser in order to demonstrate its reaction speed.

Finally, a simulation studies the dynamic behaviour of modeled electrolyser, if it had been used to provide frequency reserve service to the grid on January 27th 2017. As a conclusion, it is shown that electrolyser is capable of a sub-second stable reaction time.

Contents

List of Figures

List of Tables

List of Abbreviations, Acronyms and Definitions

Abbreviations and Acronyms

- BoP = Balance of Plant;
- FCR = Frequency Containment Reserves;
- FFR = Fast Frequency Response;
- HHV = Higher Heating Value;
- HTSE = High-Temperature Steam Electrolysis;
- LHV = Lower Heating Value;
- MEA = Membrane Electrode Assemblies;
- PEM = Proton Exchange Membrane or Polymer Electrolyte Membrane (indicating the same thing);
- PEMEL = PEM electrolyser;
- PEMFC = PEM fuel cell;
- PEMWE = PEM water electrolysis;
- PtH = Power to Hydrogen;
- RES = Renewable Energy Sources;
- RoCoF = Rate of Change of Frequency;
- SOE = Solide oxide Electrolysis;
- TSO = Transmission System Operators;
- VRES = Variable Renewable Energy Sources;

Definitions

- Balance of Plant = Auxiliary systems needed by an electrolyser
- Cell = Hydrogen production unit in PEM electrolysis;
- Droop function = The droop is the intentional loss in output power from a device as it drives a load;
- Stack = Set of cells in electrical series;

Chapter 1

Introduction

In response to the climate change they are facing, our societies have embraced energy transitions that are disrupting the way we produce, transport and consume energy. Our system is, still today, largely based on fossil energies. It should evolve towards a system based on various renewable energies and on carbon-free energy vectors, both in time and in space. If electricity is a vector that shines particularly for its almost instantaneous transport, it does not allow conservation over time. It is in an attempt to fill this need that hydrogen has been identified as a clean and flexible energy storage vector.
Hydrogen can be used to provide both electricity and heat in a multitude of sectors. It can also be used in tanks or in pipe networks, making it a transportable energy [29]. Hydrogen is a mediatic subject, it is considered as the key stone for the future energy systems by policy. Hydrogen is for example an important part of the overall EU strategy for energy system integration. With the publication of the REPowerEU plan in May 2022 [4], the European Commission completes the implementation of the European hydrogen strategy while further increasing the European ambitions for renewable hydrogen as an important energy carrier to move away from Russia fossil fuel imports. Hydrogen has a bright future and the needs will increase in the coming years.
On the other hand, hydrogen is currently used almost exclusively by industry for refining petroleum, treating metals, producing fertilizer, and processing foods. Since hydrogen is not available in its natural state, it needs to be produced. The hydrogen production is currently based on natural gas by steam reforming of methane and therefore releases carbon dioxide. Hydrogen is no exception to the decarbonisation objectives, producing "green" hydrogen is a therefore a necessity. Water electrolysis allows to produce hydrogen from pure water and electricity. Since we produce carbon-free energy, it is a good way to produce green hydrogen.
There are different electrolyser technologies. The Alkaline is the traditional and mature electrolyser. The PEM technology developed as the reverse process of fuel cells allows dynamic and flexible operation. This flexibility has for consequence that electrolysers are often designed, in the literature, to operate with an electricity production unit from a nearby renewable energy source (RES). It will not be the case here.
The power grid is at the heart of the energy transition. With the penetration of variable renewable energies sources (VRES), associated with the phasing out of conventional

generating units, we observe a paradigm shift. From a grid based on the control of generation according to demand, it is evolving towards a distributed system whose balance management must be able to play on both production and demand. The power grid faces instantaneous balancing challenges between energy production on one side and energy consumption on the other side.
In the context of this thesis, the idea using electrolysers to provide power grid services comes from the price of hydrogen production. The price of electricity in the production of hydrogen by electrolysis is currently too expensive to make electrolysis competitive with the steam reforming of methane. The ancillary services to the grid could be a source of additional income to the value of the production [30].
These challenges are perfectly illustrated by the article by Arash E. Samani et al. [30] which includes historical grid frequency data in Belgium for the year 2017. The frequency gives us an overview of the balance between generation electricity and consumption. If we are above 50Hz, the electricity production is in excess, conversely, if we are below, the electricity production is in deficit. The liberal European electricity market, known as 'Frequency containment reserve', defines the criteria under which a system can contribute to balancing and be remunerated by 'Transmission System Operators' (TSOs)[31].
Electricity demand response programs can lower prices, improve system reliability, and reduce electricity price volatility [32]. Electrolysers have been put forward as an option to ensure the stability of the network by making its power consumption, and therefore its hydrogen production, dependent on the state of the grid [33, 83]. It should therefore consume more when the grid needs consumption and consume less when the grid needs less consumption. The electrolyser can then be seen as a smart load that could consume power when needed and stop consuming it if the grid requires a slowdown in consumption. The electrolyser must therefore be able to adapt its power consumption very quickly according to the state of health of the network.
Unfortunately, assumptions about the flexibility of electrolysers are still unreliable. And there is a lack of literature investigating the ability of high power electrolysers to achieve the operational recommendations of Transmission System Operators [24]. The work of this thesis aims to provide some answers to this specific question. It has been written in the hope of making a contribution to this literature. Concretely, we are going to study how flexible and fast the electrolyser can be in its power changes. We will therefore study the response time and the speed of power change which are the central points for using electrolysers as a smart load. The study will focus on the impact of dynamic behaviour on hydrogen production, its quality, its compression, cooling and fluid circulation systems, its efficiency and the degradation of the installation, etc.

1.1 Scope and problem statement

This thesis addresses two types of audiences. First, the paper attempts to answer a question that has an essentially electrical aspect. It is about studying the ability of high capacity electrolysers to help the stability of the grid as smart loads. These could help the remunerated process of frequency restoration and even bring virtual inertia to the

grid. On the other hand, this work is mainly focused on the electrolyser as such and thus on its chemical, mechanical, pneumatic operations and the necessary infrastructure. It will therefore interest people who want to know about high capacity electrolysers and their dynamic behaviour.
Various researches already show the role that electrolysers could play in the grid. In "Novel Electrolyser Applications: Providing More Than Just Hydrogen" [24], one of the conclusions of the report can be formulated as follows: electrolysers can function as demand-side response facilities with sufficient speed and duration to participate in the regulation of energy on the grid or at final installations. In addition, electrolysers can be operated to support a variety of applications by providing hydrogen: for industrial processes, as an electrofuel in transportation or power generation, or as a fuel for combustion.
In this study of J. Eichman et al. [24], a frequency restoration test was performed to test the ability of an electrolyser to accelerate the rate at which the grid frequency can be restored. An electrically isolated microgrid consisting of a 120kW diesel generator, a load battery and a 40kW electrolyser was subjected to a change in load battery consumption of 10, 20 and 25kW. It was shown that the electrolyser could, by producing according to the state of the frequency, help the rapid recovery of the frequency. These powers, although significant, are several orders of magnitude different from a system that would significantly support the grid.
The ability of PEM electrolysis to provide grid services cannot be restricted to the study of the electrical response of the electrolyser. In this thesis, we will study the balance of plant, the fluidic circuits, the temperature regulation, the pneumatic constraints and the control and reactivity of this whole infrastructure to understand the issues from the point of view of the electrolyser.

1.2 Objectives and research questions

The main objectives of this work are to study and outline the dynamic behaviour of the electrolysers from the point of view of the grid but also to see what limits and what impact this would have on the installation.
The research topic can therefore be formulated as follows: Study of the dynamic behaviour of large scale PEM electrolysers in a fast demand response perspective.
The following questions can be asked:

- Is it possible to build a suitable model from the literature to represent the electrical response and the balance of plant of a large scale electrolyser in order to provide ancillary services on the grid?
- What are the different time responses in the electrolysis system ?
- What are the control schemes needed to properly model the balance of plant that allows the electrolyser providing ancillary service applications?

- What can we learn from electrolysers to implement the closest model to reality on the grid?
- What is the impact of demand response from electrolyser on its efficiency?
- What are the dynamical limits in the flexibility of the electrolyser power supply?

1.3 Methodology

Mathematical modeling and real time simulation of electrolysers using Simscape on Matlab Simulink is the selected research methodology. Digital real-time data of the frequency of the grid in January 2017 is used in order to know the demand response to the grid. The simulation of output as voltage/current waveform, hydrogen production, temperature of the stack, circulating pumps flow with the desired accuracy, which are representative of the behaviour of the real system being modeled. The methodology can be summarized as following:

1. Perform a state of the art review of the electrolyser modeling.
2. Define model equations and constraints.
3. Implement a model from this by modifying the MATLAB implemented one.
4. Scale up the model to reach the requirements.
5. Drawing conclusions from the model.
6. Find a simplified model in order to study electrolysers from grid perspectives.

1.4 Contribution of master thesis

This thesis contributes to the research on the use of electrolysers in power system stability. There is a lack of study on the dynamic behaviour of high power electrolysers. To be able to simulate future power systems, it is necessary to properly understand the electrolysers in the application use case.
The contributions of this work are:

- A Simulink model as complete as possible which includes the whole electrolyser.
- Impulse and transient responses of the electrolyser behaviour.
- The response time, limits and constraints of a high capacity electrolyser.

1.5 Outline of master thesis

- Chapter 2 exposes the context of hydrogen, the basis of the electrolysis theory, the different electrolyser technologies and finally the applicability to the grid services.
- Chapter 3 reviews the mathematical equations used to model the electrolysis system.
- Chapter 4 explains how the Matlab model has been modified and scaled up.
- Chapter 5 demonstrates the coherence of the model simulations and operates a validation based on the literature.
- Chapter 6 uses the model in a frequency containment reserve condition and makes observation about its operation.
- Chapter 7 provides the final conclusion.

Chapter 2

Contexts of hydrogen, demand response and electrolysis systems

This chapter provides the necessary information to understand the energy choices that make the present work relevant. First, we will look at hydrogen as a resource, in terms of demand, production and future developments. Afterwards we will look at the electrolysis process and the different existing technologies in order to produce carbon-free hydrogen assuming a carbon-free electricity mix. And finally, we will look at the grid stability and how, in this context, water electrolysis can provide power grid services.

2.1 Context of hydrogen : production, needs and perspectives

The first thing we can say is that hydrogen is an energetic fuel. One kilogram of hydrogen represents 141.9 MJ (39.4KWh) of chemical potential energy. Here below we have two combustion equations of hydrogen at 25°C for atmospheric temperature. Equation 2.1 represents the combustion of hydrogen producing liquid water and energy and Equation 2.2 represents combustion of hydrogen producing water vapour and therefore less energy since water vapour is more energetic than liquid water.

$$H_2(g) + \frac{1}{2}O_2(g) \rightarrow H_2O(l) + 285.58kJ \tag{2.1}$$

$$H_2(g) + \frac{1}{2}O_2(g) \rightarrow H_2O(g) + 241.6kJ \tag{2.2}$$

The Equation 2.1 gives an amount of energy that is called the Higher Heating Value (HHV) of hydrogen, Gross Calorific Value (GCV), or Higher Calorific Value (HCV). It indicates the upper limit of the available thermal energy produced by a complete combustion of the hydrogen. It is measured as a unit of energy per unit mass, molar or volume of substance. The HHV is determined by bringing all the products of combustion back to the original pre-combustion temperature, and in particular condensing any vapor produced by the combustion. The HHV of hydrogen for mole, kilogram and normal cube

meter[1] is represented in Table 2.1.

Unit	value
kJ/mol	285.58
MJ/kg	141.9
KWh/kg	39.41
MJ/Nm^3	11.8
KWh/Nm^3	3.28

Table 2.1: Higher Heating Values of hydrogen.

Equation 2.2 gives us another energy value for hydrogen combustion. It is the Lower Heating Value (LHV), Net Calorific Value (NCV) or Lower Calorific Value (LCV). This is another measure of available thermal energy produced by a combustion of fuel, measured as a unit of energy per unit mass or volume of substance. In contrast to the HHV, the LHV considers energy losses. Here for hydrogen the losses are represented as the energy used to vaporize water. Table 2.2 gives the LHV values.

Unit	value
kJ/mol	241.60
MJ/kg	120.1
KWh/kg	33.33
MJ/Nm^3	10
KWh/Nm^3	2.78

Table 2.2: Lower Heating Values of hydrogen.

2.1.1 Hydrogen production and needs

As we have seen, hydrogen contains chemical potential energy. On earth there is no abundant source of hydrogen, so we say that hydrogen is an energy carrier because we have to produce it with energy, before using it to recover energy.
Today, hydrogen is only very slightly a clean energy carrier. For the production, we can not say that it is clean and for the consumption we can not say that it is an energy carrier.
The production of hydrogen in Europe, represented in Figure 2.1, consists of 91% fossil fuel production, mostly using steam reformation of methane releasing carbon into the atmosphere. 7% by-product, coming from several electrochemical processes in industry, such as the production of chlorine by electrolysis of sodium chloride solution. About 1% is produced with low-carbon technologies using carbon capture and storage (CCS). Finally, only 2% of the hydrogen comes from electrolysis powered by the grid with only 0.1% of the hydrogen produced by renewable energies. In terms of use, 92% of its production

[1] Nm^3 is a m^3 of hydrogen gas at 25°C 1atm - $1Nm^3_{H_2} = 0.0899kg$

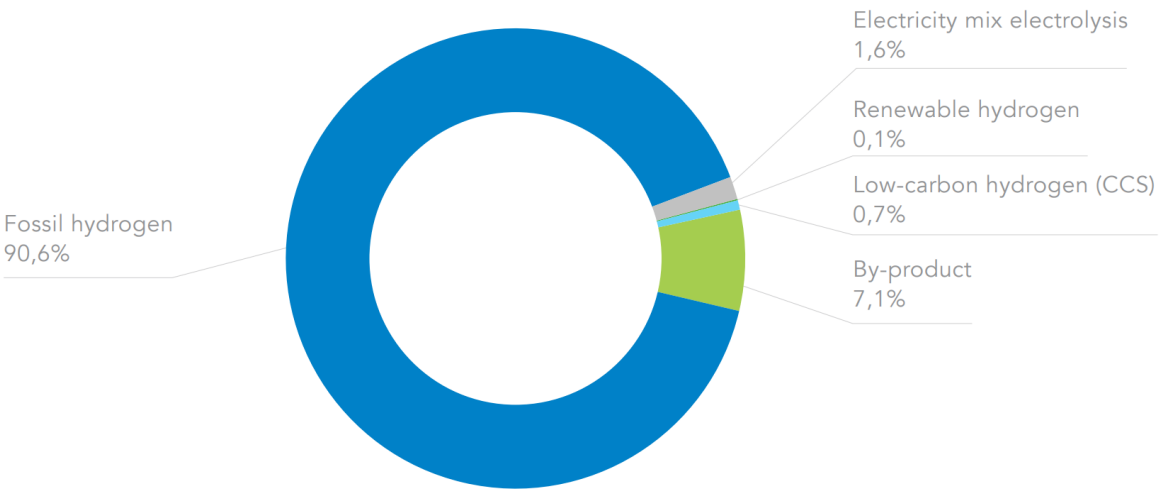

Figure 2.1: Total production for hydrogen in 2018 by technology. Taken from [1].

is reserved for the chemical industries. The refinery industry, for hydrocracking and desulfurization of hydrocarbons, and the ammonia industry, used as a base for synthetic fertilizers, together account for nearly 80% of hydrogen use. The figure 2.2 summarizes hydrogen demand by sector.

Hydrogen is really an energy carrier in its consumption in the sense that it contains

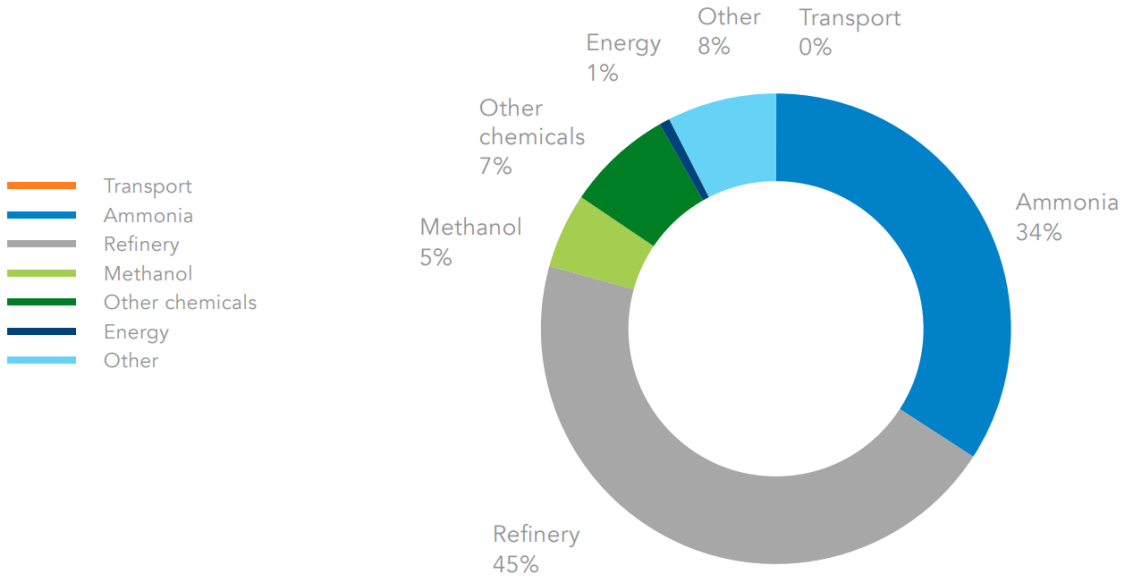

Figure 2.2: Total demand for hydrogen in 2018 by application. Taken from [1].

energy but it is not an energy carrier because it is used as a reagent in chemical reactions

(which uses its energy).
The total hydrogen consumption in Europe has been estimated at 8.3 Mt (327 TWh_{HHV}) for the year 2018 [34]. Hydrogen electrolysis produce therefore approximately 0.166Mt of hydrogen in Europe.. Hydrogen accounts for less than 2% of European energy consumption.

2.1.2 Perspectives

Europe sees hydrogen as having a great future and an important role in the decarbonisation of energy. Hydrogen can be an energy carrier seen as an electrofuel for the future. That is to say, a fuel that could create electrical power via fuel cells. It is therefore a source of power and controllable energy unlike some renewable energies such as solar panels or wind turbines. Within the framework of the decarbonisation of energies, the electrolysis of water thanks to renewable electricity seems to be an alternative that promises a wide range of solutions. Indeed, hydrogen can be a source of electricity for the grid, a source of electricity for transportation, a source of heat by combustion or used for the production of methane for which transportation chains and plants are already running.
The storage of energy in large quantities is a fairly important issue in the current energy transition strategies. It is necessary to be able to store energy in various time frames, both throughout the day and throughout the year. The term "Hydrogen Economy" heralds an economy based on hydrogen combined with electricity for energy consumption, transportation and storage. Hydrogen can then be produced by electrolysis and create electricity in fuel cells. These solutions highlight that hydrogen is an important player in the implementation of a decarbonised energy system.
Although power-to-hydrogen technologies have been available and used for decades thanks to electrolysers, the power of the installations is often measured in kW. In the coming years, we will be moving towards installations of tens of MW. There are 135MW of electrolysers in Europe and about 300MW in the world in 2021. The installed capacity of electrolysers has already grown enormously in the recent years, from 90MW in 2019 to 135MW in 2021.
In 2019, the largest capacity electrolyser in Europe was 7MW, in 2021 it was 10MW. Several 20MW electrolysers and even a 30MW one was under construction in 2021. The industry's ambitions already include several electrolysers in the order of magnitude of 100MW. These installations are intended to help the ammonia and refining industries meet their decarbonisation goals. Often industries start with pilots and plan to increase the installed capacity to meet their needs. Other late-stage projects focus on new mobility such as buses, coaches and small boats. These generation sources are generally distributed and produced on site for refueling stations. They are significantly smaller than the hydrogen production planned for industrial applications.
The figure 2.3 shows the hydrogen demand for 2030 and 2050 for 3 different scenarios divided by sector. The growth of hydrogen demand with respect to 2018 for central forecast is about 50% for 2030 and 200% by 2050 (400% growth in high demand scenario

by 2050). We can see that the scenarios for the future depend widely on the use of

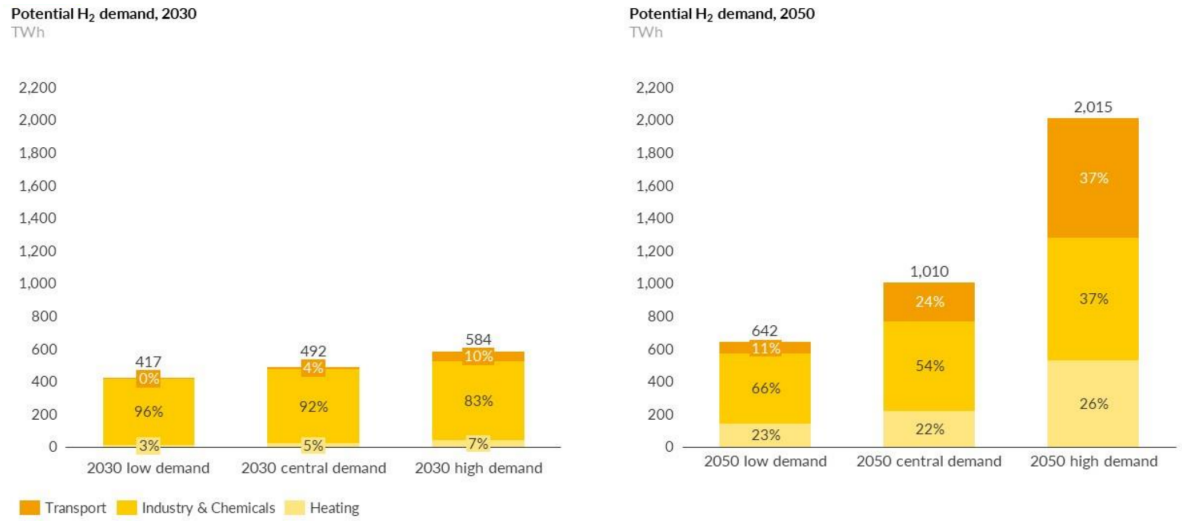

Figure 2.3: Hydrogen Demand Forecast in 2030 and 2050 for 3 different scenarios. Taken from [2].

hydrogen for heating and transport purposes. The expectations about a large use of hydrogen are already planned for 20 years with for example "The Hydrogen Economy" [35] a report from the US department of Energy that predicted the commercialization of hydrogen vehicles and did not happen. Instead, battery EV replaced the hydrogen vehicles forecast for individual cars. But this time it is a bit different. It is not only a study about alternative energy but political choices are already made about hydrogen. In July 2020, the European commission was declaring about the hydrogen strategy for a climate-neutral Europe:
... In order to implement the ambition of the European Green Deal and building on the Commission's New Industrial Strategy for Europe and its recovery plan, this Communication sets out a vision of how the EU can turn clean hydrogen into a viable solution to decarbonise different sectors over time, installing at least 6 GW of renewable hydrogen electrolysers in the EU by 2024 and 40 GW of renewable hydrogen electrolysers by 2030 and the production of up to 10 million tonnes of renewable hydrogen in the EU. 10Mt is 60 times the current electrolysis sourced hydrogen and 1200 times the renewable hydrogen. However, according to the Clean Hydrogen Monitor 2021 [3], the objective of 6GW electrolysers by 2024 will be reached and industry ambitions based on announced projects already stand at 119 GW for 2030 that is clearly bigger than European ambitions. Figure 2.4 shows the operational and planned projects based on industry ambitions by 2030.

Recently on the 18th May 2022, in the context of the Russian military aggression against Ukraine, the European Commission published the REPowerEU Plan [36]. REPowerEU is about rapidly reducing our dependence on Russian fossil fuels by fast forwarding the clean transition and joining forces to achieve a more resilient energy system and a true Energy Union. In the "communication from the European commission to the European

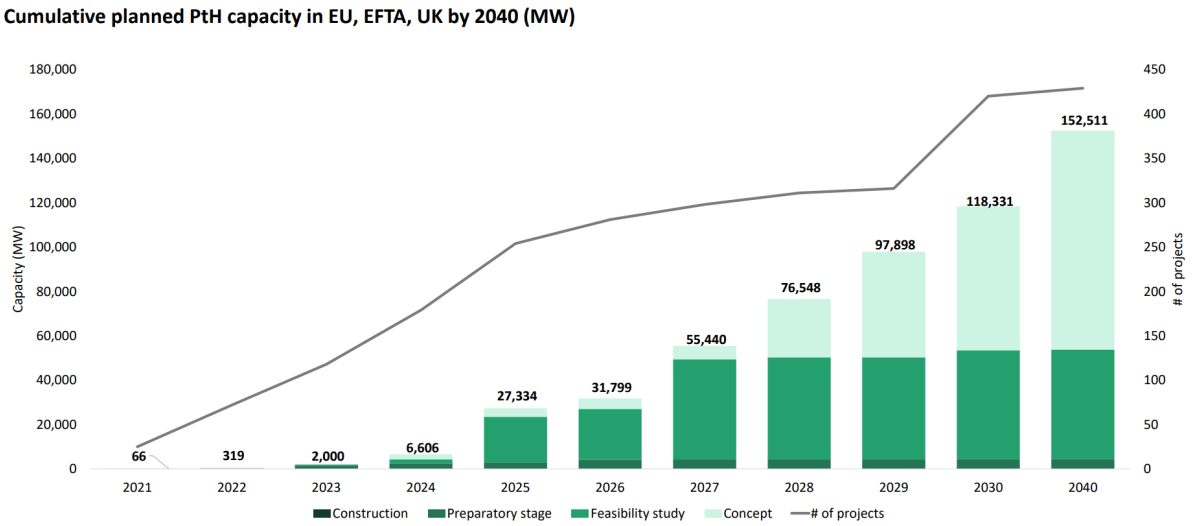

Figure 2.4: Cumulative planned and operational PtH projects by year 2021-2040 in MW and number of projects. Taken from [3].

parliament, European council, council, European economic and social committee and the committee of the regions" [4] we find this:

• *Renewable hydrogen will be key to replace natural gas, coal and oil in hard-to-decarbonise industries and transport. REPowerEU sets a target of 10 million tonnes of domestic renewable hydrogen production and 10 million tonnes of renewable hydrogen imports by 2030.*

→ 20Mt of renewable hydrogen is **twice the 2020 target.**

• *Accelerated efforts are needed to deploy hydrogen infrastructure for producing, importing and transporting 20 million tonnes of hydrogen by 2030. Cross-border hydrogen infrastructure is still in its infancy, but the basis for planning and development has already been set by the inclusion of hydrogen infrastructure in the revised trans-European networks for energy. Total investment needs for key hydrogen infrastructure categories are estimated to be in the range of EUR 28 – 38 billion for EU-internal pipelines and 6 - 11 billion for storage.*

→ 28B to 38B€ for pipelines and 6B to 11B€ for storage. **34B to 49B€ for hydrogen infrastructure.**

• *To facilitate the import of up to 10 million tonnes of renewable hydrogen, the Commission will support the development of three major hydrogen import corridors via the Mediterranean, the North Sea area and, as soon as conditions allow, with Ukraine. Green Hydrogen Partnerships will facilitate the imports of green hydrogen while supporting the decarbonation in the partner countries. Other forms of fossil-free hydrogen, notably nuclear-based, also play a role in substituting natural gas (see map).*

→ Importation of hydrogen comes **from the North, the Mediterranean sea and Ukraine**. These import corridors are available in Figure 2.5 in light gray arrows.

Figure 2.5: European infrastructure map for electricity - with the hydrogen import corridors in light gray. Taken from [4].

2.2 Water electrolysis

This section will focus on identifying how electrolysis works from the electrochemical point of vue. Water electrolysis is a technique that involves separating water molecules with a direct current in order to cause a non-spontaneous redox reaction[2]. The water is decomposed into oxygen and hydrogen gas with an electric current. A DC electrical power source is connected to two electrodes. Hydrogen will appear at the cathode (where electrons enter the water), and oxygen will appear at the anode.

2.2.1 Chemical reaction

In pure water at the negatively charged cathode, a reduction reaction takes place, with electrons (e^-) from the cathode being given to hydrogen cations to form hydrogen gas. The half reaction, balanced with acid, is:

$$\text{Reduction at cathode: } 2H^+(aq) + 2e^- \rightarrow H_2(g) \tag{2.3}$$

At the positively charged anode, an oxidation reaction occurs, generating oxygen gas and giving electrons to the anode to complete the circuit:

$$\text{Oxidation at anode: } 2H_2O(l) \rightarrow O_2(g) + 4H^+(aq) + 4e^- \tag{2.4}$$

The same half-reactions can also be balanced with the base. Therefore we find two other half reactions:

$$\text{Reduction at cathode: } 2H_2O(l) + 2e^- \rightarrow H_2(g) + OH^-(aq) \tag{2.5}$$

[2]an electron transfer reduction–oxidation is a type of chemical reaction

$$\text{Oxidation at anode: } 2OH^-(aq) \rightarrow 1/2\ O_2(g) + H_2O(l) + 2e^- \tag{2.6}$$

Combining either half reaction pair yields the same overall decomposition of water into oxygen and hydrogen:

$$\text{Overall reaction: } 2H_2O(l) \rightarrow 2H_2(g) + O_2(g) \tag{2.7}$$

The number of hydrogen molecules produced is thus twice the number of oxygen molecules. The number of electrons pushed through the water is twice the number of generated hydrogen molecules and four times the number of generated oxygen molecules.

2.2.2 Thermodynamics

In their paper LeRoy et al. [37] propose a generic approach based on the thermodynamic formalism. In this part, we will consider standard conditions that will simplify the concepts. The decomposition of water into hydrogen and oxygen at standard temperature and pressure is not favorable in thermodynamic terms. The electrolysis of water in standard conditions requires a theoretical minimum of electrical energy input to dissociate each mole of water, which is the standard Gibbs free energy of formation of water. In the case of water electrolysis the reaction enthalpy is the amount of energy (both work and heat) that has to be provided so the reaction products are at the same temperature as the reactant. As per the second law of thermodynamics, the enthalpy of the reaction is:

$$\Delta H = \underbrace{\Delta G}_{elec} + \underbrace{T\Delta S}_{heat} \tag{2.8}$$

Where ΔG° the Gibbs free energy = 237.24 kJ/mol(water) for standard conditions, T is the temperature of the reaction and ΔS the change of entropy = 163 J/K mol(water). The overall cell reaction with thermodynamic energy inputs then becomes:

$$H_2O(l) + \Delta H \rightarrow H_2(g) + \frac{1}{2}O_2(g) \tag{2.9}$$

(with $\Delta H^\circ = 285.83$kJ/mol whose $\Delta S^\circ = 48.6$kJ/mol (for standard temperature)).
Since each mole of water requires two moles of electrons (n = 2), and given that the Faraday constant represents the charge of a mole of electrons (F = 96485 C/mol), it follows the thermodynamic standard cell potential using Gibbs free energy (representing the LHV of hydrogen) can be obtained from this equation:

$$E^\circ = \frac{\Delta G^\circ}{nF} \tag{2.10}$$

(With the result that E° is the cell potential = $1.23V$ at 298K, $\Delta G^\circ = 237.24$ KJ/mol, 33.3 kWh/kg or 2.78 kWh/Nm^3).
The alternative formulation is calculated assuming that all of the energy to drive the electrolysis reaction is supplied by the electrical component of the required energy which results in a higher reversible cell voltage (using the HHV of hydrogen). This voltage is

referred to as the thermoneutral voltage. The thermoneutral voltage is a voltage drop across an electrochemical cell which is sufficient not only to drive the cell reaction, but to also provide the heat necessary to maintain a constant temperature. Just as the combustion of hydrogen and oxygen generates heat from the water vapour, the reverse reaction generating hydrogen and oxygen from liquid water will absorb more heat than LHV. The standard enthalpy of liquid water is $\Delta H^{\circ}_{H_2O} = -285.83$ kJ/mol.

$$E^{\circ}_{th} = \frac{\Delta H^{\circ}}{nF} \tag{2.11}$$

(where $E^{\circ}_{th} = 1.48$V, $\Delta H^{\circ} = 285.83$ kJ/mol, 39.4 kWh/kg(H_2) or 3.28 kWh/Nm^3.) These explanations are made for standard conditions. The temperature and the pressure in the electrolyser have a big influence on the voltage. Moreover the explanation using the thermoneutral voltage is very global. Still, this thermoneutral voltage gives an idea of the minimum voltage to be applied to perform the reaction at standard conditions.
However, calculations regarding the potential requires taking into account the additional losses. In practice when an electrochemical cell is "driven" toward completion by applying reasonable potential, it is kinetically controlled. Therefore, activation energy, ion mobility (diffusion) and concentration, membrane and conductor resistance, surface hindrance including bubble formation (causes electrode area blockage), and entropy, require a greater applied potential to overcome these factors. The amount of increase in potential required is termed the overpotential.

2.2.3 Overpotentials

Real water electrolysers require higher voltages for the reaction to proceed. The part that exceeds the open circuit voltage of equation 2.10 represents any kind of loss and nonideality in the electrochemical process. The most common representation of the electrolyser performance is the polarization curve that represents the relation between the current density and the voltage [38]. The polarization curve is composed by the thermoneutral voltage and additions of different overpotentials giving the equation 2.12 [18]. The main overpotentials of the cell voltage are the activation overpotential (to initiate the proton transfer and the electrochemical kinetic behaviour in anode and cathode), the ohmic losses (representing the losses for the conduction of the electron and the proton through respectively the conductors and the membrane) and the mass transport losses (overpotential due to the concentration of products).

$$V = E + \eta_{act} + \eta_{ohm} + \eta_{diff} \tag{2.12}$$

A PEM electrolysis system performance in static conditions can be compared by plotting the voltage versus cell current density. This essentially results in a curve that represents the power per square centimeter of cell area required to produce hydrogen and oxygen. Conversely to the PEM fuel cell, the better the PEM electrolyser the lower the cell voltage at a given current density.
As a precision, thermal needs of the reaction can be supported by the overpotentials that

are losses and end up as heat. The value of the floor voltage in Figure 2.6 can therefore be lowered to $E^{\circ} = 1.23V$ (LHV) for sufficient losses.

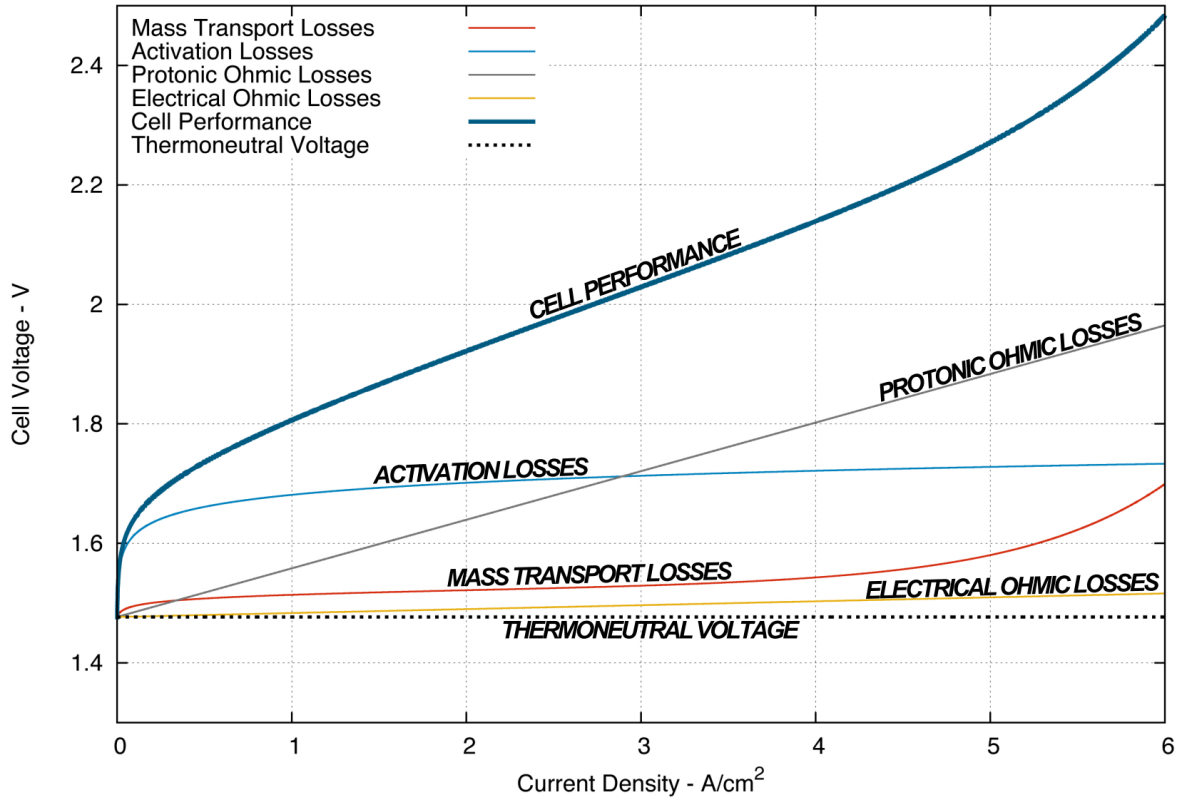

Figure 2.6: Polarization curve depicting the various losses attributed to PEM electrolysis cell operation. Taken from [5].

2.3 Electrolysers

Water electrolysis can be classified in four types, based on their electrolyte, operating conditions and ionic agents (OH^-, H^+ , O^{2-}). However operating principles are the same in all cases. The four kinds of electrolysis methods are: Alkaline water electrolysis (AWE), Solid oxide electrolysis (SOE), Microbial electrolysis cells (MEC) and PEM water electrolysis [6]. In the known industrial projects in development, we find mainly two technologies: Alkaline and PEM. Firstly, the alkaline technology, widely used today, is a mature technology. Secondly we have the PEM technology, which is in great expansion and development. The third technology is different from the first two low temperature electrolysis technologies. Its name is high temperature solid oxide electrolysis but is not yet widespread on a commercial scale. The last, the microbial electrolysis will not be addressed in this thesis since it is under development and has a low hydrogen production rate.

2.3.1 Alkaline electrolysis

The alkaline water electrolysis transforms at the cathode side two molecules of alkaline solution (KOH/NaOH) into one molecule of hydrogen (H_2) and two hydroxyl ions (OH^-). The produced H_2 eliminated from the cathode surface to recombine in a gaseous form and the hydroxyl ions (OH) transfer under the influence of the electrical circuit between anode and cathode through the porous diaphragm to the anode, where it is discharged to ½ molecule of oxygen (O2) and one molecule of water (H_2O). The O_2 recombines at the surface of the electrode and escapes as hydrogen. The mechanism is shown in Fig. 2.7. Alkaline electrolysis operates at low temperatures from 30 to 80°C with aqueous solution (KOH/NaOH) as the electrolyte. The concentration of the electrolyte is 20% to 30%. In the alkaline water electrolysis process, asbestos diaphragm and nickel materials are used as the electrodes. This diaphragm is not completely impermeable to gasses, and the gas mixture can lead to potentially dangerous conditions of flammability or explosiveness. Due to the ohmic drop across the diaphragm and liquid electrolyte, the applicable current densities are limited, on the order of $0.2 - 0.4$ Acm^{-2}. Moreover, because of the use of a liquid electrolyte, this technique can hardly be coupled to an intermittent power source (problems related to thermal management and change in electrolyte conductivity during start-up/shutdown and load variation periods). The liquid electrolyte also limits the applicable operating pressures (typically between 30 and 50 bars).

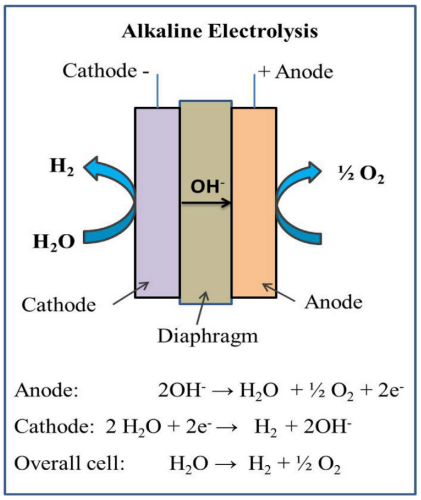

Figure 2.7: Schematic illustration of alkaline water electrolysis. Taken from [6].

Hydrogen production by alkaline water electrolysis is a well established technology up to the megawatt range. Alkaline electrolysis is mainly developed in Canada and Norway by Hydrogenics® and NEL Hydrogen®. It is coupled with nuclear power, recovered during off-peak hours, for the production of ammonia [39].

Finally, a new approach in alkaline electrolysis is under development of anion exchange membranes (AEM) made up of polymers with anionic conductivity instead of asbestos diaphragm. This innovative technology appears to be interesting in the field of alkaline water electrolysis.

2.3.2 High-temperature solid oxide electrolysis (SOE)

The solid oxide electrolysis (SOE) is a new technology first introduced by Donitz and Erdle in the 1980s. Solid oxide electrolysis has attracted an abundant deal of attention due to the electrical energy converts into the chemical energy along with producing the ultra-pure hydrogen with greater efficiency. Contrary to low temperature electrolysis technologies for which the cost of hydrogen production is 80% constituted by the cost of electricity supply, the High Temperature Steam Electrolysis (HTSE) or high temperature SOE technology is based on the contribution of a part of the energy necessary to the decomposition of the water molecule in thermal form, heat being at least three times less expensive than electricity, especially when it comes from nuclear reactors. Solid oxide electrolysis operates at high pressure and high temperatures 500–850°C. Solid oxide electrolysis process conventionally uses anioniques ceramic O^{2-} conductors. Operating principle of SOE is shown in Fig. 2.8. Nowadays, some of the ceramic proton conducting materials have been developed and studied in solid oxide fuel cells. The ceramic proton conducting materials also demonstrate high efficiency and superior ionic conductivity than O^{2-} conductors at an operating temperature of 500–700°C. However, the SOE shows some issues related to lack of stability and degradation, which have to be solved before going to commercialization on a large scale.

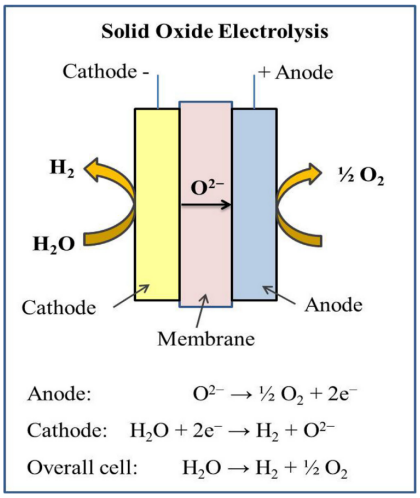

Figure 2.8: Schematic illustration of Solid Oxide electrolysis. Taken from [6].

Work on EVHT, which began in the 1980s, resumed in early 2000 after a hiatus due to a lack of market prospects, and has benefited from the research conducted on solid oxide fuel cells. This work was mainly supported by the DoE (Department of Energy) in the United States and by the European Commission (Relhy 21 project) [39].

2.3.3 PEM electrolysis

The first PEM water electrolysis was idealized by Grubb in the early fifties and was developed in 1966 by General Electric Co. to overcome the drawbacks to the alkaline water electrolysis. PEM water electrolysis technology is similar to the PEM fuel cell technology, where solid polysulfonated membranes (Nafion, fumapem) was used as an electrolyte (proton conductor). These proton exchange membranes have many advantages such as lower gas permeability, high proton conductivity, lower thickness and high-pressure operations. In terms of sustainability and environmental impact, PEM water electrolysis is one of the favorable methods for conversion of renewable energy to highly pure hydrogen. It has also other great advantages such as compact design, high current density (above 2 A/cm^2), high efficiency, fast response, small footprint, operates under lower temperatures (20–80°C) and produces oxygen as a byproduct. Additionally, balancing PEM electrolysis plants is very simple, which is more attractive for industrial applications. Furthermore, compared to alkaline technology, PEM is particularly suitable for coupling to renewable energy sources, as it has a rapid response and a good dynamic behaviour [40].

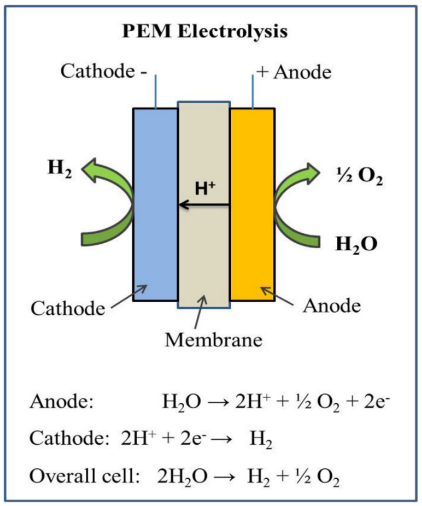

Figure 2.9: Schematic illustration of PEM water electrolysis. Taken from [6].

The state-of-the-art electrocatalysts for PEM electrolysis are high activity of noble metals such as Pt/Pd as the hydrogen evolution reaction (HER) at the cathode and IrO_2/RuO_2 as the oxygen evolution reaction (OER) at the anode, which makes PEM more expensive than alkaline water electrolysis. Therefore, one of the main challenges in PEM water electrolysis is to reduce the production cost while maintaining the high efficiency.

2.3.4 Technology selection

First of all, it is interesting to compare the state of the art and the target performances of the different technologies because they are not at the same stage of development. Data are available in tables 2.3, 2.5 and 2.4[3].

[3]available online: https://www.fch.europa.eu/soa-and-targets

Parameter	Unit	State of the art		FCH 2 JU target		
	year	2012	2017	2020	2024	2030
Generic system						
Electrical energy @nominal capacity	kWh/kg	57	51	50	49	48
Capital cost	€/(kg/d)	8000	1600	1250	1000	800
O&M cost	€/(kg/d)/yr	160	32	26	20	16
Stack						
Degradation	%/1000hrs	/	0.13	0.12	0.11	0.1
Current density	A/cm2	0.3	0.5	0.7	0.7	0.8
Use of critical raw materials as catalysts	mg/W	8.9	7.3	3.4	2.1	0.7

Table 2.3: State-of-the-art and future targets for hydrogen production from renewable electricity for energy storage and grid balancing using **alkaline electrolysers** [25, 26].

Parameter	Unit	State of the art		FCH 2 JU target		
	year	2012	2017	2020	2024	2030
Generic system						
Electrical energy @nominal capacity	kWh/kg	na	41	40	39	37
Availability	%	na	na	95%	98%	99%
Capital cost	€/(kg/d)	na	12000	4500	2400	1500
O&M cost	€/(kg/d)/yr	na	600	225	120	75
Specific system						
Reversible efficiency	%	na	50%	54%	57%	60%
Reversible capacity	%	na	20%	25%	30%	40%
Stack						
Production loss rate	%/1000hrs	na	2.8	1.9	1.2	0.5

Table 2.4: State-of-the-art and future targets for hydrogen production from renewable electricity for energy storage and grid balancing using **high temperature SOE** [25, 26].

Efficiency of modern hydrogen generators is measured by energy consumed per standard volume of hydrogen (kWh/Nm3), assuming standard temperature and pressure of the H_2. The lower the energy used by a generator, the higher its efficiency would be. Efficiency is crucial since the cost of hydrogen production of the two main technologies is based on 80% on electricity. If we neglect all losses and heat needs, a 100%-efficient electrolyser would consume 33.3 kWh per kilogram of hydrogen or 2.78kWh/Nm^3 following (Eq. 2.10 or Table 2.2 about LHV). Practical electrolysis may consume 51 kWh/kg (4,58 kWh/Nm^3) for alkaline electrolysers, 41 kW/kg (3,69 kWh/Nm^3) for high-temperature SOE and finally 58 kWh/kg (5,21 kWh/Nm^3) for PEM electrolysers at nominal capacities. The electrical efficiency of Alkaline electrolysers systems is around 63%–73% (compared to

Parameter	Unit	State of the art		FCH 2 JU target		
	year	2012	2017	2020	2024	2030
Generic system						
Electrical energy @nominal capacity	kWh/kg	60	58	55	52	50
Capital cost	€/(kg/d)	8000	2900	2000	1500	1000
O&M cost	€/(kg/d)/yr	160	58	41	30	21
Specific system						
Hot idle ramp time	sec	60	10	2	1	1
Cold start ramp time	sec	300	120	30	10	10
Footprint	m2/MW	/	120	100	80	45
Stack						
Degradation	%/1000hrs	0.375	0.25	0.19	0.125	0.12
Current density PEM	A/cm2	1.7	2.0	2.2	2.4	2.5
Use of critical raw materials as catalysts PGM	mg/W	/	5.0	2.7	1.25	0.4
Use of critical raw materials as catalysts Pt	mg/W	/	1.0	0.7	0.4	0.1

Table 2.5: State-of-the-art and future targets for hydrogen production from renewable electricity for energy storage and grid balancing using **PEM electrolysers** [25, 26].

LHV), while the ultimate goal is 70%–80%. A PEM electrolyser system has a lower efficiency of around 60%-70%, which is expected to be improved to 82%–86% before 2030 according to "Fuel Cells and Hydrogen Joint Undertaking" the predecessor of Clean Hydrogen [41]. The theoretical efficiency of PEM is very high. The loss of efficiency comes also from the compression of hydrogen to high pressure for example for storage purposes. This is the main reason electrolysers operate at high pressure,even if it is bad for them efficiency, is to have a pressurized hydrogen production because pressurizing afterwards would be even worse in terms of overall energy efficiency.
The positive aspects of the PEM electrolysers are the high current density (>2A/cm^2), the good partial load range (10%-100%), the rapid system response (<1s), the high gas purity (99.99%) and the dynamic operation [27]. A comparison about the different water electrolysis is available in Table 2.6.
There is no bad choice for hydrogen production by water electrolysis. Alkaline technology still has a good future since there is an enormous quantity of renewable hydrogen in Europe until 2030. SOE is still at a laboratory stage and not yet fit for large scale operation. On the other hand PEMWE has good dynamic behaviour and large scale opportunities which we need as the grid is changing its paradigm and needs new high power demand response in order to support the stability. But before dwelling on the PEM operation and its action on the power grid, we will present the different issues of grid stability.

Electrolysis process	Advantages	Disadvantages
Alkaline Electrolysis	Well established technology. Non-noble electro catalysts. Low cost technology. The energy efficiency is (70–80%). Commercialized.	Low current densities. Formation of carbonates on the electrode decreases the performance of the electrolyser. Low purity of gasses. Low operational pressure (3–30 bar). Low dynamic operation.
Solid Oxide Electrolysis	Higher efficiency (90–100%). Efficiency>100% with hot steam. Non-noble electro catalysts. High working pressure.	Laboratory stage. Large system design. Low durability. No dependable cost information.
PEM Electrolysis	High current densities. Compact system design and Quick Response. Greater hydrogen production rate with high purity of gasses (99.99%). Higher energy efficiency (80–90%). High dynamic operation.	New and partially established. High cost of components. Acidic environment. Low durability. Commercialization is in near term.

Table 2.6: Advantages and Disadvantages of different water electrolysis technologies. Taken from [6] and [27].

2.4 Grid stability, Demand response, frequency containment reserve

For a proper functioning, the grid needs stability. The stability of a power system is the property that allows it to reach an acceptable steady-state following a disturbance (like a connection or disconnection of a large load or a large generator). There are different types of stability. The rotor angle stability, generally defined as the ability of a power system to maintain machines synchronous operation when subjected to a disturbance [9]. Voltage stability, based on fault or on the inability of the generation-network system to provide the power required by the loads (due to real and reactive power that leads to congestion, reliability problems). And the frequency stability, based on the balance between the consumption and the production of electrical power.
Electrolysis is studied to play a role in supporting the grid in a demand response perspective. The voltage stability is inherently a distribution issue related to local infrastructures and power flows. Electrolysers could play a role in the evolution of the distribution topologies for example to avoid congestion by consuming local production. But voltage stability will not be the subject here. More practically, hydrogen production could offer a

demand side response to the grid in order to provide short term frequency control. Figure 2.10 resumes the different aspects of the power system stability. In this thesis we will focus on how hydrogen production could contribute to stability as Frequency Containment Reserves (FCR) and Synthetic Virtual Inertia (as Fast Frequency Response - FFR).

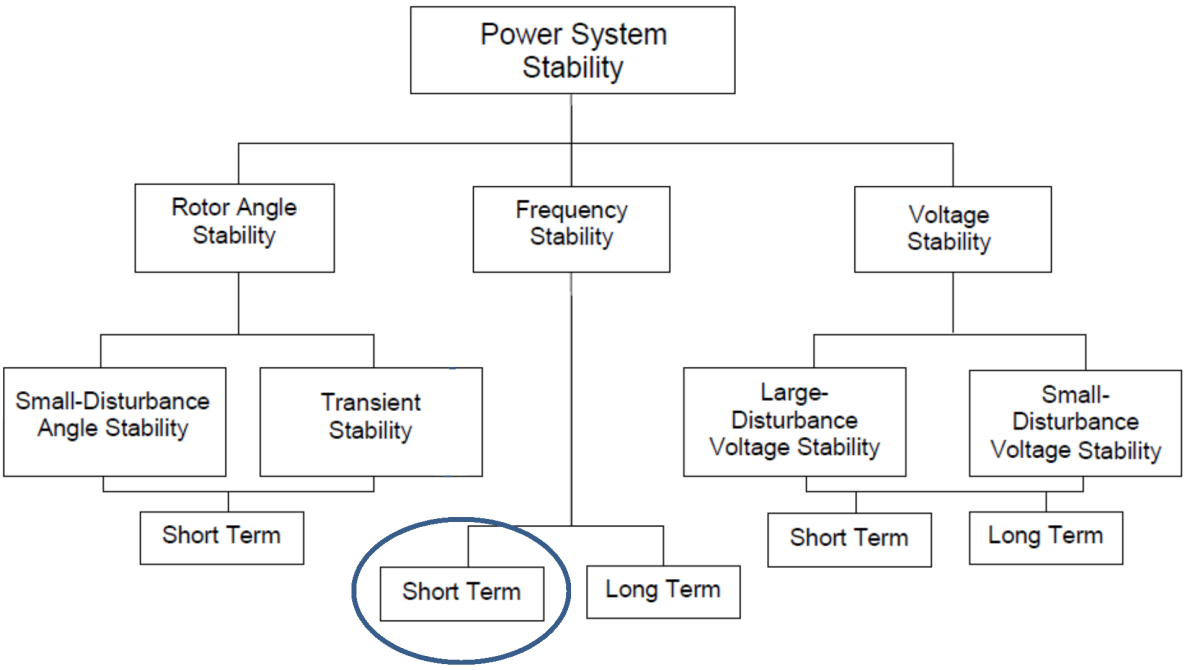

Figure 2.10: Scheme of the different types of stability. Taken from [7].

2.4.1 Economical and quantization of frequency stability

Liberalization of the electric market has taken place since the 1990s. Utilities are no longer vertically integrated companies. The coordination necessary for reliable system operation, including frequency control, is provided by the transmission system operators (TSOs). The frequency control framework had to be adapted to the market environment in the sense that the frequency support from individual power plants is provided and paid by the TSOs. The organization of the ancillary services market in Europe are dependent on the specific rules of the different national TSOs [42]. To assist the electrical network, a large consumption capacity is required. According to ENTSOE, the overall FCR capacity is 3,000 MW in 2016 in the synchronous interconnected area of continental Europe.
Also, inertia used to be widely available when electricity is produced by rotating machines but the loss of inertia could lead to a compensation mechanism to synthetic inertia providers in the future. The prevision of reduction of inertia is given in the ENSTO-E insight report : "The inertia challenge in Europe – Present and long-term perspective" from January 2021. The total kinetic energy (inertia) in continental Europe will be at minimum 1000 GWs and at maximum 1800 GWs according to ENTSOE [43] for the

NT2030 scenario for 2030. By 2025 the minimum inertia constant in continental Europe synchronous grid will be between 2 and 2.5 seconds, and by 2040 it will be between 1 to 1.5 seconds.
The synthetic inertia is called the FFR (Fast Frequency Response), with a delivery time in less than 2 seconds and is a service that is not currently used according to the report "Economic grid support services by wind and solar PV" of 2014 of REserviceS [44]. This may become a service in the liberal electricity market in the coming years in order to guarantee stability.

2.4.2 Frequency stability

This frequency stability refers to the ability of a system to maintain a steady frequency after a significant imbalance between generation and load. The link between frequency stability and power balance can be understood as following. The generators are creating electrical power while they are rotating. The rotating speed is named the working point of the machine and the frequency of the grid. The working point is also associated with a power or a couple for each machine. After a disturbance, if the balance shifts to underproduction, the working point changes and the load will decrease because of the energy balance, the generators will slow down, decreasing the frequency of the grid. On the other hand, if the power equilibrium moves toward a power overproduction, the mechanical power on the generator increases and the generator will speed up to find a new working point where the mechanical power is equal to the electrical power. The physics of generators explain why the power balance influences the frequency of the grid. In the steady state the idealized power–speed characteristic of a single generating unit is given by equation 2.13 [45]. The frequency difference is linear to the power difference from the steady state.

$$\frac{\Delta\omega}{\omega_n} = -\rho\frac{\Delta P_m}{P_n} \text{ or } \frac{\Delta P_m}{P_n} = -K\frac{\Delta\omega}{\omega_n} \tag{2.13}$$

where ρ is referred to as the speed–droop coefficient or simply the droop. The reciprocal of droop $K = \frac{1}{\rho}$ is the effective gain of the governing system. $\Delta\omega$ and ΔP_m are respectively the difference of pulsation of the AC current and the difference of power on the system. ω_n and P_n are the nominal pulsation and the nominal power of the system. The pulsation can be converted to the frequency of the AC current and we keep the same relation. The nominal frequency of the European grid is 50Hz.
Figure 2.11 represents the frequency restoration process. There is a classification according to the time a frequency control system can respond. The first response in case of disturbance is inertia caused mainly by the mechanical inertia of the rotating machines. This is not a compensated frequency control until today but it has an essential impact on the dynamic behaviour of the grid in the first seconds of a disturbance. The primary control called FCR (frequency containment reserves) are the operating reserves activated for stabilizing System Frequency after an imbalance in the scale of a few seconds (within 30s) at a steady-state value. It is a joint action of FCR within the whole synchronous area. Definition of fast frequency response: fast frequency response is the controlled contribution

of electrical torque from a unit which responds quickly to changes in frequency in order to counteract the effect of reduced inertial response.
The secondary control responses (frequency restoration reserves with automatic activation and with semi-automatic or manual activation) in the scale of a few minutes (between 30s and 15min) are activated to control the frequency toward its set point value and replace FCR. The replacement reserves or tertiary control provided by resources with a slower response time that can be called upon to replace or supplement the primary and secondary control in restoring system stability that is afterwards taken into charge by a generation rescheduling.

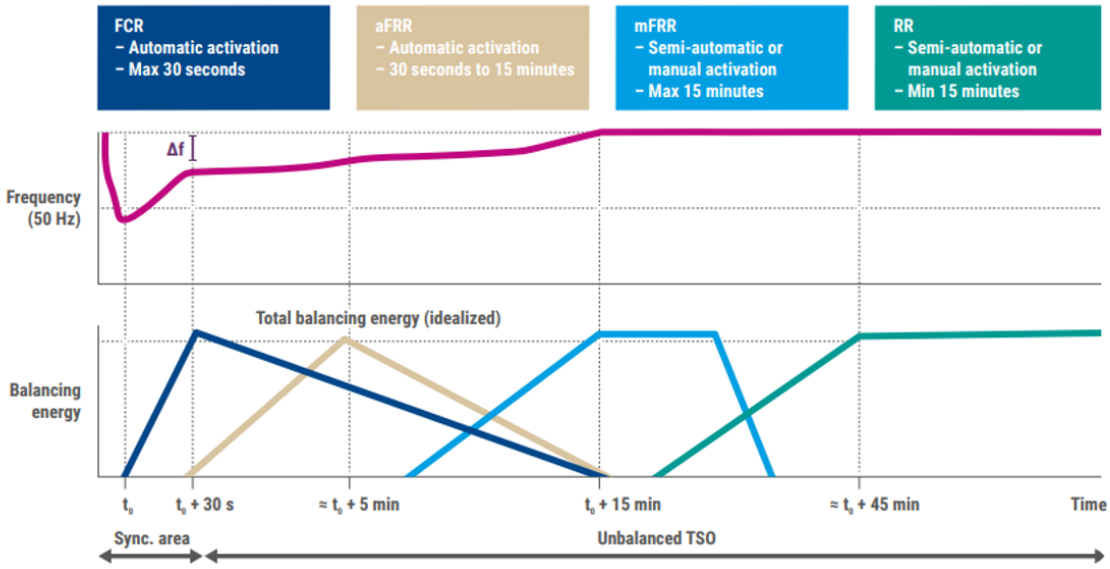

18 // **ENTSO-E** Annual Report // 2020 Edition

Figure 2.11: Frequency restoration process by ENTSO-E. Taken from [8].

2.4.3 Inertia in traditional power systems

The renewable sources of energy are driving power systems toward low-inertia conditions and frequency stability challenges [46]. Inertia refers traditionally to the kinetic power of the rotating machines. In general, inertia is defined as the resistance of a physical object to a change in its state of motion, including changes in its speed and direction. Applying this definition to a traditional electrical power system, the physical objects that are in motion are the rotating machinery (synchronous generators and turbines, induction generators, etc.) connected to the power system and the resistance to the change in rotational speed is expressed by the moment of inertia of their rotating mass [9]. To explain the inertia, let's take the example of the power angle curve of a synchronous machine in Figure 2.12.

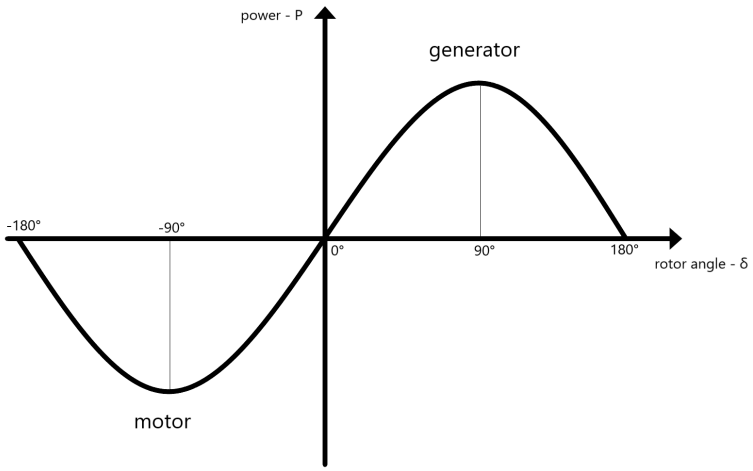

Figure 2.12: Power angle curve of a synchronous machine.

The synchronous machines are the electrical generators of the grid. The rotor angle of the synchronous machine is the phase shift between the grid phase applied on the stator windings and the rotor phase (divided by the number of poles). An intuitive way to understand this type of machine is that if the rotor has a phase advance (called rotor angle), the machine is in generating mode and will pull the voltage of the stator (of the grid). The bigger the rotor angle is, the more power the machine produces, according to the power angle curve, as shown in Figure 2.11. After a loss of frequency, the grid frequency will slow down resulting in a slow down of the stator voltage frequency. This will therefore increase the rotor angle (because the rotor is rotating faster) and the produced couple (or power) of the generators will increase. Of course the mechanical power of the generator has not changed and therefore the generator will not produce this additional power in the long term. Virtual inertia means that when the grid frequency drops, the plant uses the energy stored in the rotating mass, in chemical reactions... to produce more electrical power to the grid. The objective is to limit the drop in the frequency of the grid voltage. Definition of synthetic inertia: synthetic inertia is defined as the controlled contribution of electrical torque from a unit that is proportional to the rate of change of frequency (RoCoF) at the terminals of the unit [47]. RoCoF is graphically represented in Figure 2.13. This response is temporary and the grid requires counter balancing events, that is the frequency restoration process in Figure 2.11 and 2.13 in order to keep the frequency stable.

Inertia can be measured as the inertia constant. The inertia constant represents the time period the inertia energy could provide nominal power only using the kinetic energy stored in the rotating mass and is expressed in Eq. 2.14 [9].

$$H_{SG} = \frac{E_{SG}}{S_{SG}} = \frac{\frac{J_{SG} \cdot \omega_{e,0}^2}{2}}{S_{SG}} \tag{2.14}$$

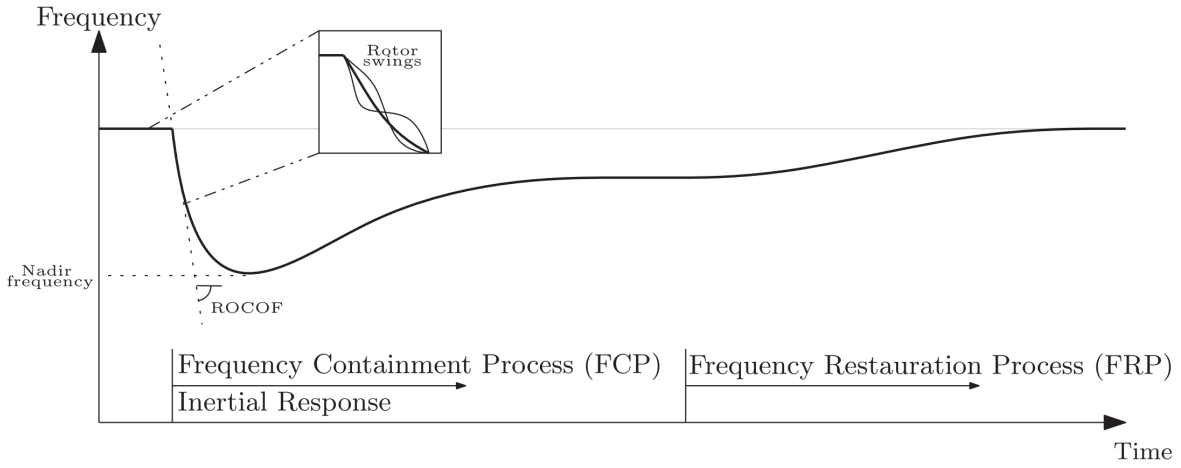

Figure 2.13: Classification of frequency control mechanisms. Taken from [9].

where H_{SG} is the inertia constant, generally expressed in [s] but more exactly in [Ws/VA], E_{SG} the energy stored in the synchronous machine in [Ws] and S_{SG} the apparent power of the generator in [VA]. J_{SG} the moment of inertia in [kgm^2] of the rotating mass and $\omega_{e,0}^2$ the nominal speed of rotation in [rad/s].

2.4.4 Low inertia impact on power system stability and control

In order to ensure a stable system operation and control, it is necessary to assess the impact of this reduced synchronous inertia on the dynamics of the power system. Figure 2.14 is a general overview of different power system phenomena and controls are given together with the time scales involved.
There is a close link between inertia and the dynamics of interest for frequency stability and rotor angle stability.

Rotor angle stability

In general, lowering the inertia of synchronous generators results in larger rotor swings and makes the system more vulnerable to disturbances in terms of transient stability.

Frequency stability

Reducing the amount of synchronous inertia mainly influences the frequency stability of a power system. If the power/consumption balance is not restored, large frequency swings occur which may result in tripping of generating units and/or load. The reduction in inertia influences both the RoCoF and the minimum value of frequency reached during the transient period (nadir frequency, represented graphically in Fig. 2.13), two parameters which both play an important role in the activation of system protection devices. This increased RoCoF can be considered as one of the main barriers to operate a system with

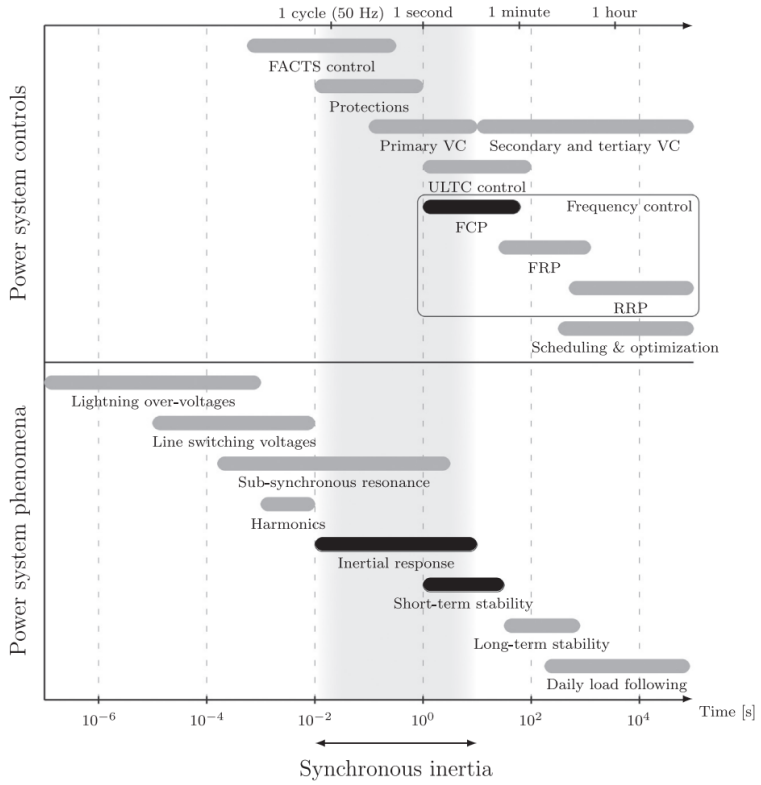

Figure 2.14: Overview of time scales covered by power system phenomena and controls and synchronous inertia. Taken from [9].

low inertia in a safe and secure way. Figure 2.14 will see the inertia response shortened. It reduces the time period for the governor control to react before the frequency exceeds thresholds at which load/generation shedding is initiated, but moreover it also has an impact on current protection schemes and the operation of synchronous units.

Operating systems with low inertia

In "The relevance of inertia in power systems" [9], Pieter Tielens and Dirk Van Hertem develop the two main approaches about operating systems with low inertia:

- *A first approach mainly focuses on adapting the current power system equipment, grid codes and protection to cope with higher RoCoF and larger frequency swings.*
- *The second approach tries to accommodate more converter connected generation by providing different forms of inertia (such as virtual inertia) or incentives for more flexible plants or plants with a higher synchronous inertia. This virtual inertia is also identified as a future grid support service in the REserviceS project [44] which sets some technical and economic guidelines and recommendations for the design of a European market for ancillary services. Some studies even propose to implement an inertia constraint within the unit commitment problem to ensure that a minimum amount of system inertia is always available.*

2.4.5 On the ability of pem water electrolysers to provide power grid services

The research question of this thesis is oriented, at the end, about the support of the power grid in a fast demand response perspective. As for short-term stability and for synthetic inertial responses are overlapping in time range (in Fig 2.14), PEM electrolyser is seen to help at this range of time response. To conclude the first chapter of this thesis, let's review the different research made on similar approaches.

On the ability of pem water electrolysers to provide power grid services [10]

In 2019 a research publication by L. Allidières et al. was studying the ability of pem water electrolysers to provide power grid services [10]. A set of key performance indicators (KPIs) has been designed in Figure 2.15 to measure the level of development of PEM water electrolysers, to measure the impact of operation with transient power sources (for grid services) on the performances, and to facilitate the comparison of commercial products available on the market. The conclusion is that there are two main critical issues that are limiting the performances of existing technology and will require further developments: (i) the need for operation in isothermal conditions in order to reduce efficiency losses and degraded power responses; (ii) the need to reduce power fluctuations down to the appropriate level on power plateaus.

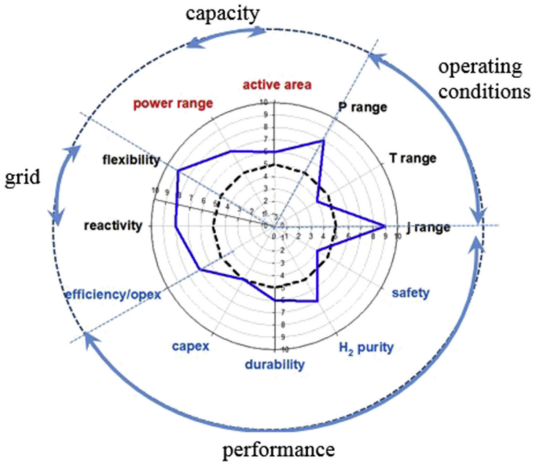

Figure 2.15: KPIs of PEM water electrolysis technology. (- -) reference case (stationary, 2015); (—) test results from the paper (transient PEM, 2017). Taken from [10].

Secondary Frequency Control for the IESO [11]

In 2018, Hydrogenics in partnership with Enbridge installed 2.5MW of PEMWE stacks that are supporting the secondary frequency control for the IESO (Canadian TSO). Since 13th January 2022 this hydrogen is blended to the natural gas networks to reduce the heating carbon footprint[4]. This electrolyser has a 2 second response time and a 2MW/s ramp rate. The electrolyser is functioning at 1.3MW and is varying between 0.25MW and 2.35MW (+/-1.05MW). This project is therefore proving that this type of application is already possible. The power profile of the PEM electrolyser is available in Figure 2.16.

[4]available on Enbridge site: https://www.enbridgegas.com/about-enbridge-gas/newsroom/newsdetail?releaseId=122757

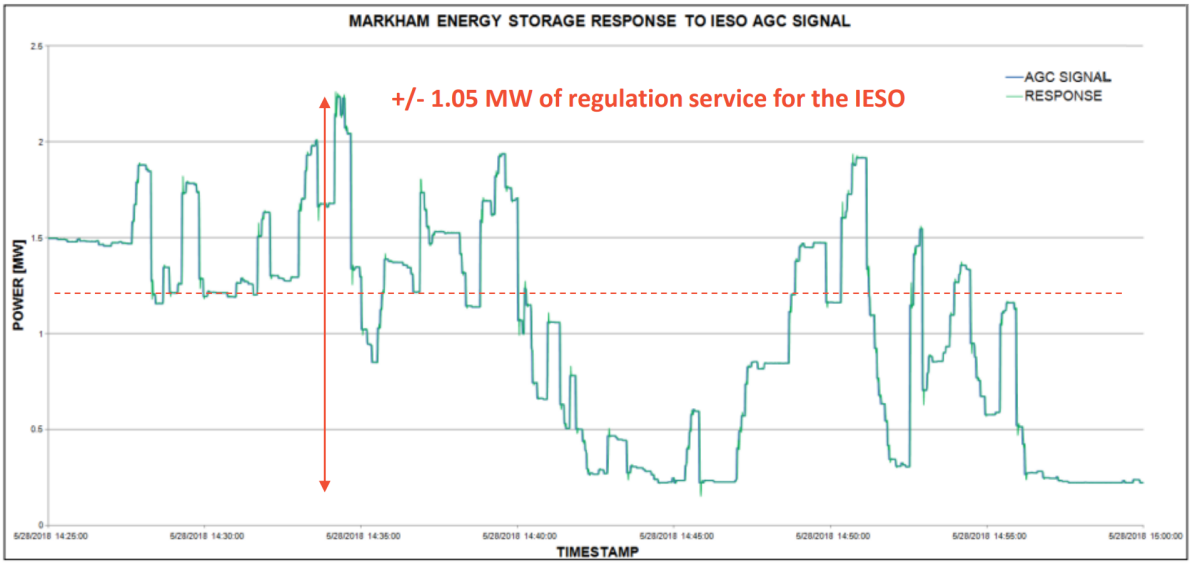

Figure 2.16: Markham energy storage response to IESO AGC signal, Taken from [11].

Chapter 3

Mathematical modeling of an electrolyser

Our objective is to develop a computer model able to represent the dynamic behaviour of large scale PEM electrolysers. PEM electrolyser modeling has seen over years a strong growth in the number of research works, as illustrated by the following figure Fig. 3.1, showing the number of papers on electrochemical modeling classified by year.

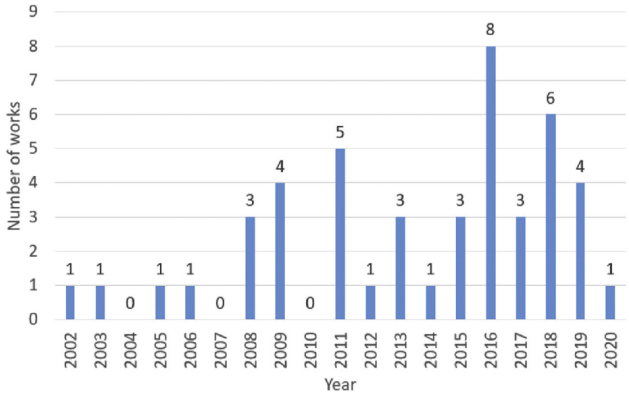

Figure 3.1: Evolution of the number of works about voltage to the year for the PEM electrolyser taken from [12].

In this chapter, we will review the electrolyser modeling with a focus on the specifics of PEM. This section borrows its structure from the state of the art done by Pierre Olivier for his 2016 thesis [23] and in the paper [48]. We will enrich it with information crucial to the needs of the analysis that we will do in the following sections of this work.

Model categories

In order to model an electrolyser as a whole, it is necessary to look at each of its constituent aspects. Pierre Olivier classifies models according to 5 categories [23]:

- Electrochemical models are used to describe the electrochemical response of electrolysis cells and stacks.
- Electrical models describe the electrical phenomena taking place within the other electrical components of the system (converters, pumps, cold group, etc.)
- Thermal models calculate the different temperatures within the system and their evolution, in particular to include the impact of temperature on the electrical response of the electrolysis stack and therefore on its performance.
- Mass transfer models are used to describe mass transport phenomena within an electrolysis cell.
- Fluidic models are used to describe the circulation of the electrolyte within the system and to calculate the different flow rates and pressures within the system.

In the real world, these different aspects of the electrolyser interact with each other and are more or less coupled. However, the models we present are intended to be modular in their designs. Some models only use either an electrochemical, thermal or mass transport representation in the membrane.
The different models presentation looks at the following aspects of the model:

- The modeling approach
- The dynamic character
- The modeling scale

The modeling approach

There are several approaches.
The empirical approach aims to find mathematical equations which allow the most accurate representation of the system observations. The empirical equations can therefore have a number of parameters that do not all have a physical meaning.
The analytical approach is based on physical, electrochemical or thermal theory and principles. This approach constitutes analytical equations that represent the different phenomena involved and formalize the losses, non-idealities... Therefore the parameters have a physical meaning.
The semi-empirical model takes the terms developed by the theoretical analysis of the analytical approach and adds empirical variables to better fit the observations.

The dynamic character

Static models are built on algebraic equations on a set of variables that does not include a time variable $X = f(Y)$.
Dynamic models with localized parameters are built from ordinary differential equations, with variables that only depend on time. These models are of the input/output (I/O) type

and are adapted to the analysis and synthesis of control laws (control and monitoring). Dynamic models with distributed parameters are made of partial differential equations, integrating the spatial distribution of the different variables and parameters. These complex models are mainly used for the dimensioning, analysis and design of processes in process engineering.
Quasi-static models are derived from dynamic models. The equations used are no longer differential equations, but time equations assuming the temporal evolution of the different variables as quasi-static $X(t + \Delta t) = X(t) + \Delta t \cdot K$

The modeling scale

Most electrolyser system models are based on the operation of a cell or a stack and PEM cell. It is assumed that a stack is then composed of cells operating in the same way. Other works integrate the modeling of a system. There is the modeling of the stack but also the Balance of Plant and the auxiliary components.

3.1 Electrochemical model

This type of model is also called (stack or cell) voltage model because it describes the voltage of a stack. Most electrochemical models are based on the scale of the electrolysis cell and consider the stack as an electrical series of several cells. Static models are mainly used in the development of electrochemical models. The very short response time of PEM cells allows, in many applications, not to bother with the dynamic aspect. Dynamic models are developed for the study of converters and the electrical response of electrolysers [49]. In the framework of this work, as it is important to find an accurate model both in relation to the operating points and internal states of the electrolyser and in its dynamic response from the point of view of the power supply, both static and dynamic analyses will be of interest.

3.1.1 Faraday's law

According to Faraday's law, the production rate of hydrogen in water electrolysis is directly proportional to the number of electrons traveling at the electrodes, so proportional to the electrical current in the external circuit. Hence, the total hydrogen production rate in an electrolyser, which consists of several cells connected in series, can be expressed as:

$$\dot{n}_{H_2} = \eta_F \frac{n_c I}{nF} \tag{3.1}$$

where

$\dot{n}_{H_2}$	hydrogen production rate, $mol \cdot s^{-1}$
η_F	Faraday efficiency
n_c	number of cells in series
n	number of moles of electrons per moles of water, $n = 2$
F	Faraday constant, $F = 96,485\ C \cdot mol^{-1}$

Some models consider the Faraday efficiency equal or very close to 1 and this is mostly true for high current densities as we can see in Fig. 3.2. For this reason, the Faraday efficiency is very little addressed for PEM electrolysers and concerns more alkaline electrolysis. Other models describe the Faraday efficiency by empiric equations which depend on operating conditions such as temperature or current. Ulleberg gives an empirical expression (Eq. 3.2) for Faraday efficiency in [50] for a given temperature.

$$\eta_F = \frac{(I/A)^2}{f_1 + (I/A)^2} f_2 \tag{3.2}$$

Where f_1 and f_2 are empirically determined and are linear to temperature (pressure neglected).

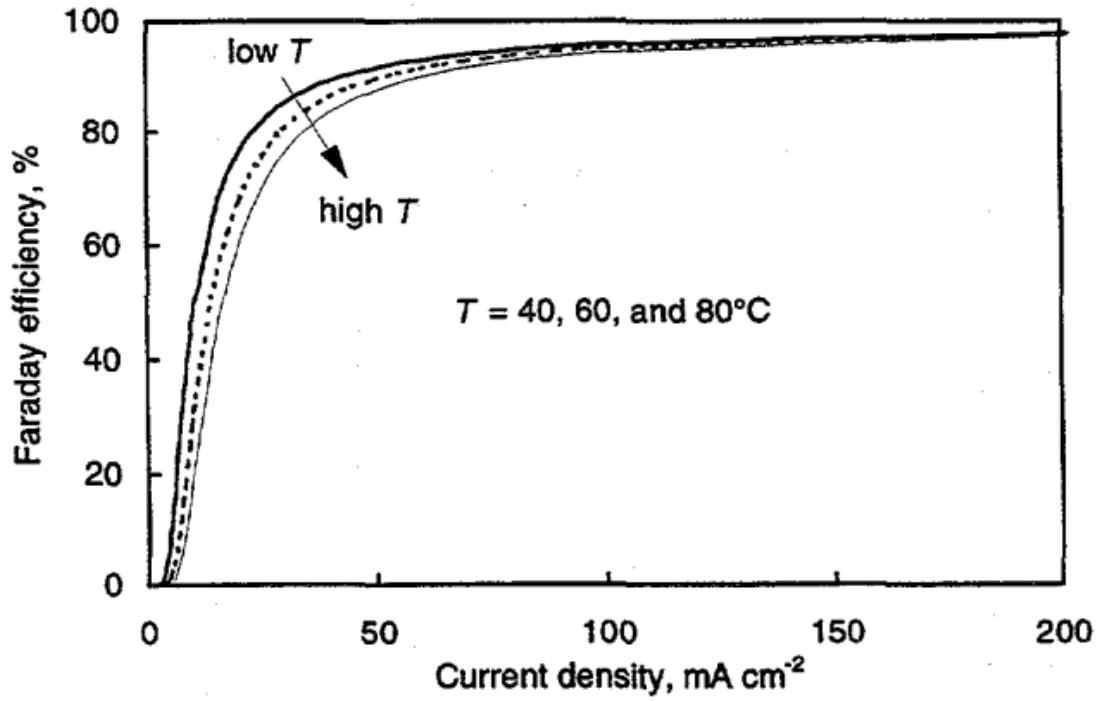

Figure 3.2: Typical Faraday efficiency curves for an electrolyser cell. Taken from [13].

Since the Faraday efficiency is caused by parasitic current losses, it is often called the current efficiency [13]. In order to characterize cell efficiency, it is necessary to link electrical power input to hydrogen flow output. Thus, Faraday's law is not sufficient an electrical response of cell electrolysis has to be described by the voltage model. The electrical response of the electrolysis cell can be either considered as static or dynamic.

3.1.2 Static modeling

The initial electrical response of an electrolyser stack is very fast (less than 15ms) and the total response time is 0.2s according to J. Eichman et al. [24] which is extremely

low compared to the global system and for normal use of electrolysers. It is therefore common for the static approach to be used in most models. These models consider the stack as a non-linear resistance. The description of the current-voltage characteristic is therefore defined by the polarization curve, which takes into account other parameters such as temperature and pressure.

Analytical models

The analytical models repeat the developments of section 2.3 and adopt the equation 2.12 repeated below.

$$V = E_{Nernst} + \eta_{act} + \eta_{ohm} + \eta_{diff} \tag{3.3}$$

Each term from the reversible potential to the different overvoltages can be described theoretically as in F. Maranggio's et al. theoretical model [18]. In the following, you will find a development for each term from Eq. 3.3.

Reversible potential
The open circuit potential (also called Nernst potential because it uses the Nernst equation) gives us the redox equilibrium potential that represents the reversible conditions for the reaction and therefore the minimum voltage. In equation 3.4 we have the minimum thermodynamic voltage as we saw in the theoretical part.

$$E_{Nernst} = \frac{\Delta G}{-2F} \tag{3.4}$$

The Nernst equation is a good way to find the open-circuit voltage. The Nernst equation expresses the voltage with respect to the standard reversible potential and a term describing the variation according to the operational conditions [51]. The potential is given by

$$E_{oc} = E^0_{rev} + \frac{RT}{nF} \ln\left(\frac{P_{H_2} \cdot \sqrt{P_{O_2}}}{a_{H_2O}}\right) \tag{3.5}$$

With E^0_{rev} the reversible potential without the effect of pressures, $R = 8.3144 J/molK$ the gas constant, T the temperature in Kelvin, n is the number of electrons involved in the half-reaction (equal to 2), $F = 96487 C/mol$ the Faraday constant, P_i the partial pressure of gas i and a_i the thermodynamic activity of species i.
The Gibbs free energy is temperature-dependent [52] and therefore, the reversible potential can be changed in a temperature dependent reversible potential (for standard conditions of pressure) and an empirical expression is used to model this behaviour. There are different empiric models such as the one developed by Harrison et al. [53] that find the expression 3.6 or the one by Roy at al. [54] in expression 3.7.

$$E^0_{rev}(T) = 1,229 - 0.9 \cdot 10^{-3} \cdot (T - 298K) \tag{3.6}$$

$$E^0_{rev}(T) = 1.485 - 1.49 \cdot 10^{-4} \cdot T - 9.84 \cdot 10^{-8} \cdot T^2 \tag{3.7}$$

Activation overvoltage
The activation voltage drop results from the proton transfer and chemical reaction velocity, it represents the electrochemical kinetic behaviours. The activation voltage drop $E_{act,k}$ can be deduced from the Butler–Volmer equation (3.8).

$$I = I_{0,k}\left[\frac{C_{PE}}{C_{PS}} \cdot \exp\left(\frac{\alpha_k nF \cdot E_{act,k}}{RT}\right) - \frac{C_{RE}}{C_{RS}} \cdot \exp\left(-\frac{(1-\alpha_k)\, nF \cdot E_{act,k}}{RT}\right)\right] \quad (3.8)$$

With C_{PE}, C_{RE}, C_{PS} and C_{RS} the different concentrations of products (P) and reagents (R) respectively near the electrode (E) and in the solution (S), α_k and $I_{0,k}$ respectively the charge transfer coefficient and the current exchange density of the half-reaction occurring at electrode k.
To find a simplified expression to get the activation overpotential in function of current density we first assume that the diffusion is not limiting the process during the reaction and that the concentration can be considered equal and therefore equal to 1. This assumption is made because we consider a diffusion overpotential in case of high current density. When the current density is high, the second exponential (that is a negative exponential) can be neglected. After the development done by Guillaume Fontès for his thesis on page 48 [55], $E_{act,k}$ can be rewritten, in function of the current I as the equation 3.9 named the Tafel law:

$$E_{act} = \frac{RT}{n\alpha^* F} \ln\left(\frac{I}{I_0^*}\right) \quad (3.9)$$

where α^* and I_0^* are respectively the transfer coefficient and the exchange current defined by equation 3.10 and 3.11.

$$\alpha^* = \frac{\alpha_a \alpha_c}{\alpha_a + \alpha_c} \quad (3.10)$$

where α_a is the transfer coefficient of the anode and α_c is the one of the cathode.

$$I_0^* = I_{0,a}^{\frac{\alpha_c}{\alpha_a+\alpha_c}} I_{0,c}^{\frac{\alpha_a}{\alpha_a+\alpha_c}} \quad (3.11)$$

Ohmic overvoltage
The resistance R_{mem} of the membrane is the main cause of the ohmic voltage drop. The conductivity value σ_{PEM} (in $\Omega^{-1}cm^{-1}$) is often given by empirical relation such as equation 3.12 proposed by [56].

$$\sigma_{\mathrm{PEM}} = (0.005139.\lambda - 0.0326)\exp\left[1268\left(\frac{1}{303.15} - \frac{1}{T}\right)\right] \quad (3.12)$$

λ is the water content of the membrane.
The conductivity of the rest of the stack is considered negligible. To compute the overpotential, we can use the equation 3.13.

$$E_{ohm} = \frac{J \cdot l}{\sigma_{\mathrm{PEM}}} = \frac{I \cdot l}{A \cdot \sigma_{\mathrm{PEM}}} \quad (3.13)$$

Where J is the current density, I the current, l is the length and A the area of the membrane.

Diffusion overvoltage
For high current densities, the reaction is no longer just controlled by electronic transfer but by matter transfer. This phenomenon named diffusion overvoltage (or concentration overpotential) has an impact on the polarization curve. First we have to come back to the Butler-Volmer equation 3.8. The hypothesis of same concentration between the electrode and the solution in order to neglect the diffusion is not possible anymore. Therefore we can find the equation 3.14 for activation and diffusion overpotential.

$$E_{act,k} + E_{diff,k} = \frac{RT}{nF} \ln\left(\frac{C_{PS}}{C_{PE}} \frac{I}{I_0^*}\right) \tag{3.14}$$

By identification we can find the diffusion overpotential (3.15). We have an overpotential for each electrode [18].

$$E_{diff,k} = \frac{RT}{nF} \ln\left(\frac{C_{PS}}{C_{PE}}\right) = \frac{RT_a}{nF} \ln\left(\frac{C_{PS,O_2}}{C_{PE,O_2}}\right) + \frac{RT_c}{nF} \ln\left(\frac{C_{PS,H_2}}{C_{PE,H_2}}\right) \tag{3.15}$$

Some model have a different approach of the diffusion overpotential by integrating it to the activation overvoltage with a "diffusion limiting current density" in equation 3.16.

$$E_{act,k} + E_{diff} = \frac{RT}{n\alpha^* F} \ln\left(\frac{\frac{I}{I_0^*}}{1 - \frac{I}{I_{lim}}}\right) \tag{3.16}$$

We can find the diffusion overpotential by deducing it from equation 3.16 and we find the results of [55] with equation 3.17.
(Note that there is a sign ambiguity, the diffusion overpotential is always positive from the ln*. From general perspective, all the overvoltages are considered positive and added to the thermoneutral voltage)*

$$E_{diff} = -\frac{RT}{n\beta F} \ln\left(1 - \frac{I}{I_{\text{lim}}}\right) \tag{3.17}$$

With β empiric coefficient taking in account the charge transfer coefficient α^* and I_{lim} the first limit current that can be fixed or empiric.

Impact of bubbles on the polarization curve
The electrolysis of water produces gas bubbles into the electrolysis cell. These bubbles have different impacts. The bubbles are covering a part of the surface of the electrodes. This phenomenon is simply modeled by a reduction of the area in equation 3.18.

$$A_{\text{aviable}} = A_{\text{total}} - A_{\text{obstructed}} \tag{3.18}$$

The problem is that the ion H^+ are in solution in water and must go through the membrane and this can increase the protonic ohmic overpotential. An other impact of this phenomenon is to increase the electrical ohmic overpotential and

that the bubbles do not conduct the electrons. In PEM electrolysis, the electrical ohmic losses can be neglected compared to the protonic one. A last impact is the limitation impact on water diffusion in the anode. The bubbles in PEM electrolysers are formed at the anode. The anode overpotential has been modeled in 3.19 [57].

$$E_{bubbles} = \frac{RT}{n\alpha_a \beta F} \ln(1 - \theta_b) \tag{3.19}$$

Where θ_b is the fraction of the anode surface blocked by the bubbles (3.20).

$$A_{\text{obstructed}} = A_{\text{total}} \cdot \theta_b \tag{3.20}$$

Semi-empirical models

In static models, there are also empirical or semi-empirical models. This approach is a simple way to model the polarization curve (current-voltage curve). The principle of the empirical model is to find a form of the equation $V = f(I)$ that is closest to the experimental states. The best known semi-empirical model is the Ulleberg model developed in 1998 for alkaline electrolysers but applicable to PEM electrolysers. It is defined in the equation 3.21. It is based on theoretical thermodynamics and empirical electrochemical data.

$$V_{\text{cell}} = V_{\text{rev}} + r \cdot I_{\text{cell}} + s \cdot \log[k \cdot I_{\text{cell}} + 1] \tag{3.21}$$

where V_{rev} , r, s, and k are parameters defined to approximate the experimental results. They can be defined as constant or they can depend on temperature, pressure, Gibbs energy change. V_{rev} is the reversible potential defined by the Gibbs free energy, $r \cdot I_{\text{cell}}$ represents the potential due to ohmic losses and $s \cdot \log[k \cdot I_{\text{cell}} + 1]$ are the activation and diffusion overpotentials. Temperature plays an important role in the performance of an electrolyser. The Ulleberg model can be extended to the final Ulleberg model 3.22. Dividing by the membrane area, we find the voltage versus the current density as shown on the polarization curve.

$$V_{\text{cell}} = V_{\text{rev}} + \left(\frac{r_1 + r_2 \cdot T}{A}\right) \cdot I_{\text{cell}} + s \cdot \log\left[\left(\frac{k_1 \cdot T^2 + k_2 \cdot T + k_3}{A \cdot T^2}\right) \cdot I_{\text{cell}} + 1\right] \tag{3.22}$$

To go further with the Ulleberg model, the article [58] takes into account, in addition to the temperature, the pressure on the gasses. The model is presented in equation 3.23.

$$V_{\text{cell}} = V_{\text{rev}} + [(r_1 + d_1) + r_2 \cdot T + d_2 \cdot P] \cdot I_{\text{cell}} + s \cdot \log\left[\left(k_1 + \frac{k_2}{T} + \frac{k_3}{T^2}\right) \cdot I_{\text{cell}} + 1\right] \tag{3.23}$$

3.1.3 Dynamic approach

Although the response of the stack is very fast, the behaviour of the stack can still be studied dynamically. For this purpose, the stack is not only a non-linear resistive element

but it is possible to use an equivalent electrical circuit with imaginary impedance. The charge double layer phenomenon which takes place at the electrode-electrolyte interface, is modeled by a capacitance in parallel with the activation and mass transport resistances. The major point with the dynamic approach is that the model developed is often intended to be used for grid studies [14, 59, 60] or for power electronics testing application [12, 28, 61, 49, 62], it does not model the electrochemical reactions and thermal phenomena in detail but the simplified models are expected to be sufficiently accurate for the electrical study.

Double layer capacitance

A double layer (DL) is a structure that appears on the surface of an object when it is exposed to a fluid. Double-layer capacitance is the important characteristic of the electrical double layer which appears, for example, at the interface between a conductive electrode and an adjacent liquid electrolyte. At this boundary two layers of charge with opposing polarity form, one at the surface of the electrode, and one in the electrolyte. These two layers, electrons on the electrode and ions in the electrolyte, are typically separated by a single layer of solvent molecules that adhere to the surface of the electrode and act like a dielectric in a conventional capacitor. As activation overpotential, there are two double layer capacitance, one at each electrode. These capacitances are evaluated empirically in the literature and are considered to be equal at each electrode [15].

Equivalent electrical circuit

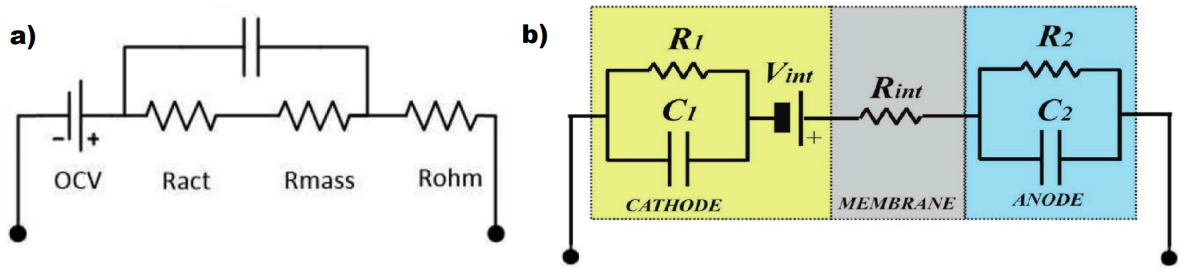

Figure 3.3: a) Electrolyser system components. Taken from [14]. b) Electrolyser electric scheme of the PEM electrolyser (EL). Taken from [15].

In figure 3.3 there are two equivalent electrical models used in two different articles. The first by Bart W. Tuinema et al. and the second by Damien Guilbert et al. [14, 15]. Globally the two circuits are simplifications of the same idea.

- The reversible voltage is represented by a fixed DC voltage modeling the power converted into hydrogen. This DC voltage is "OCV" and "Vint" in the schemes a) and b).

- Ract (R1&R2), Rmass (neglected) and Rohm (Rint) represent the activation, mass transport and ohmic losses, respectively in circuit a) (b)).
- The capacitor in the two circuits is the effect of the double layers capacitance.

Simplification of the PEM stack model is mainly dependent on the decision which losses are included and based on several assumptions:

- The mass transfer losses are not significant for low and moderate current densities if the flow field is appropriate for gas removal. Thus, the mass transfer overpotentials can be neglected for up to 3 A/cm2. This is the case for a).
- Activation losses are dominant at low-current densities, while the ohmic overpotential becomes dominant at medium-current densities according to the logarithmic resistive effect over current of the activation overpotential.
- Pressure and temperature are assumed constant.

Transient

The study of the transient of PEM stacks is that it is studied on low current density [63, 15]. Low current densities induce slower response. The time constant τ is dependent (decreasing) on the current because the resistance of the activation overpotential decreases with higher current.

$$\tau = R_{act} \cdot C_{DL} \tag{3.24}$$

$$R_{act} = \frac{E_{act}}{I} = \frac{\frac{RT}{n\alpha^* F} \ln\left(\frac{I}{I_0^*}\right)}{I} = K\frac{\ln(I)}{I} \tag{3.25}$$

where K can be assumed constant at operation point.
Table 3.1 shows different time constants for low current densities. Therefore, we have that for high current densities, we find the time constant below 1s.

Input current	τ
0 to 0.02 A/cm^2	5 s
0.1 to0.12 A/cm^2	4.5 s
0 to 0.2 A/cm^2	1.05s
0.2 to 0 A/cm^2	2.3s

Table 3.1: Time constant for different transients, from [28].

3.2 Electrical model of the power supply and the balance of plant consumption

The electrical model is focusing on the power supply of the electrolyser plant and on the consumption of the pumps, chillers, etc known as the balance of plant (BoP). The stacks are already studied in the electrochemical model and will not be addressed in this part. This part will study the modeling of the electrical consumption and the dynamic behaviour of the converters feeding the electrolyser and the electrical consumption of the balance of plant.

3.2.1 Converters

Power electronics converters are used to supply large electrolysers with DC electrical power. Modern power converters have been widely developed since the 1960's with the appearance of semiconductors in the 1950's and for example the commercialization of thyristors by General Electric in 1960 and 1961 [64]. There are now a large number of converter topologies for electrolysers. The topologies use different configurations of rectifier diodes or thyristors and choppers (i.e. buck converters). Several analysis of these topologies have been done in the literature [61] [65] [66].
Each electrolysis system is equipped with converters in order to adapt input current to the U-I characteristics of the stack(s) and other electric equipment. The dynamical aspect of the converter is crucial in the study of electrolysers dynamics. Dynamic models can be found in the literature. The study of the converters dynamic is not the main goal of this thesis.
The losses are about 1.5kWh/kg from Figure 3.4, these losses represent therefore 0.135kWh/Nm^3 on a HHV of 3.28kWh/Nm^3. This represents a loss of about 4%. This is coherent with the efficiency of ancillaries such as AC-DC converters mainly based on thyristors, which feature high energy efficiency (around 97%)[61].

3.2.2 Other components

When the power consumption of the balance of plant components are considered, they are aggregated in a unique electrical consumption which can be constant or linearly described with stack power (3.26).

$$P_{BOP} = P_0 + k \cdot P_{stack} \tag{3.26}$$

where P_0 is the constant part of the power consumed by the BoP as soon as the system is powered on and P_k the proportionality coefficient. In figure 3.4 we can see that the impact of balance of plant on the production is decreasing with the system load. This means that the BoP needs a relatively high constant part and that the proportionality is rather low. In the reviewed literature, no model with a detailed representation of BoP components to describe separately their comportment and power consumption was found. [67] develops the design, implementation, and practical experimentation of an optimized

BoP for a medium-size PEM electrolyser.

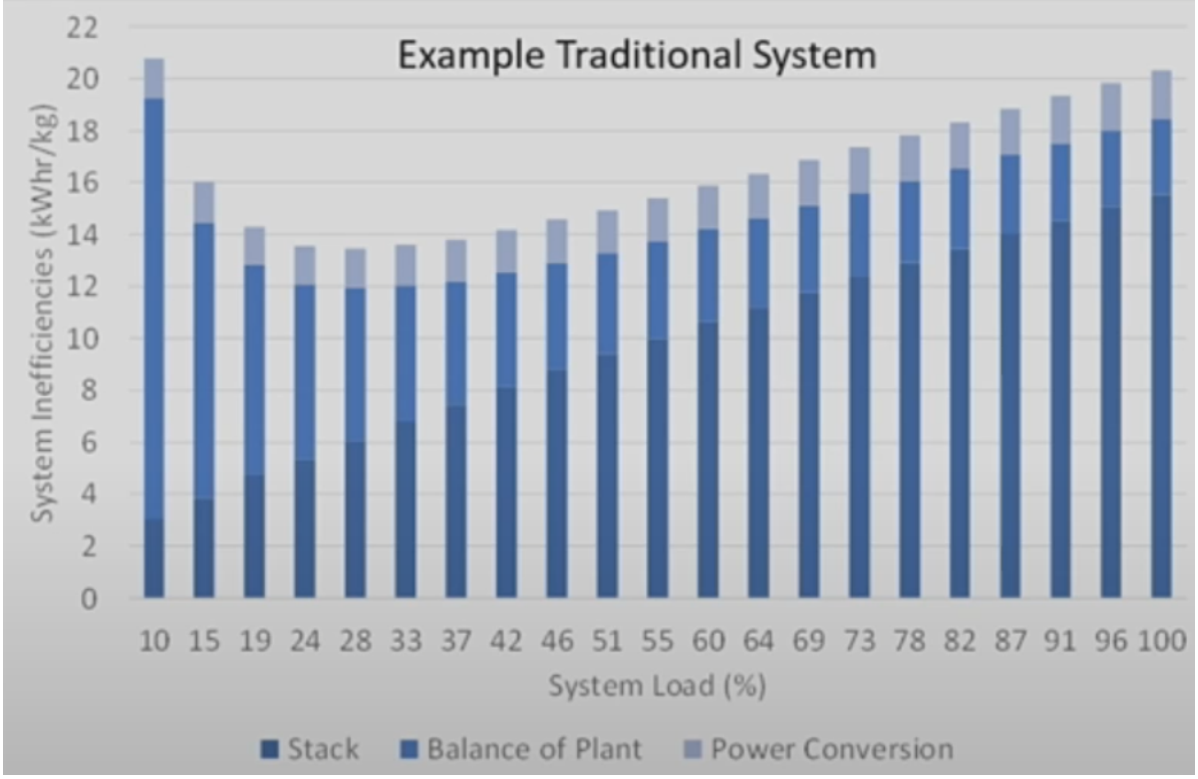

Figure 3.4: Share of energy in hydrogen production losses for different system loads. Taken from [16].

3.3 Thermal model

As we have seen in the thermodynamic development and electrochemical models of the stack, the cell potential decreases with temperature. The thermoneutral voltage is decreasing for higher temperature but the influence of the temperature on the I-U curves is mainly due to the temperature dependence of the overvoltages (Fig. 3.5).

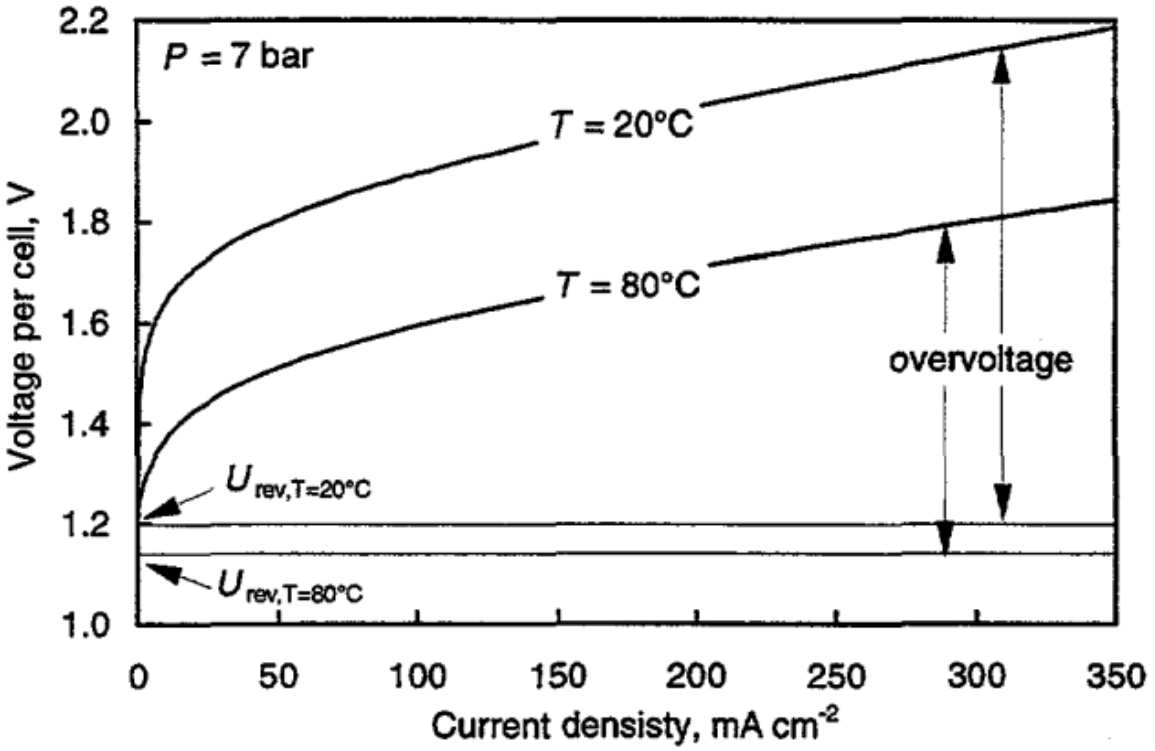

Figure 3.5: Typical I-U curves for an electrolyser cell at high and low temperatures. Taken from [13].

In electrochemical models, the stack temperature is almost always used as a modeling parameter. However, the temperature regulation is not always modeled. The temperature regulation can be considered as perfect and the temperature as an adjustment variable. However, maintaining the temperature at a desired value can be complicated, especially when the electrolyser is used dynamically. Therefore, we have thermal models designed to complement the electrochemical model of the stacks. These models focus on the thermal equilibrium and the quantities of thermal energy accumulation, thermal energy production, exchange and transport within the electrolyser system. Two types of models are distinguished in the literature: models based on ordinary differential and partial differential equations.

3.3.1 Lumped parameters model

The stack is considered as a unique thermal capacitance C_p (lumped thermal capacitance) and its temperature is assumed to be homogeneous. The overall thermal energy balance can be expressed as a linear, first order, non-homogeneous differential equation. The standard component library TRNSYS17 [68] provides 3 different ways to calculate the temperature in Type 160 "Advanced Alkaline Electrolyser" :

- Mode 1: T is known and therefore given as input
- Mode 2: T is calculated from a simple quasi-static thermal model
- Mode 3: T is calculated from a complex lumped thermal capacitance model

These models are based on the analytical characterization of thermal accumulation, production, exchange and transport terms and the resolution of thermal balances.
The overall energy model described in Ulleberg model [13] and [50], by Rafael et al. [69] or by Lebbal and Lecoeuche [70]:

$$\dot{\mathrm{Q}}_{\mathrm{gen}} = \dot{\mathrm{Q}}_{\mathrm{store}} + \dot{\mathrm{Q}}_{\mathrm{loss}} + \dot{\mathrm{Q}}_{\mathrm{cool}} \tag{3.27}$$

With

$$\dot{\mathrm{Q}}_{\mathrm{store}} = C_p \frac{dT}{dt}, \tag{3.28}$$

The thermal capacitance modeling the stack of value C_p.
The decomposition of electrical power allows isolating thermo-neutral voltage U_{tn} (Eq. 3.29 and 3.30).

$$We = U \cdot I = \frac{I}{2F} \Delta rH + N_{\mathrm{cell}} \left(V_{\mathrm{cell}} - U_{\mathrm{th}} \right) I \tag{3.29}$$

The first term is the work needed for the reaction where ΔrH is the enthalpy of water dissociation reaction (J mol-1) and the second term is the part of the work that is transformed into heat $\dot{Q}_{\mathrm{gen}}$:

$$\dot{Q}_{\mathrm{gen}} = N_{\mathrm{cell}} \left(V_{\mathrm{cell}} - U_{\mathrm{th}} \right) I \tag{3.30}$$

The energy loss can be modeled linearly with the ambient in Eq. 3.31

$$\dot{Q}_{\mathrm{loss}} = \frac{1}{R_{\mathrm{th}}} \left(T_{\mathrm{stack}} - T_{\mathrm{amb}} \right) \tag{3.31}$$

With R_{th} the thermal resistance of the stack

$$\dot{Q}_{\mathrm{cool}} = \dot{n}^{in}_{H_2O} \cdot H^{in}_{H_2O} - \dot{n}^{out}_{H_2O} \cdot H^{out}_{H_2O} - \dot{n}^{out}_{H_2} \cdot H^{out}_{H_2} - \dot{n}^{out}_{O_2} \cdot H^{out}_{O_2} \tag{3.32}$$

With $\dot{n}^{in}_i$ and $\dot{n}^{out}_i$ respectively the input and output molar flow of species i, H^{in}_i and H^{out}_i respectively the input and output molar enthalpy of species i. That can be simplified:

$$\dot{Q}_{\mathrm{cool}} = \dot{n}_{\mathrm{in},H_2O} \cdot C_{p,H_2O} \left(T_{\mathrm{in},H_2O} - T_{\mathrm{stack}} \right) \tag{3.33}$$

Assuming the output temperatures are equal to the stack temperature and the input temperatures are equal both at anode and cathode compartments. The different output energy flows are simplified by considering a water circuit without electrolysis and perfect heat transfer with the stack.
We obtain a generic expression for the stack thermal balance (Eq. 3.34).

$$C_p \frac{dT}{dt} = N_{\text{cell}} \left(V_{\text{cell}} - U_{\text{th}}\right) I + \frac{1}{R_{\text{th}}} \left(T_{\text{stack}} - T_{\text{amb}}\right) + \dot{n}_{\text{in},H_2O} \cdot C_{p,H_2O} \left(T_{\text{in},H_2O} - T_{\text{stack}}\right) \tag{3.34}$$

The equation (3.34) has 4 different terms:

- $\left(C_p \frac{dT}{dt}\right)$ the accumulation term
- $((E_{cell} - V_{th}) \cdot I)$ the heat production term
- $\left(\frac{1}{R_{\text{th}}} \left(T_{\text{stack}} - T_{\text{amb}}\right)\right)$ the losses term
- $\left(\dot{n}_{\text{in},H_2O} \cdot C_{p_{H_2O}} \left(T_{\text{in},H_2O} - T_{\text{stack}}\right)\right)$ the exchange term with circulating water

In mode 2 the electrolyser temperature is simply calculated by assuming constant heat generation and heat transfer rates for a given time interval. Thus, Equation 3.27 can be rewritten as

$$T_{\text{stack}} = T_{\text{stack},ini} + \frac{\Delta t}{C_p} (\dot{\text{Q}}_{\text{gen}} + \dot{\text{Q}}_{\text{loss}} + \dot{\text{Q}}_{\text{cool}}) \tag{3.35}$$

where

Δt	time interval, s
$T_{\text{stack},ini}$	temperature of stack at initial conditions, °C

Mode 3 will not be implemented since Simscape already implements thermal capacitances. The final model can be understood as Equation 3.36.

$$T_{\text{stack}} = T_{\text{stack},ini} + \frac{dt}{C_p} (\dot{\text{Q}}_{\text{gen}} + \dot{\text{Q}}_{\text{loss}} + \dot{\text{Q}}_{\text{cool}}) \tag{3.36}$$

3.4 Mass transfer model

The electrolysis is a continuous reactor. The reagents and products are continuously flowing into and out of the reactor. The phenomenon of mass transfer has a big impact on the dynamic behaviour of the stack and its electrochemical conversion efficiency. There is also a transfer of the reagents through the membrane. The mass transfer models have been developed in order to be coupled with the electrochemicals models. The main goals are to determine the impact of the mass transfer on the dynamic behaviour, to compute reversible potential and diffusion overvoltage calculations by determining species concentration and pressure and to evaluate the impacts of gas cross-permeation on cell efficiency, cell degradation, gas purity and security constraints. Fig. 3.6 represents a PEM cell with the different parts used to describe the mass transfer.

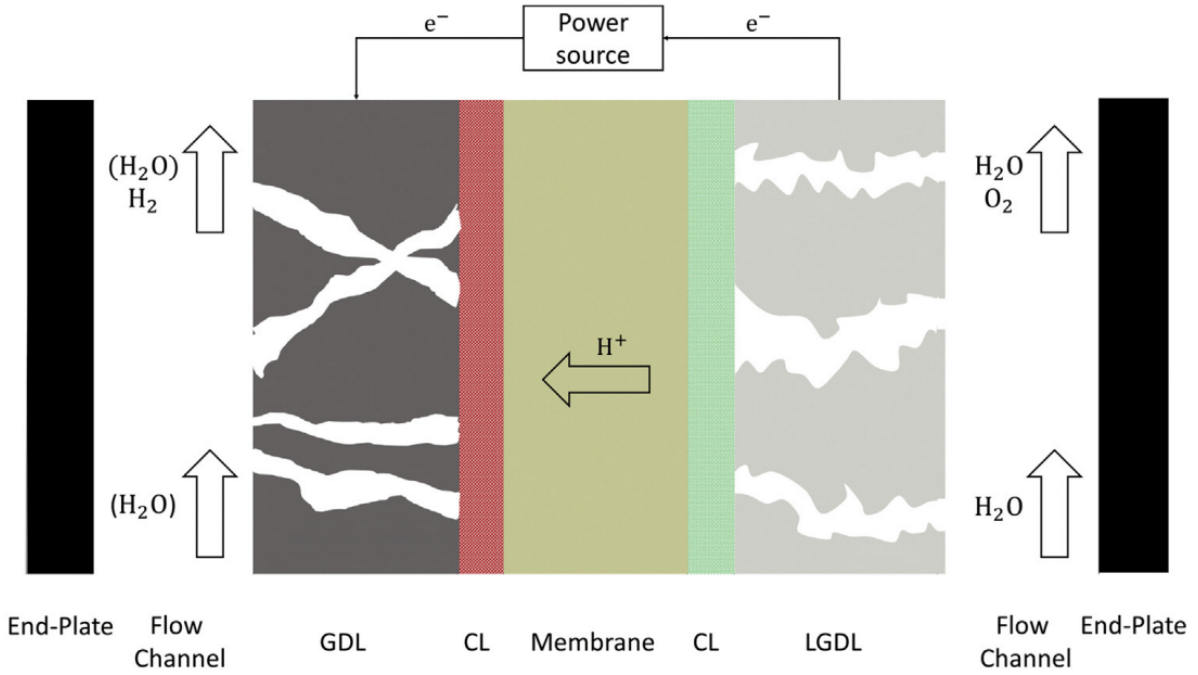

Figure 3.6: A single-cell PEMWE with end-plates, flow channel, liquid-gas diffusion layer (LGDL), gas diffusion layer (GDL), and catalyst coated membrane (CCM). Schematic of components and mass flows in a PEMWE. Taken from [17].

In this part, we will use an existing model related to mass transport and its characterization for PEM electrolysers. To go further on this specific and crucial topic for the improvement of PEM cells, the review of Maier et al. [17] addresses the current knowledge of mass transport, considering the flow channels, liquid-gas diffusion layer, and polymer electrolyte membrane in particular.

3.4.1 Mass transfer in the PEM

Figure 3.7 shows the mass flows inside the electrolysis cell (expressed in mol/s). Here below the explanation of the different fluxes.

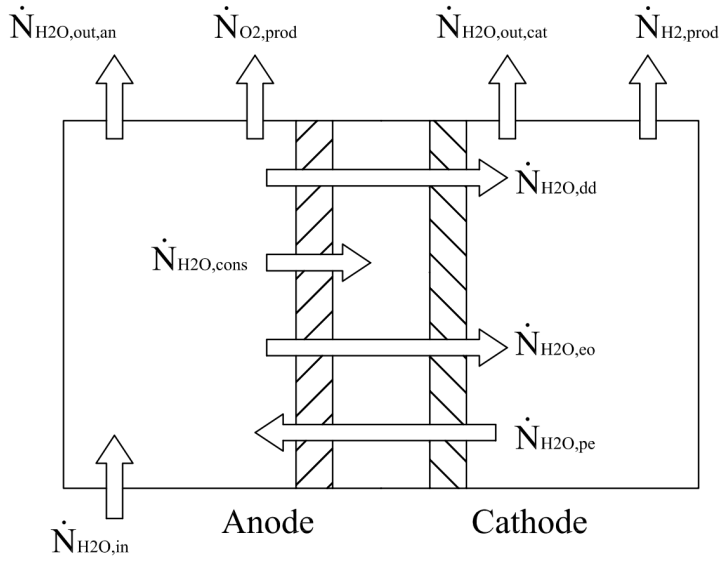

Figure 3.7: Mass flows inside the cell. Taken from [18].

$\dot{N}_{H_2O,\text{in}}$ is the molar water inlet flow at the anode.

$\dot{N}_{H_2O,\text{out,an}}$ is the molar water outlet flow from the anode.

$\dot{N}_{H_2O,\text{out,cat}}$ is the molar water outlet flow from the cathode.

$\dot{N}_{O_2,\text{prod}}$ is the molar oxygen flow produced at the anode.

$\dot{N}_{H_2,\text{prod}}$ is the molar hydrogen flow produced at the cathode.

$\dot{N}_{H_2O,\text{dd}}$ is the molar water flow due to the concentration gradient.

$\dot{N}_{H_2O,\text{drag}}$ is the molar water flow from the anode to the cathode, due to the electro-osmotic drag.

$\dot{N}_{H_2O,\text{pe}}$ is the molar water flow from the cathode to the anode, due to the pressure effect.

$\dot{N}_{H_2O,\text{cons}}$ is the molar water flow consumed by the electrochemical reaction and split into hydrogen and oxygen.

Anode

First we can consider that the total water flux entering the cell is known. The pumps circulate the water at specific flux in order to help the regulation of the water.
According to Faraday's law, the consumption of water in an electrolyser cell is directly proportional to the electrical current density. Assuming a Faraday's efficiency of 1 (as explained in section 3.1.1). The total mass flux of consumed water $\dot{G}_{H_2O,\text{cons}}$ [kg s^{-1}] can be described by [71] as:

$$\dot{G}_{H_2O,\text{cons}} = N_{\text{cell}} \frac{I}{2F} \cdot M_{H_2O} \tag{3.37}$$

where N_{cell} the number of cells [-], I is the current[1] [A], M_{H_2O} is the molar weight of water [kg mol^{-1}] and F is the Faraday constant [s A mol^{-1}].
The produced mass flux of oxygen gas is therefore [71]:

$$\dot{G}_{O_2,\text{prod}} = N_{\text{cell}} \frac{I}{4F} \cdot M_{O_2} \tag{3.38}$$

where M_{O_2} is the molar weight of oxygen.
The global mass flux of water out of the anode is equal to the inlet flux of water at the anode minus the consumed water and the water across the membrane:

$$\dot{G}_{H_2O,\text{out,an}} = \dot{G}_{H_2O,\text{in}} - \dot{G}_{H_2O,\text{cons}} - \dot{G}_{H_2O,\text{mem}} \tag{3.39}$$

Cathode

The produced molar and mass flux of hydrogen gas are:

$$\dot{N}_{H_2,\text{prod}} = N_{\text{cell}} \frac{I}{2F} \tag{3.40}$$

$$\dot{G}_{H_2,\text{prod}} = N_{\text{cell}} \frac{I}{2F} \cdot M_{H_2} \tag{3.41}$$

where M_{H_2} is the molar weight of hydrogen.
The global mass flux of water out of the cathode is equal to the flux of water across the membrane:

$$\dot{G}_{H_2O,\text{out,cat}} = \dot{N}_{H_2O,\text{out,cat}} \cdot M_{H_2O} = \dot{N}_{H_2O,\text{mem}} \cdot M_{H_2O} \tag{3.42}$$

Membrane

Water crosses the membrane from anode to cathode. This is composed of three phenomena exposed in Fig 3.7 above: water diffusion, electro-osmotic drag and hydraulic pressure.

$$\dot{N}_{H_2O,\text{mem}} = \dot{N}_{H_2O,\text{diff}} + \dot{N}_{H_2O,\text{drag}} + \dot{N}_{H_2O,\text{pe}} = \dot{N}_{H_2O,\text{out,cat}} \tag{3.43}$$

Water diffusion

[1] assumed to be uniformly distributed [72]

Diffusion of water refers to the transport of water from high to low concentration regions prevalently from anode to cathode as water is formed at anode side. Fick's law is used to calculate the water transport by integrating water concentration across the membrane between the two electrodes [20]. Assuming a linear water concentration gradient, we can simply calculate the concentration gradients across the membrane as a difference instead of using integral function:

$$\dot{N}_{H_2O,\text{diff}} = \frac{AD_w}{\delta_{mem}} \left(C_{H_2O,mem,cat} - C_{H_2O,mem,an}\right) \tag{3.44}$$

where A is the air of the membrane, D_w is the membrane water diffusion coefficient, δ_{mem} is the thickness of the membrane and $C_{H_2O,mem,cat}$ and $C_{H_2O,mem,an}$ are the water concentration at the electrolyte/electrode interfaces at cathode and anode.

Electro-osmotic drag
When the proton moves through the PEM, water molecules also accompany the proton through the membrane by the electric field. This phenomenon is well known as the electro-osmosis drag. To model this phenomenon, we use a coefficient, named n_{drag}, representing the number of water molecules dragged per hydrogen core H^+ through the membrane [$\text{mol}_{H_2O}/\text{mol}_{H^+}$]. This linear dependence can be expressed as [18]:

$$\dot{N}_{\text{drag}} = n_{\text{drag}} \dot{N}_{H^+,\text{through}} = n_{\text{drag}} N_{\text{cell}} \frac{I}{F} \tag{3.45}$$

where $\dot{N}_{\text{drag}}$ represents the water molar transfer, $\dot{N}_{H^+,\text{through}}$ the molar transfer of proton through the membrane and therefore the mass flux is expressed as [71]:

$$G_{\text{drag}} = n_{\text{drag}}(2 \cdot G_{H_2O,\text{cons}}) \tag{3.46}$$

For temperatures around 353 K, n_{drag} is approximately 5.0. We obtain G_{drag} is about 10 times $G_{H_2O,\text{cons}}$ [71]. Therefore the dehumidification at the cathode will be necessary.
The coefficient n_{drag} has been measured experimentally by different authors and resulting values have shown large variance. The electro-osmosis drag depends linearly on the temperature according to Onda et al. [73]:

$$n_{\text{drag}} = 0.0134 \cdot T + 0.03 \tag{3.47}$$

The relationship 3.48 below is function of temperature and pressure [74]:

$$n_{\text{drag}} = 0.0252 P_c - 1.9073 I + 0.0189 T - 2.7892 \tag{3.48}$$

Hydraulic Pressure
Water transport due to pressure asymmetry, Δp, between anode and cathode depends on permeability of the membrane and can be calculated using Darcy's Law. The relationship is function of K_{darcy} the membrane permeability to water, μ_{H_2O} the viscosity, and M_{H_2O} the molar mass of water:

$$\dot{N}_{H_2O,\text{pe}} = K_{\text{darcy}} \frac{A \rho_{H_2O}}{\delta_{mem} \mu_{H_2O} M_{H_2O}} \Delta p \tag{3.49}$$

Partial pressure

The partial pressures of the species i at the electrode k is given by:

$$p_i = X_i P_k \tag{3.50}$$

where p_i is the partial pressure of the species, $X_{i,k}$ is the molar fraction of the species at electrode k and P_k is the pressure at the electrode k. The molar fractions at the anode can be expressed as

$$X_{\mathrm{O}_2,an} = \frac{\dot{N}_{O_2,\mathrm{prod}}}{\dot{N}_{O_2,\mathrm{prod}} + \dot{N}_{H_2O,\mathrm{out,an}}} \tag{3.51}$$

$$X_{\mathrm{H}_2O,an} = \frac{\dot{N}_{H_2O,\mathrm{out,an}}}{\dot{N}_{O_2,\mathrm{prod}} + \dot{N}_{H_2O,\mathrm{out,an}}} \tag{3.52}$$

The partial pressures of the hydrogen and water at the cathode are calculated according to Eq. 3.50. The molar fractions at the cathode can be expressed as:

$$X_{\mathrm{H}_2,cat} = \frac{\dot{N}_{H_2,\mathrm{prod}}}{\dot{N}_{H_2,\mathrm{prod}} + \dot{N}_{H_2O,\mathrm{out,cat}}} \tag{3.53}$$

$$X_{\mathrm{H}_2O,cat} = \frac{\dot{N}_{H_2O,\mathrm{out,cat}}}{\dot{N}_{H_2,\mathrm{prod}} + \dot{N}_{H_2O,\mathrm{out,cat}}} \tag{3.54}$$

3.5 Fluidic model

The fluidic model will be implemented with the Simscape library of Simulink which allows to take into account the flow rates, the pressures on the fluids at different places.

3.6 Efficiency

The efficiency calculation is computed from the produced hydrogen to the global power consumed. The total energy demand is the theoretical energy required for H_2O electrolysis without any losses. In real systems, losses are inevitable and the performance of the system concerned can be evaluated in terms of energy efficiency. This efficiency can be defined [75] as:

$$\eta_{\text{en}} = \frac{\text{LHV}_{\text{H}_2} \cdot \dot{N}_{\text{H}_2,\text{out}}}{Q_{\text{electric}} + Q_{\text{heat,PEM}} + Q_{\text{heat,H}_2\text{O}}} \tag{3.55}$$

where LHV_{H_2} is the lower heating value of H_2, $\dot{N}_{\text{H}_2,\text{out}}$ is the outlet flow rate of H_2, Q_{electric} and $Q_{\text{heat,PEM}}$ are the rate of electric energy input and the rate of thermal energy input for the PEM electrolyser respectively, $Q_{\text{heat,H}_2\text{O}}$ is the rate of thermal energy input to the heat exchanger with the H_2O.
As soon as there is no thermal energy input in the PEM, $Q_{\text{heat,PEM}} = 0$. The thermal input of water can be considered to be zero at standard conditions or even negative when the water is cooled with heat revaluing e.g. by cogeneration.

Chapter 4

Modeling with MATLAB®

This chapter explains the new electrolyser model provided by Matlab and the modifications that we made to better support the dynamic aspects of the large PEM electrolysers.
MATLAB, version R2022a released on 15 March 2022, provides a first electrolyser model[1]. This model cites 2 articles [20, 78] and presents a lot of similarities with the modeling of Adbin et al. [72]. It is a Simulink® model using Simscap™ to create models of physical systems. Simscape has physical components and connections that directly integrate with block diagrams and other modeling paradigms. It is possible to create custom component models using the MATLAB® based Simscape language, which enables text-based authoring of physical modeling components, domains and libraries. The model parameters and design control systems for the physical system can be driven using Matlab variables and expressions.
Fig. 4.1 is a view of the model. It can be split into five parts. The Electrolyser part in purple represents the stack and therefore the central part of the electrolyser system. The Electrical supply in green has to provide a DC current to the electrolyser. The three last parts are commonly called balance of plant and manage the thermal and pressure regulation, provide water to the electrolyser and manage the gas produced. The hydrogen chain is the blue area, the water circuit, thermal control and oxygen release is in yellow and the thermal output in orange is used to model the exchange heat of the stack.
On Fig. 4.2, we see that the scheme of PEM electrolyser done for the off-the-shelf M series electrolyser by NEL ASA company is very close to the model. The biggest difference is the water circulation at the cathode with the hydrogen/water separator.

[1]available on https://www.mathworks.com/help/physmod/simscape/ug/pem-electrolysis-system.html

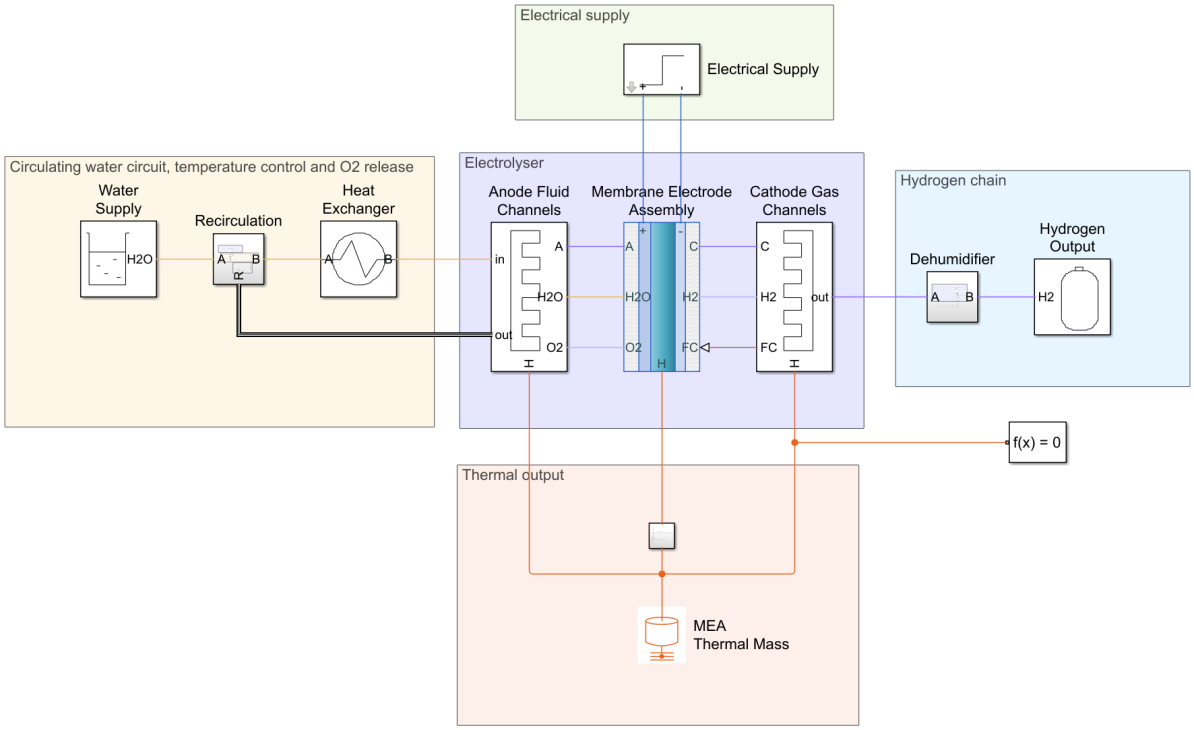

Figure 4.1: Matlab electrolyser model overview.

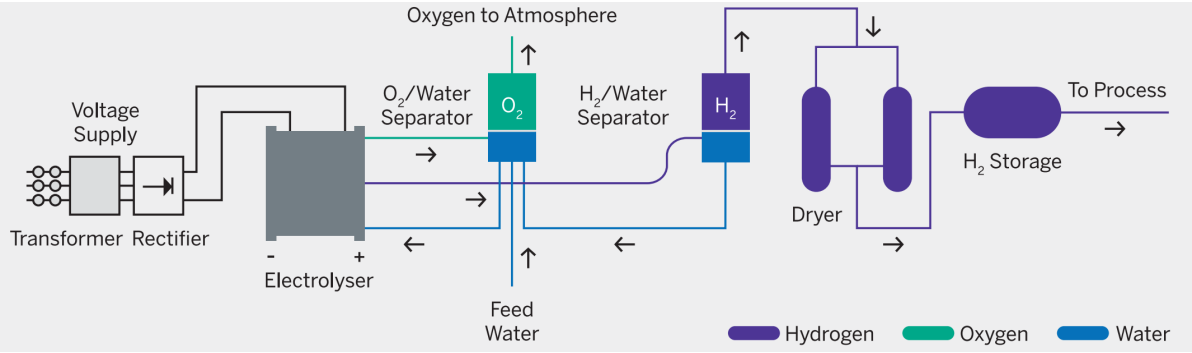

Figure 4.2: Nel electrolyser scheme available in their brochure [19].

Nel ASA is a global Norwegian company founded in 1998. Nel provides solutions for the production, storage and distribution of hydrogen from renewable energy sources. The company is already producing 1.25 MW PEM electrolyser modules. These modules are combined to install modular plants up to hundreds of MW (under the product name M series).

4.1 Stack model

The electrolyser stack can be represented as a black box interacting with the balance of plant and the electrical supply. The stack in itself can be decomposed in 3 blocks, the Membrane Electrode Assemblies, the anode and the cathode fluid channels. The fluid channels are the pipes and the interface where the water and the gas (oxygen, vapor and hydrogen) are consumed or produced inflows and outflows. The Membrane Electrode Assemblies is a custom block from Simscape. The code of this block implements the different equations to model PEM electrolysis.

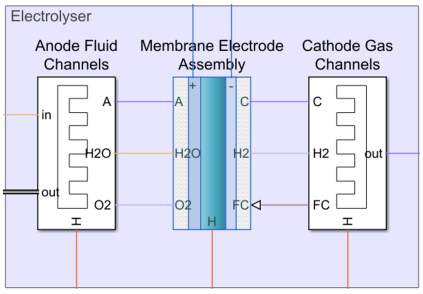

Figure 4.3: Stack model from matlab model.

4.1.1 Membrane Electrode Assemblies (MEA)

This block is defined within a Simulink code. The code is available in Annex A. It models a stack of membrane electrode assemblies (MEA) for a PEM electrolyser. The power supply is given through the + (positive) and - (negative) electrodes. Water is consumed from the connected anode flow channels on port "H2O". Oxygen and hydrogen are produced at the connected anode and cathode fluid channels, respectively on port "O2" and "H2". Waste heat is modeled through the port "H" to the equivalent MEA thermal mass.

Voltage model

The stack voltage can be modeled in many different ways. As we have seen in Chapter 3, in the dynamic approach, some models use the static approach to model the voltage as a non-linear varying resistance. Other models use different approaches such as non real impedance (resistive and capacitive behaviour).
The voltage model is the number of cells times the cell voltage. The cell voltage is the sum as in equation 4.1 of the Nernst voltage and the different over-potentials. We can see that activation and diffusion over-potentials are included in the same over-potential as in 3.16.

```
343        % Stack voltage
344        v == N_cell * (v_nernst + v_ohm + v_act_diff);
```

$$V_{cell} = V_{nernst} + V_{ohm} + V_{act,dif} \tag{4.1}$$

The Nernst potential is given by the equation 3.5. In the original code, the logarithm in the expression is $\ln\left(\frac{a_{H_2,C} \cdot a_{O_2,A}^{0.5}}{a_{H_2O,A}}\right)$. This is using the activities of the gas and not the

partial pressures. We can change the expression of V_{nernst} and get Eq. 4.2, the same as in Chapter 3.

```
250     % Nernst voltage
251     E_cell = G_H2O/(-2*F) - {0.0009, 'V/K'}*(T_stack-{298,'K'})
252     % ORIGINAL VERSION
253     %v_nernst = E_cell + R_u*T_stack/(2*F) * log((a_H2_C * a_O2_A^0.5) / a_H2O_A);
254     % MODIFIED VERSION
255     v_nernst = E_cell + R_u*T_stack/(2*F) * log((p_ws_ratio_C * p_ws_ratio_A^0.5)/ a_H2O_A);
```

$$V_{nernst} = E^0_{cell} + \frac{R \cdot T_{stack}}{2 \cdot F} \cdot \ln\left(\frac{P_{H_2,C} \cdot P^{0.5}_{O_2,A}}{a_{H_2O,A}}\right) \tag{4.2}$$

In the original version of the MEA code, the standard potential was given by $E^0_{cell} = \frac{G_{H_2O}}{-2 \cdot F} = 1.2289V$ but it has been modified according to equation 3.6, the thermoneutral voltage depends on the temperature and is plotted in Figure 4.4.

$$E^0_{cell} = \frac{G_{H_2O}}{-2 \cdot F} - 0.0009 \cdot (T_{stack} - 298) \tag{4.3}$$

For the ohmic losses, the original Matlab model uses the same empirical model for the

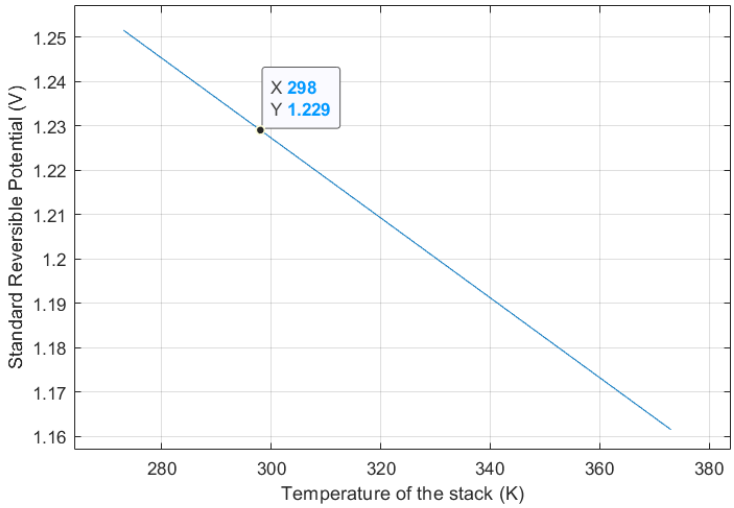

Figure 4.4: Reversible voltage in function of stack temperature at atmospheric pressure.

conductivity from Harrison et al. [53] used in many PEM electrolysis models. We find therefore the equivalent resistance in Eq. 4.4.

$$R_{ohm} = \frac{l_{membrane}}{(0.005139.\lambda - 0.0326)\exp\left[1268\left(\frac{1}{303.15} - \frac{1}{T}\right)\right]} \tag{4.4}$$

The voltage in Eq. 4.5 is given by Ohm's law.

$$V_{ohm} = R_{ohm} \cdot i_{cell} \tag{4.5}$$

```
273         % Resistive voltage loss
274         v_ohm = R_ohm * i_cell;
```

Now comes the activation overpotential. The original equation implemented in Matlab was the same as the activation overpotential we found at Eq. 3.9. Now we see that the diffusion overpotential is not modeled so we can transform the activation potential and use the Eq. 3.16. The limiting current density is defined around 9.4A/cm^2 in [55] (for PEM fuel cell) but [69] explains that however, in commercial PEMWE the mass-transport limitation effect is hardly seen because the working current densities are never high enough to raise the limiting current.

```
257         % ORIGINAL VERSION
258         %v_act = if ge(i_cell, io), b*log(i_cell/io) else 0 end;
259         % MODIFIED VERSION
260         v_act = if ge(i_cell, io), b*log((i_cell/io)/(1-(1/i_lim))) else 0 end;
```

$$V_{act} + V_{diff} = \frac{R \cdot T_{stack}}{2 \cdot \alpha \cdot F} \cdot \ln\left(\frac{\frac{i_c cell}{io}}{1 - \frac{1}{i_{lim}}}\right) \tag{4.6}$$

The activation potential is subject to several simplifications. For example, there is no question of activation at the anode and at the cathode and these two activations are combined in the same over-potential. The exchange current density of the model is $I_o* = 8cdot10^{-5}$ A/cm^2 and the charge transfer coefficient are $\alpha* = 0.5$. With the data of the electrolyser of Z. Abdin [72], we get values of $3.7 \cdot 10^{-3}$ A/cm^2 and 0.19. By implementing these parameters in the simulations, the activation over-voltage decreases a bit for high current densities. The original values were kept by default to preserve the initial characteristics of the modeled cells.
The bubbles are not modeled in this case. It is an important study field to increase the efficiency of electrolysers but it is never included in PEMWE models. It needs more empiric data and is not known enough to take it into account in the model.

Thermal model

In the thermal model, we have a simple thermal capacitance representing the stack temperature (see subsection 3.3.1 Lumped parameters model). The capacitance represents the energy stored in the stack. Its name is "MEA thermal mass" in the Simulink model. From the MEA custom block, the only thermal flux is the heat generated by the different losses. All the over-potentials end up in heat generation. Therefore the heat is the entire electrical power minus the effective power needed for the chemical reaction. In the original code, we find this idea in Eq. 4.7:

$$P_{dissipated} = P_{elec} - P_{net} \tag{4.7}$$

The electrical power is easy to get because we have already defined the voltage and the current is controlled. Now we have to define the net power. In chapter 3 we defined the net power as the thermoneutral voltage compared to the cell voltage in equation 3.30.

$$\dot{Q}_{\text{gen}} = N_{\text{cell}} \left(V_{\text{cell}} - E_{\text{Nernst}} \right) I \tag{4.8}$$

In the original code of Matlab it is defined by the following expression:

$$P_{net} = P_{rxn} - P_{delta,std} - P_{trans} \tag{4.9}$$

P_{rxn} is the energy consumed by reaction at standard temperature

$$P_{rxn} = HHV_{H_2} \cdot \dot{G}_{H_2,\text{prod}} / M_{H_2} \tag{4.10}$$

where HHV_{H_2} is the higher heating value of hydrogen expressed as kJ/mol.
$P_{delta,std}$ is the energy gain in membrane due to bringing reactants and products to standard temperature

$$\begin{aligned} P_{delta,std} = \dot{G}_{H_2O,\text{cons}} \cdot ((\Delta H_{H_2O,A} - \Delta Hvap_{H_2O,A}) - (\Delta H_{H_2O,std} - \Delta Hvap_{H_2O,std})) \\ + \dot{G}_{O_2,\text{prod}} \cdot (\Delta H_{O_2,A} - \Delta H_{O_2,std}) + \dot{G}_{H_2,\text{prod}} \cdot (\Delta H_{H_2,A} - \Delta H_{H_2,std})) \end{aligned} \tag{4.11}$$

where $\delta H_{i,k}$ is the heat stored in the species i at the electrode k or std and $\delta Hvap_{i,k}$ is the same for vaporization heat.
P_{trans} is the energy gain in membrane due to water transport

$$P_{trans} = \dot{G}_{H_2O,\text{mem}} \cdot (\Delta H_{H_2O,A} + \Delta H_{H_2o,C} - \Delta HvapH_2O, A) \tag{4.12}$$

and we have therefore the generated heat through the loss of electrical power. This heat generation is sent to the thermal mass.

$$\dot{Q}_{\text{gen}} = P_{dissipated} \tag{4.13}$$

Mass model

The mass model ensures that the material flows are respected. In the MEA, we will model the flows of consumed water and produced gas.
The following equation is removing water from the "H2O" port:

$$\dot{M}_{H_2O,\text{delete}} = \dot{M}_{H_2O,\text{cons}} + \dot{M}_{H_2O,\text{trans}} \tag{4.14}$$

where $\dot{M}_{H_2O,\text{cons}}$ is the mass flow of consumed water by the chemical reaction and $\dot{M}_{H_2O,\text{trans}}$ is the total flow crossing the membrane.
As we are consuming water at the anode, a part of the circulating water is caught. The thermal liquid port must also define the heat flows. Equation 4.15 ensures that the heat flow of the water consumed is brought to the MAE:

$$\Phi_{H_2O} = \dot{M}_{H_2O,\text{delete}} \cdot h_{H_2O} \tag{4.15}$$

where $h_{H_2O} = u + P\nu$ with u is the specific internal energy of the system, P is the pressure of the system and ν is the specific volume. The mass flows are represented below in the same way as in section 3.4.1.

$$\dot{M}_{H_2O,\text{cons}} = N_{cell} \cdot \frac{J_{cell} \cdot A_{cell}}{(2 \cdot F)} \cdot M_{H_2O} \tag{4.16}$$

$$\dot{M}_{O_2,\text{prod}} = N_{cell} \cdot \frac{J_{cell} \cdot A_{cell}}{(4 \cdot F)} \cdot M_{O_2} \tag{4.17}$$

$$\dot{M}_{H_2,\text{prod}} = N_{cell} \cdot \frac{J_{cell} \cdot A_{cell}}{(2 \cdot F)} \cdot M_{H_2} \tag{4.18}$$

Water crosses the membrane by three phenomena: electroosmosis, diffusion and permeation. Water flows from the anode to the cathode by electroosmosis, proportional to the current, and by diffusion due to the chemical equilibrium. From the cathode to the anode by permeation due to the pressure difference between the electrodes.

$$\dot{M}_{H_2O,\text{trans}} = (\dot{n}_{H_2O,\text{diff}} + \dot{n}_{H_2O,\text{drag}} + \dot{n}_{H_2O,\text{hydraulic}}) \cdot M_{H_2O} \cdot N_{cell} \tag{4.19}$$

The equations implemented for each phenomena are the same as in section 3.4.1 but at the cell scale. This is multiplied by the number of cells in Equation 4.19.

$$\dot{N}_{H_2O,\text{diff}} = \frac{AD_w}{\delta_{mem}} (C_{H_2O,mem,cat} - C_{H_2O,mem,an}) \tag{4.20}$$

$$\dot{N}_{\text{drag}} = n_{\text{drag}} \frac{I}{F} \tag{4.21}$$

$$\dot{N}_{H_2O,\text{hydraulic}} = K_{\text{darcy}} \frac{A\rho_{H_2O}}{\delta_{mem}\mu_{H_2O}M_{H_2O}} \Delta p \tag{4.22}$$

4.1.2 Anode Fluid Channels

The anode fluid channels subsystem is the interface where the water flows in the stack, flows out and where oxygen is produced. In Figure 4.5 we see the different elements representing these channels. We have 2 pipes from the Thermal Liquid library in yellow. The pipe "Water Channels Inflow" brings the water to the stack and the pipe "Water Channels Outflow" allows the water to circulate in order to have a thermal regulation and avoid too much heating. We also have a pipe from Moist Air library for the Oxygen production. This pipe is connected at side "A" to a "CAP" which is a terminus of the moist air network. The source "S" is connected to the MEA for oxygen production. All pipes are connected to the thermal mass and represent the thermal transfer of these channels.
On the right hand side we find the 3 nodes of the MEA block. The input "A" allows to transmit the anode fluid properties, the port "H2O" is the water flowing in the membrane and the port "O2" is the oxygen production. On the left, we have 3 ports. The port "in" is the water flowing in and the port "out" is the 2 separated channels outflows for water and oxygen. This is a simplification made for modeling purposes. Simscape has no easy way to mix oxygen into the thermal liquid.

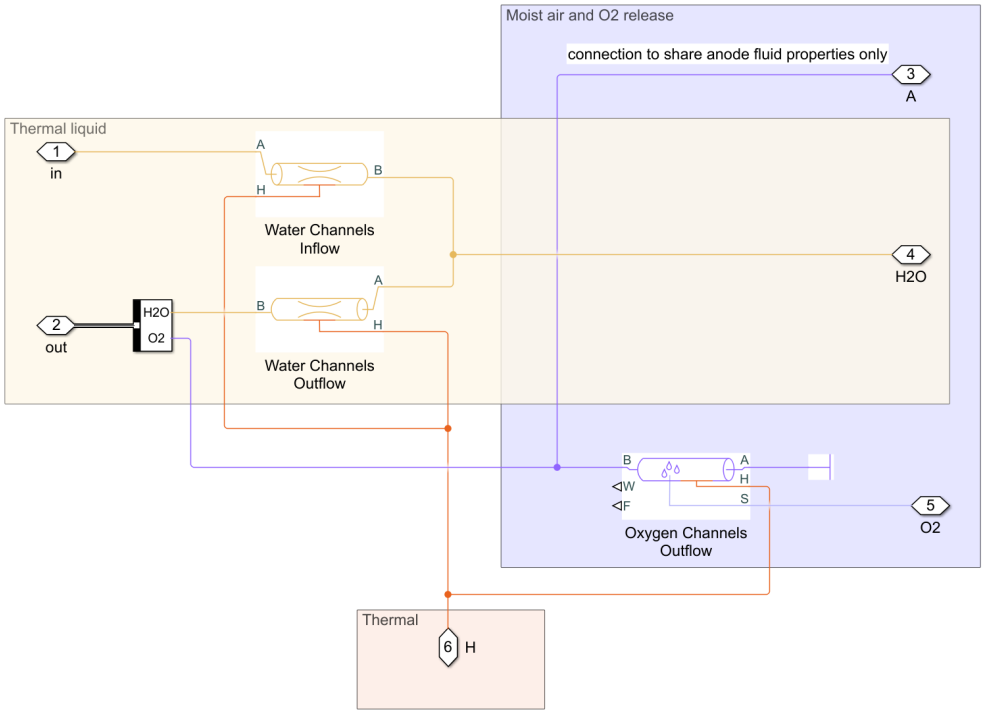

Figure 4.5: Anode Fluid Channels.

4.1.3 Cathode Gas Channels

At the cathode side, there are no in-flowing fluids. The out-flowing ones are only gasses. Therefore the subsystem is named Cathode Gas Channels and it is only designed with moist air elements in Figure 4.6. We have the same structure as the oxygen production with a CAP as terminus, a pipe with the source "S" producing moist hydrogen and all this is flowing out the Cathode gas channels by the port "out".
The ports on the left are "C" for the cathode fluid properties, "H2" for the production of hydrogen and water vapor and "FC" for the internal states of the cathode gas channels. We have below the thermal output for the pipe and at the right port, we have moist air going to the dehumidifier.

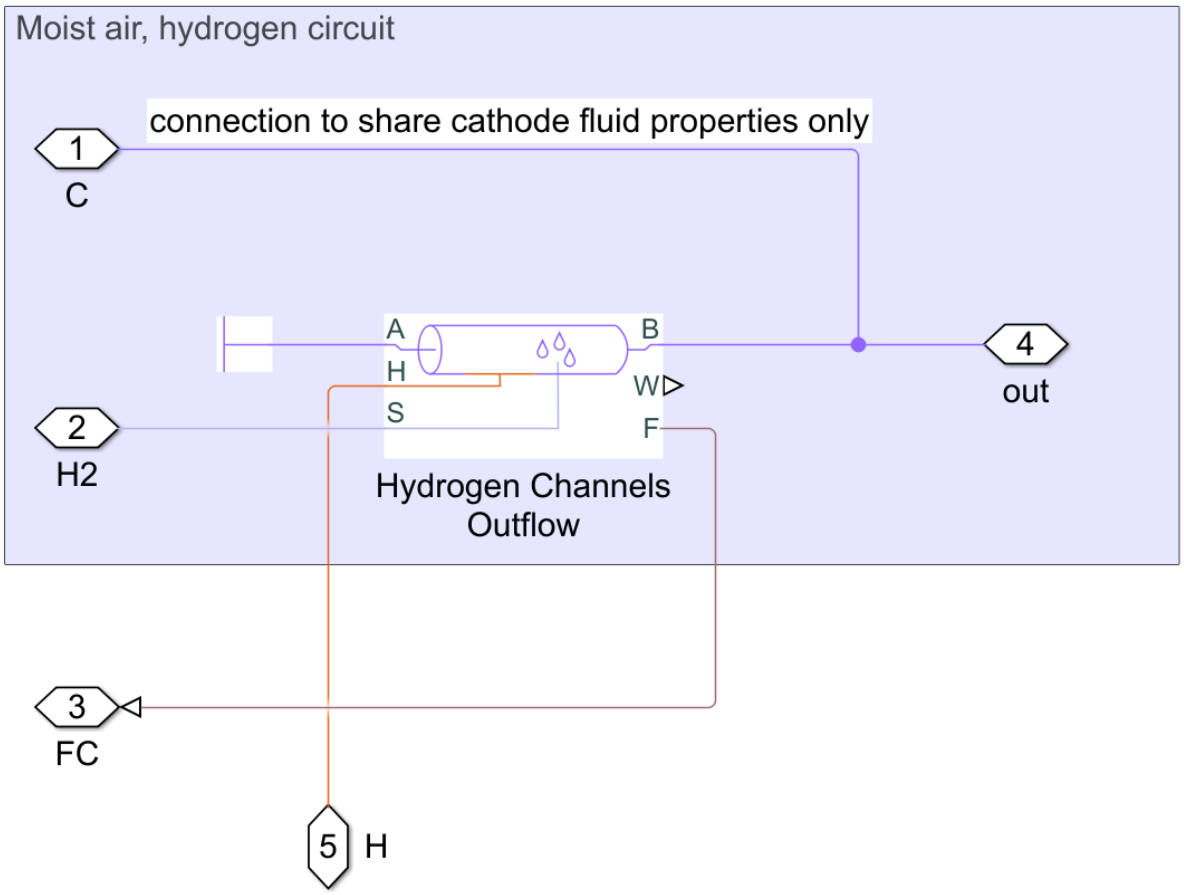

Figure 4.6: Cathode Gas Channels.

4.2 Balance of Plant

The operation of the stack requires subsystems to provide and manage the needs of the electrolyser. These components are collectively known as balance of plant (BoP). The balance of plant will mainly be constituted by the water (and oxygen) circuit, the hydrogen circuit and the thermal circuit. Each circuit can be composed of circulating pumps, heat exchanger, pipes, reservoirs, dehumidifiers, compressors...

4.2.1 Water circuit

The water circuit feeds the electrolyser stack with reagents, does the thermal regulation of the stack by circulating the water and rejects the oxygen produced in the atmosphere. The rejection is not required and oxygen can also be valued, however many electrolyser designs simply reject the oxygen produced.

Water supply

The water supply subsystem (Fig. 4.7) is composed of a reservoir and a pump. The water properties are given by the block with the same name. The mass of circulating water by the supply pump is controlled by a control chain and a max flow gain that converts a control input between 0 and 1 to the command in kg/s. The control chain for the supply pump is based on a PI controller with the parameters in Table 4.1 and a delay block. The only input of this subsystem is the port "L_tank" that gives the water level in the separator tank. The supply pump is therefore ensuring there is always enough water in the water circuit.

Controller	Proportional gain (P)	Integral gain (I)
Water supply	-100	0.001

Table 4.1: Water supply controller gains.

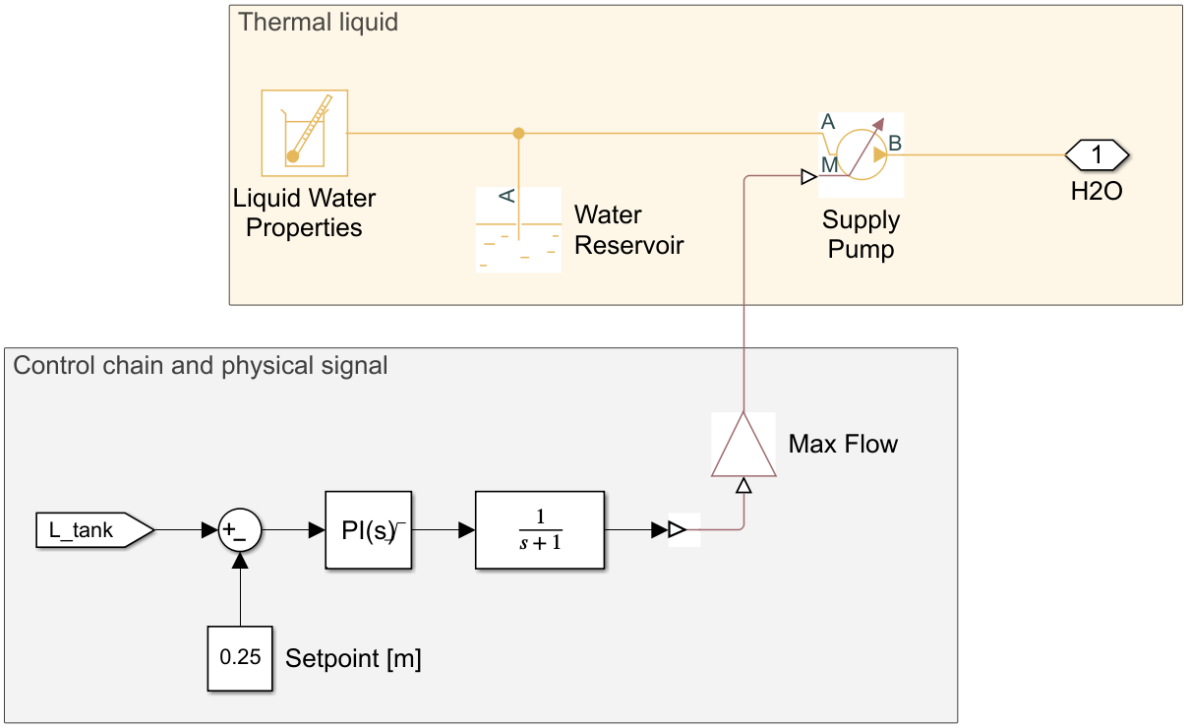

Figure 4.7: Water supply.

Recirculation

The recirculation subsystem (Fig. 4.8) includes as input, the ports "A" which is the water from the water supply subsystem, the port "R" which is the water coming from the electrolyser and the oxygen produced not mixed, and the temperature of the stack as an

information for the thermal regulation.
The circulation pump is controlled by a control chain in order to regulate the stack temperature. The control chain is provided by a PI controller with the parameters in Table 4.2 and a delay. The "Max Flow" gain allows it to go from a 0 to 1 command to a [kg/s] command with the max flow equal to the gain.

Controller	Proportional gain (P)	Integral gain (I)
Recirculation	1	0.1

Table 4.2: Recirculation controller gains.

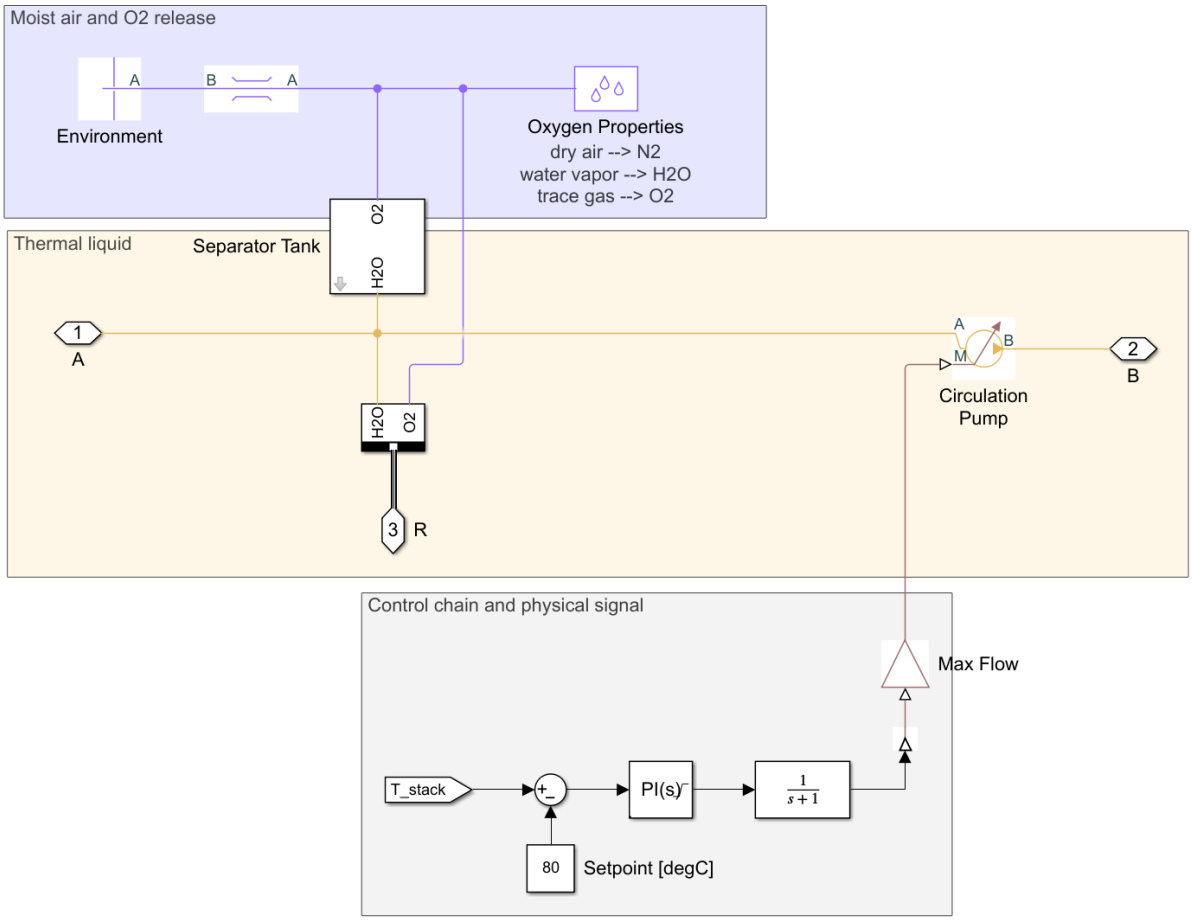

Figure 4.8: Recirculation.

The separator tank would probably be the physical manner to separate the excess dissolved oxygen in the water coming from the electrolyser. The principle is to release the pressure in order to separate, operating on the principle of density, the two components: gas on top, and water at the bottom.
In this model, the separator tank is more a sort of measurement tool to control the

supply pump as we will discuss below.
For the oxygen, we have the block properties to set the physical properties of O_2, H_2O and N_2. We have a link with the separator that works like a measurement and we find a flow resistance before rejecting the gas into the environment. A flow resistance represents a generic pressure loss in a moist air network.

Separator tank

The separator tank is a mask for a subsystem. The separator is available in Figure 4.9. This consists of two Translational Mechanical Converters (one for thermal liquid causing positive force and the other for moist air causing negative force) and a Ideal Translational Motion Sensor. The idea is to compute the difference of pressure of the fluids to be sure that there is enough water in the circulating water circuit. If the mechanical force is low, it means that there is a need for more water in the circulation circuit.

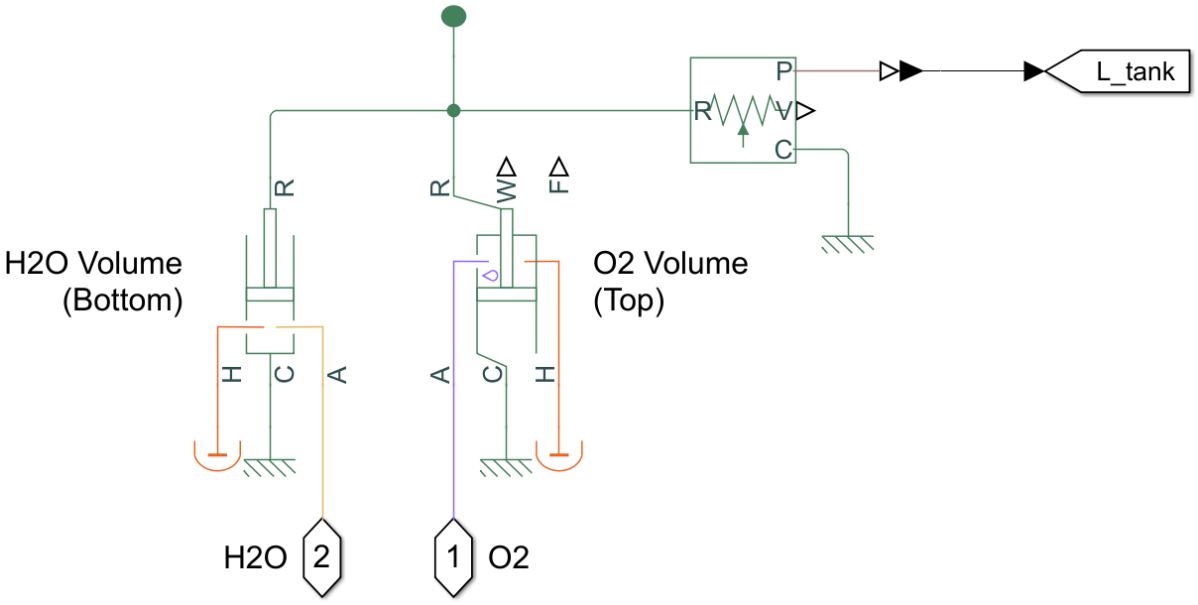

Figure 4.9: Separator tank.

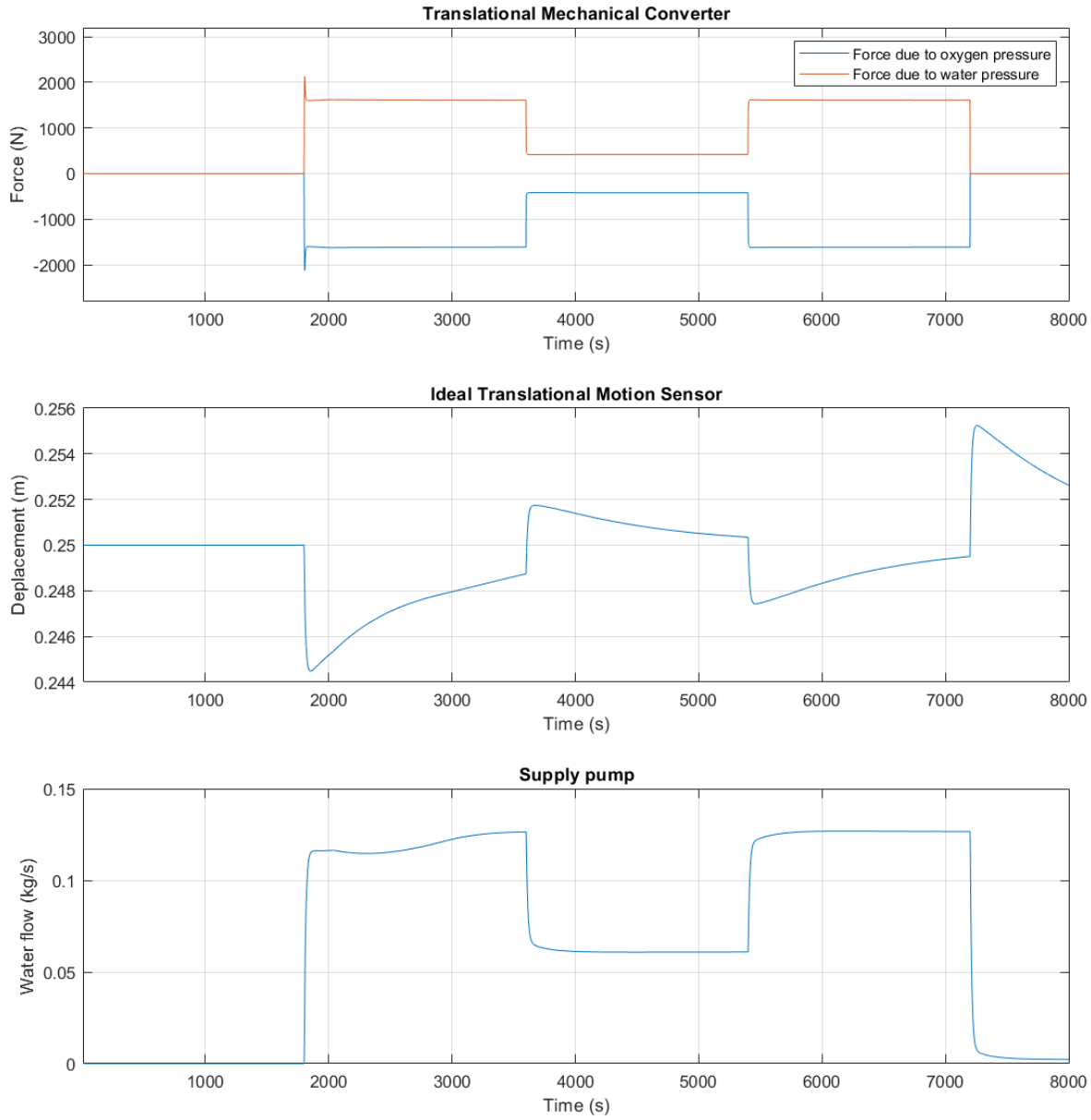

Figure 4.10: Separator tank analysis from 5.2. From model.

Heat exchanger

The heat exchanger subsystem (Fig. 4.11) represents the loss of thermal power in order to regulate the temperature of the thermal circuit. A pipe named "Heat Exchanger" is cooling the thermal liquid with the environment through the Convective Heat Transfer block. This Convective Heat Transfer block implements the heat transfer coefficient of the interface area of the Heat Exchanger with the ambient. The subsystem does not

have any control or variable because it is the circulating pump that adapts its flow in function of the temperature of the stack in order to maintain 80°C.

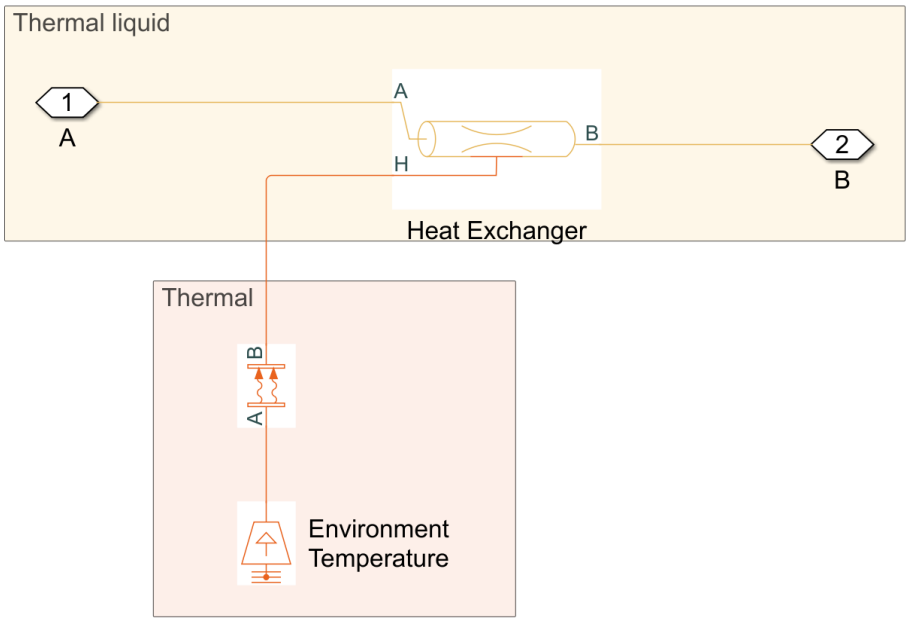

Figure 4.11: Heat exchanger.

The maximum heat flow of the heat exchanger in Equation 4.23 is based on the parameters of Table 4.3 at 80°C.

$$\dot{Q}_{\text{exch}} = U \cdot A \cdot (T_{353.15K} - T_{amb}) = 2MW \tag{4.23}$$

Parameter	Value
Heat transfer coefficient (U)	300 [W/Km^2]
Overall radiator length	1 [m]
Overall radiator width	0.3 [m]
Overall radiator height	0.5 [m]
Number of coolant tubes	25
Height of each coolant tube	0.0015 [m]
Fin spacing	0.002
Fin efficiency	0.7
Equivalent heat transfer area (A)	111.8 [m^2]

Table 4.3: Heat exchanger parameters.

4.2.2 Hydrogen circuit

The hydrogen circuit begins after the hydrogen production and the outflow of moist hydrogen from the cathode. The hydrogen circuit serves to remove the water from the hydrogen, maintain constant pressure at the cathode and depressurize at output.

Dehumidifier

The first subsystem of the hydrogen circuit is the dehumidifier in Figure 4.12. The two ports of the subsystem are the input port "A" of moist hydrogen and the output port "B" of dry hydrogen.
The "Dehumidifier Pressure Loss" flow resistance implies a loss of pressure in order to isolate the dry gas from the cathode gas channels and set up a one-way system. The dehumidifier volume represents a drying column. The dehumidification is done at 99.9% ("Fraction Removed") thanks to the moisture remover that is a controlled moisture source consuming the negative gain times the measure of moisture. It is more a modeling trick than the real manner to model the dehumidification.

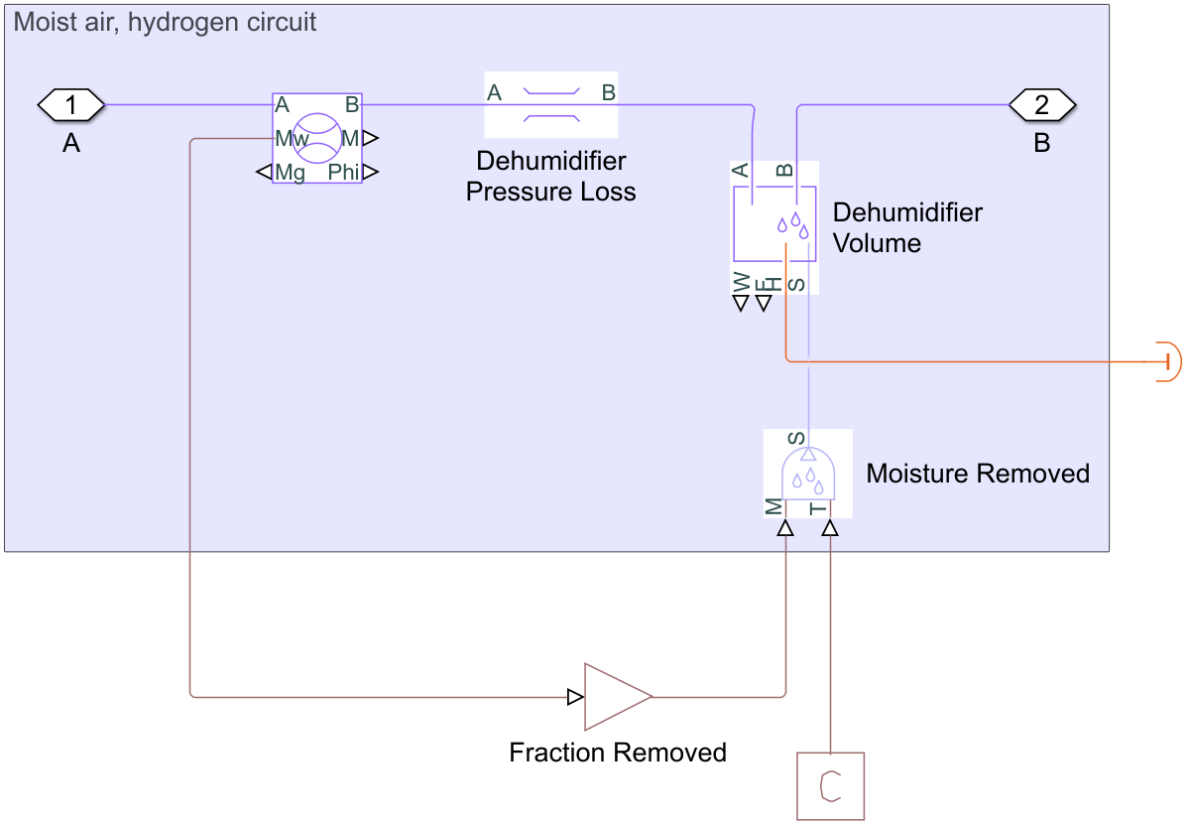

Figure 4.12: Dehumidifier.

Hydrogen output

The hydrogen output subsystem (Fig. 4.13) is composed of a pressure regulator, a pipe and the hydrogen reservoir as a way out. The hydrogen properties are given by the block with the same name. The pressure of hydrogen at the electrolyser side (port "H2") is regulated by the pressure regulator controlled by a control chain and a gain. The control chain for the supply pump is based on a PI controller with the parameters in Table 4.4 and a delay block.

Controller	Proportional gain (P)	Integral gain (I)
Hydrogen circuit	0.1	0.1

Table 4.4: Hydrogen circuit controller gains.

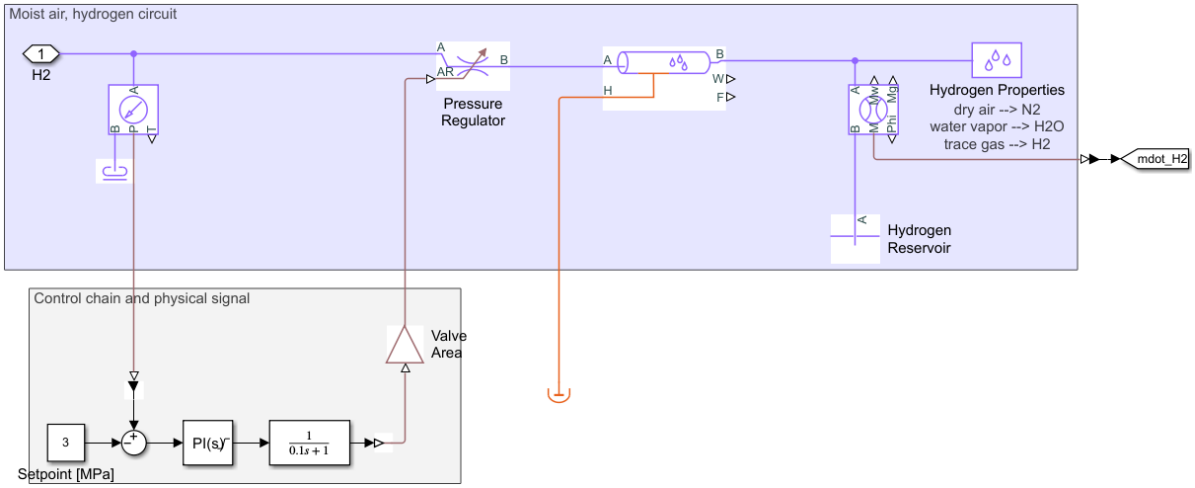

Figure 4.13: Hydrogen output.

4.2.3 Thermal circuit

The thermal circuit makes the thermal modeling for the system. In the MEA code, we have the heat generated by the electrical losses $\dot{Q}_{\text{gen}}$. The thermal circuit is composed of the heat generation connected to the MEA thermal mass that is a capacitance as explained in 3.3.1. The circuit is also connected to the pipes from the electrode fluid channels that represent the heat exchange with the circulating fluids. In 3.35, we have the different aspects of thermal modeling. For the loss with the ambient, the model could take the following form.

$$\dot{Q}_{\text{loss}} = \frac{1}{R_{th}}(T_{stack} - T_{amb}) \tag{4.24}$$

In the original model there is no thermal resistance between the stack and the ambient (can be understood as $R_{th} = \infty \rightarrow \dot{Q}_{\text{loss}} = 0$). A loss could be easily implemented if it

becomes necessary but requires data on the equivalent thermal resistance of the stack. The thermal model becomes therefore:

$$T_{\text{stack}} = T_{\text{stack},ini} + \frac{dt}{C_t}(\dot{Q}_{\text{gen}} + \dot{Q}_{\text{cool}}) \tag{4.25}$$

Where the initial temperature of the stack is the ambient temperature and is always considered as constant at 20°C. The only negative thermal flows are the heat flowing through the heat exchanger and the heat flowing out in the gas produced. The heat flow in the exchanger depends on the control chain that directs the water flow. The recirculation is controlled in order to maintain the stack temperature at 80°C. At steady state operation $\dot{Q}_{\text{gen}} = \dot{Q}_{\text{cool}}$ where $\dot{Q}_{\text{cool}} = \dot{Q}_{\text{exch}} + \dot{Q}_{\text{gas}}$.

Measurements

The subsystem in thermal output zone in Fig. 4.1 is represented below and allows the measurements of the electrical power transformed in heat and the temperature of the stack.

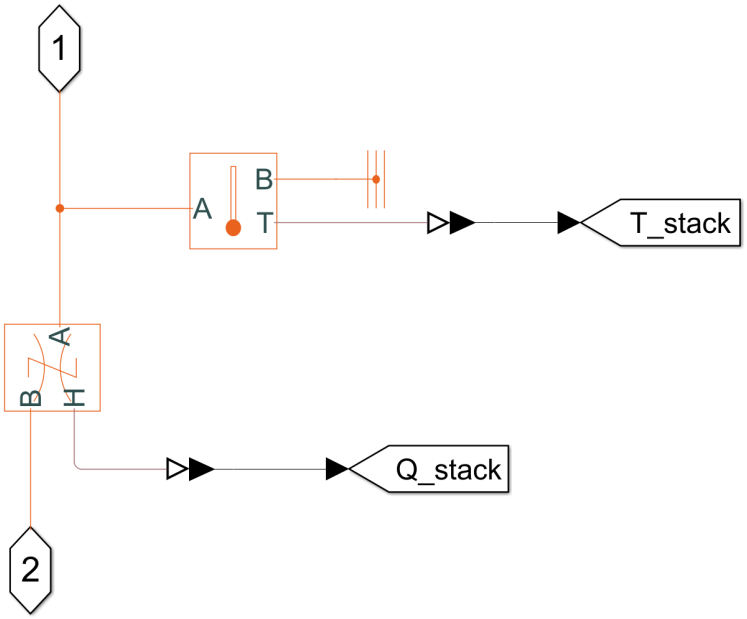

Figure 4.14: Thermal measurements subsystem.

4.2.4 Electrical supply of the balance of plant

The balance of plant does not require modeling of electrical supply. The different blocks of the libraries do not require power but just a command. With Simscape, the mechanical power consumption of the pump or compressor is given. This will be taken into account later for the efficiency calculations.

4.3 Electrical supply

The best electrical supply for an electrolyser is a DC current source. In this model, we use simply a controlled current source that generates the wanted current to supply power to the electrolysis system. Different types of scenarios will be applied to the power supply in the next chapter.
During the running of the model, applying square currents could cause problems to the solver. Moreover, the stack model used to be static and not dynamic. For these purposes, the current profile comes from a model of electrolyser based on the dynamic electrical equivalent model in Figure 4.15. This allows the current in Figure 4.16 to be closer to reality[2]. Table 4.5 gives the parameter of the equivalent circuit.

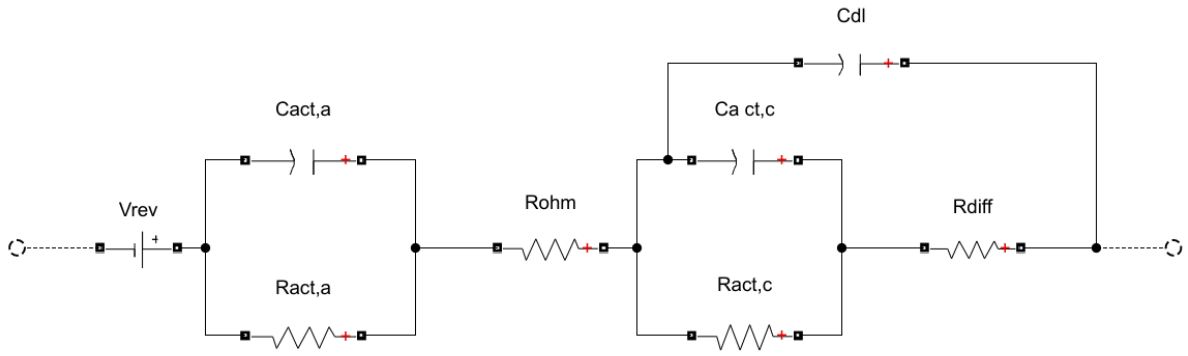

Figure 4.15: Equivalent circuit of the electrolyser.

Vrev	1.4 V
Ract,a	0.12 Ω
Cact,a	4.1 F
Rohm	0.3818 Ω
Ract,c	0.0132 Ω
Cact,c	4.1 F
Cdl	0.5455 F
Rdiff	0.3318 Ω

Table 4.5: Value of the equivalent electrolyser cell parameters.

[2]The time constant and the different resistance are not varying according to the current or other parameters, further analysis could be required but will not be done in the scope of this work.

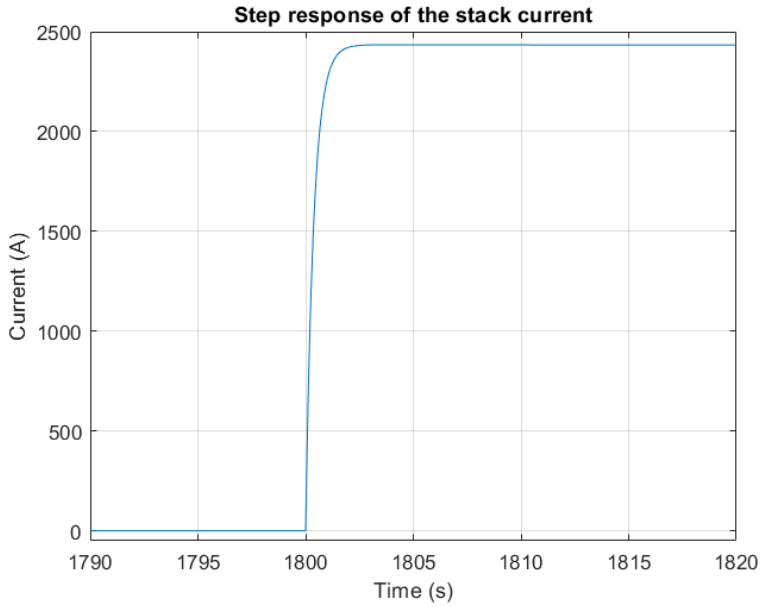

Figure 4.16: Stack current response to step power command.

4.4 Modifications

4.4.1 Modification of the MEA code

Dynamics of electrochemical model

The first idea for the modification of the MEA code was to add the capacitive behaviour of the electrochemical model. The idea is to use one of the model developed in the dynamic approach in section 3.1.3. The problem is that it is not possible to have this kind of non-linear resistance varying according to the temperature, the pressure, the current density... Therefore it was not implemented in the MEA to model. The electric dynamics are implemented in the electrical supply part in order to be able to model the rest of the electrolyser as close as possible to reality.

Electrochemical model

The electrochemical model is very close to the analysis made independently in chapter 3. Some modifications were necessary in order to reach the model described. These modifications are minor and are described directly in the stack model in 4.1.1.

4.4.2 Upscaling of the electrolyser system

The original electrolyser model is able to reach up to 140kW. Many manufacturers are able to build a basic unit of 1MW which is scalable in order to reach bigger power. This can be seen as the current state of the industry [81]. The objective of the study is therefore to develop a 1MW electrolyser by scaling up the model. There are different

ways to scale up the model. From the stack point of view, it is constituted of different cells electrically in series. The number of cells is therefore linearly correlated to the nominal power (for DC power in static mode, we assume only the resistivity of the cell). The size of a cell has also a big influence. The bigger the cell, the higher the production of hydrogen and power consumed.
The power of the stack is a function of the current. We generally express it in current density. To increase the nominal power we can increase the nominal current. PEM can reach high current densities and have improved the nominal current densities over the years. For this design, the current density of 2.3A/cm^2 is chosen as it is about the state of the art in Table 2.5.
The area of a cell is 1000 cm^2. It represents a square with sides of about 31 cm. This is quite a big cell compared to electrolysers in the literature since no large scale studies were found.
The number of cells in series allows to scale up the voltage. With 250 cells we can reach 1MW at nominal power.
The biggest difficulties during the scale up was not to find the adequate parameters but to scale up the pipes, the pumps and the compressor dimensions.

4.4.3 Minor modifications

Thermal Mass

The thermal mass is the heat capacitance consisting of the MEA storing heat. The mass and the specific heat of the MEA was given by the membrane and the diffusion layers. It did not include the bipolar plates, the microporous layers and the catalyst layers. From the study of Yang et al. [79] working on a fuel cell, we can find a table with the cell properties that allows us to compute a new mass and specific heat to represent the Thermal Mass in Table 4.6. As a reminder, the thermal capacitance can be computed as

Thermal mass	Overall density ρ_{MEA}	Overall specific heat c
Membrane Electrode Assembly	1051 kg/m^3	1552 [J/(kg K)]

Table 4.6: Thermal mass properties of the cell.

follows:

$$C_p = c \cdot m_{MEA} \tag{4.26}$$

where c is the specific heat and m_{MEA} is the mass which is obtained with:

$$m_{MEA} = \rho_{MEA} \cdot A \cdot (t_{mem} + t_{gdl,A} + t_{gdl,C} + t_{CL}) \cdot N_{cell} \tag{4.27}$$

Pressure

The output pressure is set at 3MPa in the original project. The pressure for large scale electrolysers is generally higher in order to have high pressure hydrogen that is easier to store.

We can adapt the set point to have a higher pressure (for example on 13MPa, which is still quite low). It leads to a higher delay at hydrogen output because the pressure must increase longer before starting to let the hydrogen out. Some tests were performed at 13MPa, but the pressure rating remained at 3MPa for the operating point.

4.4.4 Degradation

The manufacturer usually limits the control system to avoid an excessive power supply dynamic which would imply accelerated cell degradation. This limit may be binding [80]. In the dynamic study we cannot restrict ourselves to this type of limits and we will therefore have to study the effect of the dynamic behaviour on the cell and the degradation of it. From [25, 26] and Table 2.5 we have that the global degradation of the cell is about 0.2%/1000hrs. Unfortunately, No in-depth studies have been conducted on the link between the degradation of the electrolyser MEA and its dynamic behaviour. One thing we can say is that the fact that the pressure and the temperature are kept constant is a good thing. We will not go further for degradation analysis since we can not make any link with the dynamic behaviour.

4.5 Final electrolyser and model

In Table 4.7 we can find a summary of the main information about the electrolyser that we will use.

Technology	PEM
Nominal power	1MW
Number of stacks	1
Number of cells per stack	250
Area of one cell	1000cm^2
Nominal production of hydrogen	200Nm^3/h
Nominal current density	2.3A/cm^2
Nominal temperature	80°C
Nominal hydrogen pressure	3MPa
Operating range	10%-100%

Table 4.7: Technical specifications of the Matlab model.

Annex B shows the parameters of the Matlab Simulink Model.

Chapter 5

Validation

This part will help to defend and convince the reader of the merits of the model. Unfortunately, the lack of access to real world equipment forces us to remain at the level of mathematical modeling without being able to compare the model to an actual electrolyser. The validation will therefore be done by comparing our simulation results with experimental results found in the scientific literature.

5.1 Static analysis

A good static run is essential to verify that the model works before moving on to dynamic analyses. This section therefore focus on the validation of the static point of view. Four points are discussed: voltage modeling, thermal model, mass transfer across the membrane and electrolyser efficiency. In this analysis bellow, the nominal operating point is 80°C and 3MPa. However, it can sometimes move, so if it differs, it will be mentioned.

5.1.1 UI characteristic

This static result implies that the measure is done for a stable state of the system. The voltage of the cell must be evaluated for the same parameters of temperature and pressure. In order to compute the voltage in function of the current, one applies a ramp current density from 0A/cm^2 up to the nominal current around 2.3A/cm^2. This test is done for 80°C and for 13MPa in Figure 5.1.

The voltage of the model is given by the electrochemical model in Equation 5.1. This model is a good representation of the operation of an electrolyser and depends on its parameters.

$$E_{cell} = \underbrace{E^0_{rev} + \frac{RT}{nF}\ln\left(\frac{P_{H_2}\cdot\sqrt{P_{O_2}}}{a_{H_2O}}\right)}_{\text{Nernst potential}} + \underbrace{\frac{I\cdot l}{A\cdot\sigma_{\text{PEM}}}}_{\text{Ohmic overpotential}} + \underbrace{\frac{RT}{n\alpha^* F}\ln\left(\frac{\frac{I}{I_0^*}}{1-\frac{I}{I_{lim}}}\right)}_{\text{Activation and diffusion overpotential}} \tag{5.1}$$

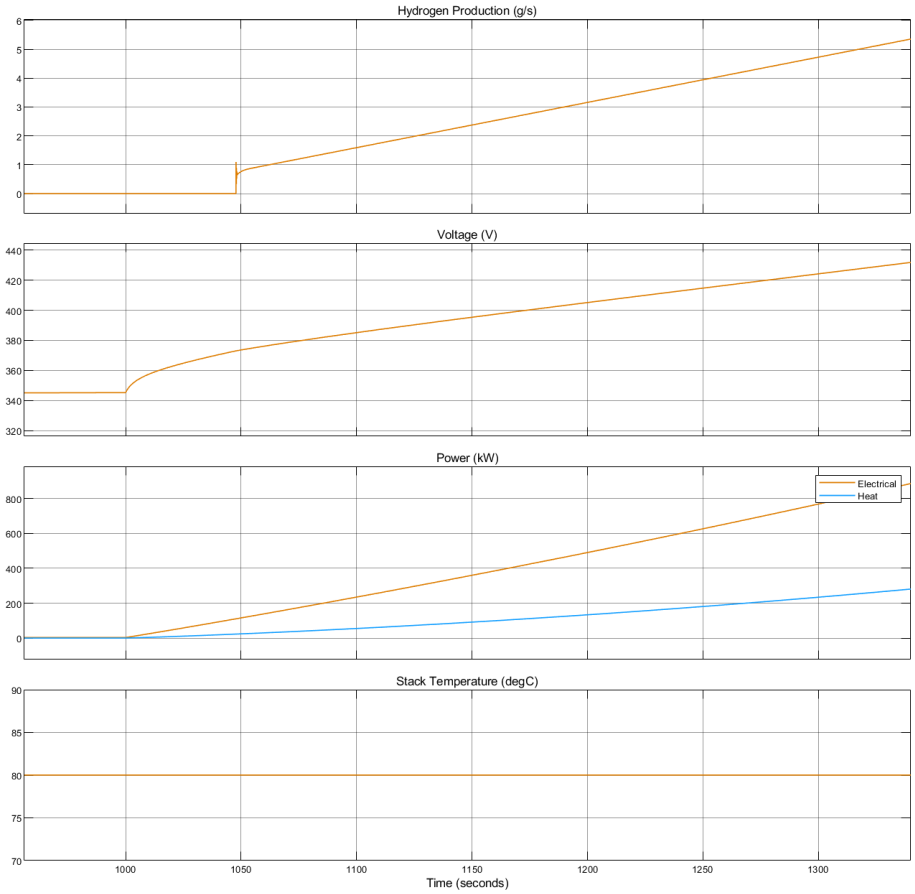

Figure 5.1: Ramp current test in order to evaluate the voltage as function of the current density for 80°C and 13MPa. From model.

Where the parameters in Table 5.1 can be empirically identified in order to fit to any electrolyser. These parameters are quite simplified since α^*, I_0^* are defined as constant but could be dependent on the temperature in order to be even more precise. Such precision is not relevant since we have no empiric electrolyser results to compare to.

Parameter	Value
E_{rev}^0	see Eq. 3.6
l	125 μm
A	1000cm^2
σ_{PEM}	see Eq. 3.12
α^*	0.5
I_0^*	$8 \cdot 10^{-5}$ A/cm^2
I_{lim}	9.4 A/cm^2

Table 5.1: Electrochemical model parameters.

The UI curves represent the cell voltage in function of the current density in Figure 5.2

at 13MPa for different temperature.

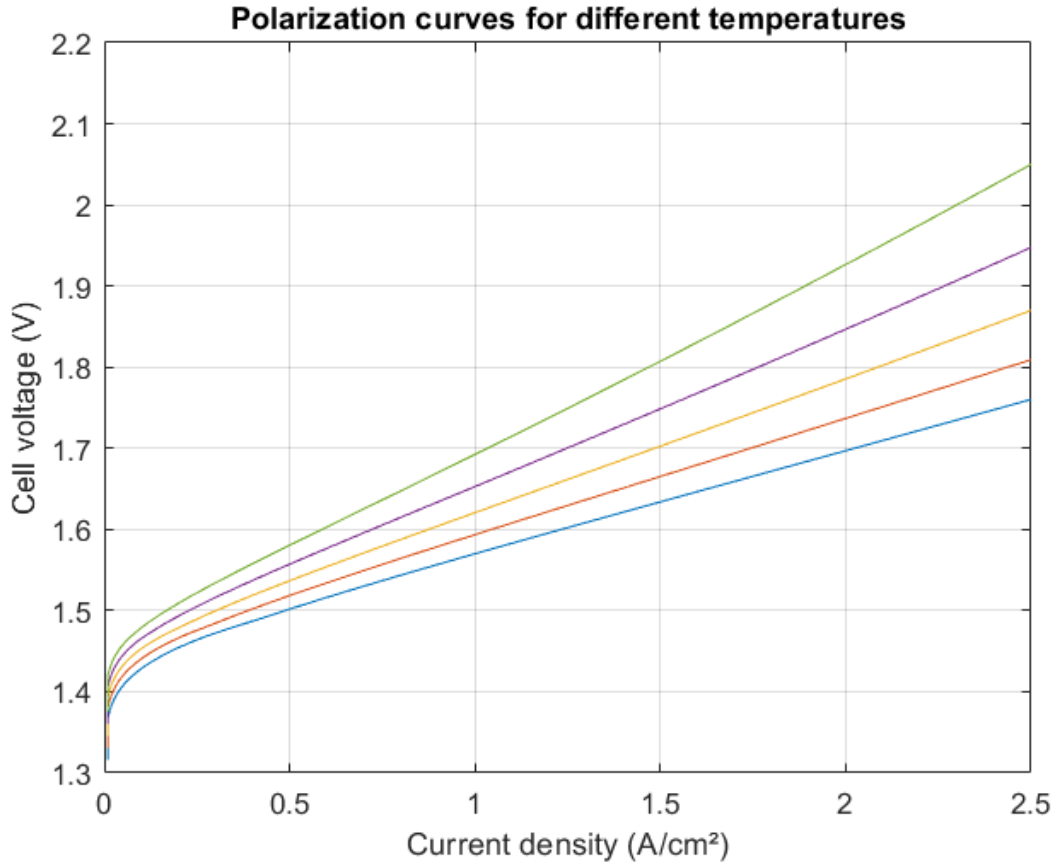

Figure 5.2: U-I characteristic for different temperatures at 3MPa. From model.

When comparing the curves from Figure 5.2 to the curves from the literature in Figure 5.3, the results obtained by the model are globally similar. The temperature of the stack (80°C) is within the highest temperature values for low temperature electrolysers. A high temperature reduces the Nernst potential but mainly decreases the slope of the ohmic overpotential and increases the efficiency of the process. In Figure 5.3, we see static analysis found in 4 different papers. We can see that we are in the right range to simulate the PEM stack characteristics.

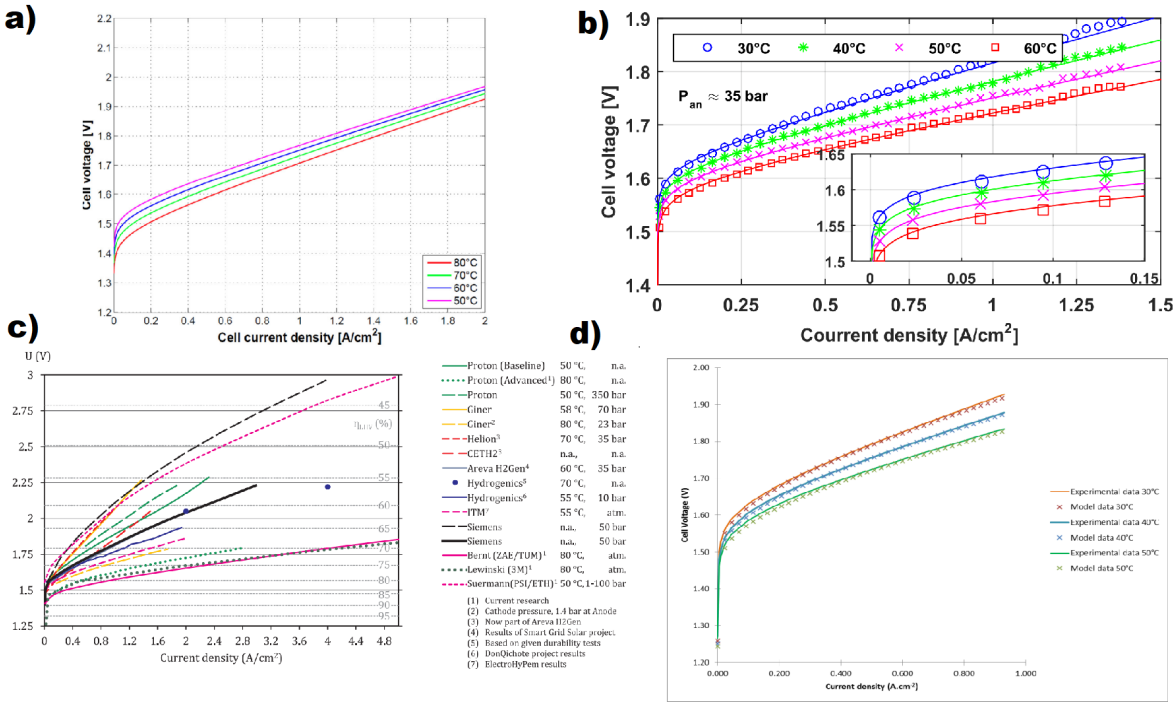

Figure 5.3: 4 polarization curves analysis from [20, 21, 22, 23].

We see that the low current density voltage can be considered as undervalued compared to some electrolysers. In this case, the activation overpotential is undervalued and it can be modified according to the parameters α^* and I_0^* in Table 5.1.

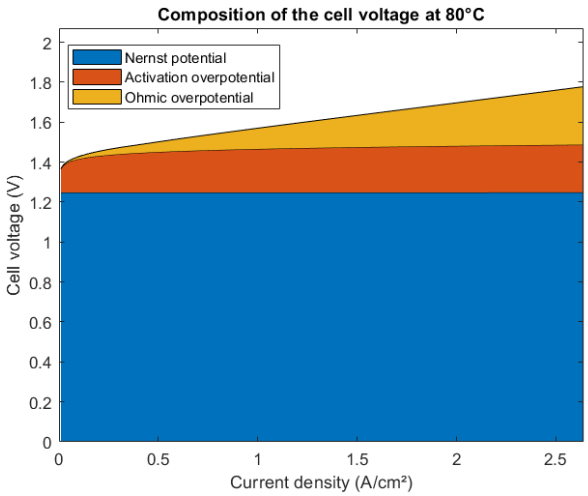

Figure 5.4: U-I characteristic composition at operating point. From model.

The Figure 5.5 shows the cell voltage according to the different voltage components. . When we compare the voltage composition at 80°C to the composition at 50°C we see

that the Nernst potential is somewhat lower for higher temperature and that the ohmic overpotential decreases significantly.

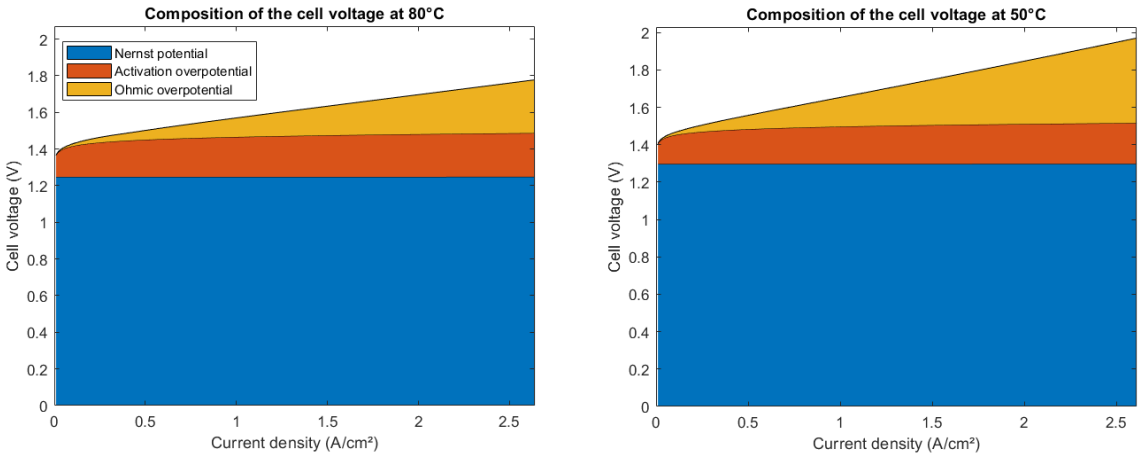

Figure 5.5: U-I characteristic composition at 3MPa for 80°C and 50°C. From model.

The pressure of the stack increases the Nernst voltage.

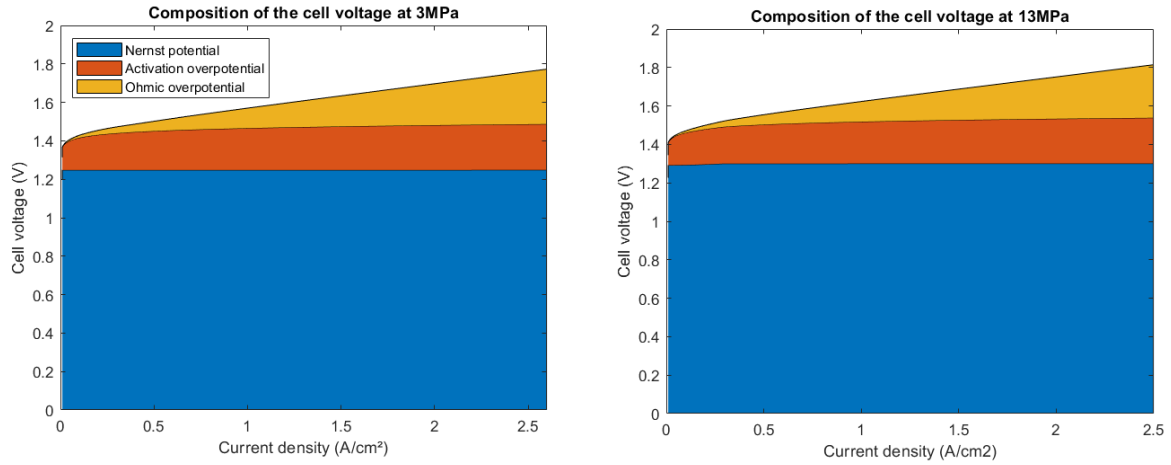

Figure 5.6: U-I characteristic composition at 80°C for 3MPa and 13MPa. From model.

5.1.2 Thermal analysis

The thermal model shows that heat is produced from electrochemical losses and that it is dissipated in the circulating water. The heat escapes the system from the heat exchanger in the circulation circuit. In order to compute all the different static analysis, we have placed a temperature source block to maintain 80°C whatever the heat production. The temperature source is an ideal energy source in a thermal network that can maintain a constant absolute temperature at the port regardless of the heat flow rate.
The thermal analysis can compare the power dissipated in the PEM stack by the losses in function of the current density. Figure 5.7 and 5.8 show the cell heat dissipation per mole from the model and literature.

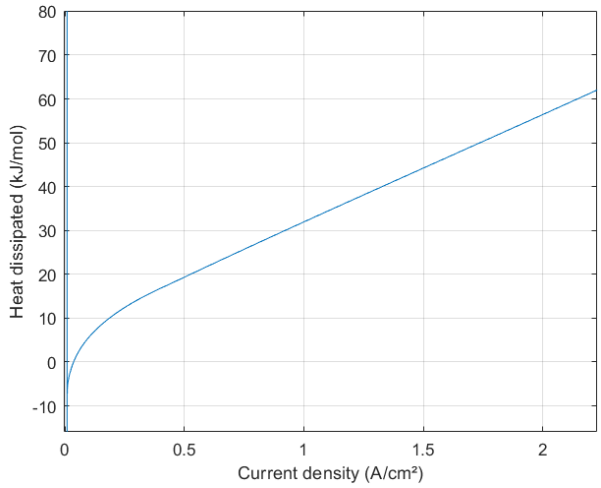

Figure 5.7: Heat dissipation per produced mole along different current densities. From model.

The two heat dissipation profiles are similar. At low current density, heat dissipation is negative, meaning that the cell absorbs heat from the surroundings. This is due to the high temperature of the stack[1]. When hydrogen production is low, the enthalpy change of the electrochemical reaction is higher than the electrical work. At high current density, a high increase in heat dissipation is to be expected.

[1]This cannot happen without the temperature source in our model because there is no heat provided to the stack.

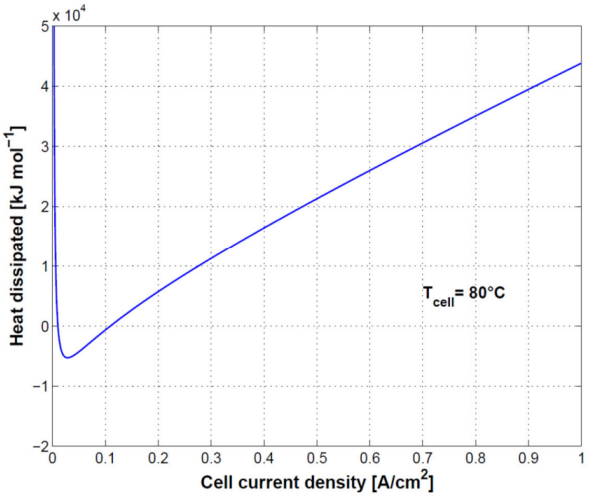

Figure 5.8: Heat dissipation by produced mole along different current densities. Taken from [20].

5.1.3 Mass transfer

The mass balance is represented in Figure 5.9. We observe that the sum of the mass of the products is equal to the consumed mass. We also see that the transported water mass across the membrane is due to the 3 phenomena described in 3.4.1.

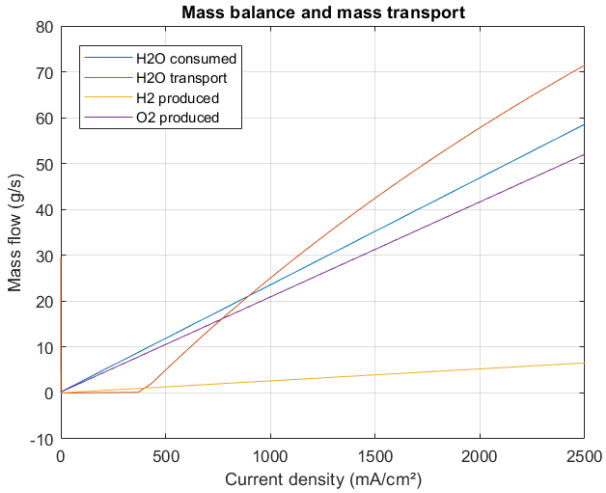

Figure 5.9: Mass balance and mass transport across the membrane. From model.

5.1.4 Efficiency

The efficiency can be computed from the HHV or the LHV according to the theoretical development in 2.2.2. Figure 5.10 represents the efficiency along different current densities. We can observe that high efficiency can reach values higher than 100% at low current density due to cell heat absorption and strongly reduces with the increase of current density by around 30% over the current density range of operation. Our results are close to the efficiency curves that we can find in the literature (Fig. 5.11).

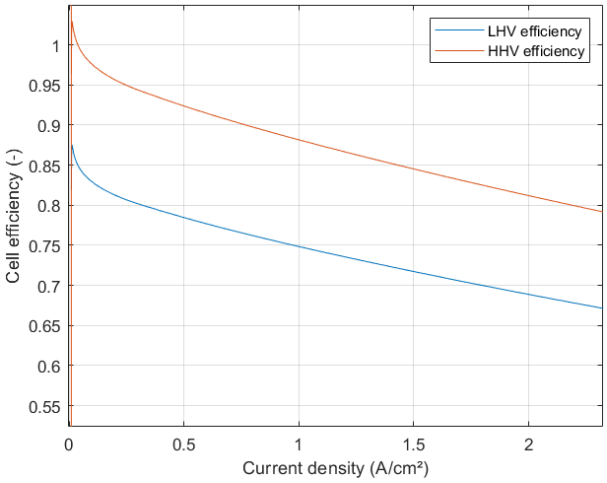

Figure 5.10: Cell efficiency curve along different current densities. From model.

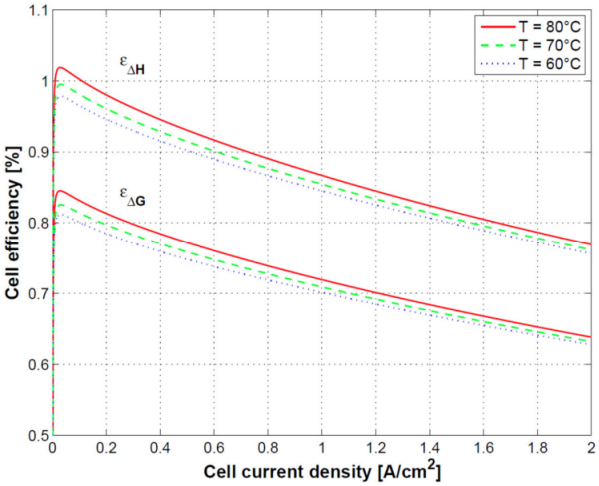

Figure 5.11: Cell efficiency curve along different current densities. Taken from [20].

5.2 Dynamic analysis

The dynamic behaviour of the electrolyser can be analysed with step responses. Three scenarios will be studied. A cold start from 0% to 100% of power, a ramp down from 100% to 50% and a ramp up from 50% to 100%. Figure 5.12 and 5.13 represent the applied current to the electrolyser and can be compared to the Figure 5.14 from the literature. Annex C shows the global behaviour of the electrolyser.

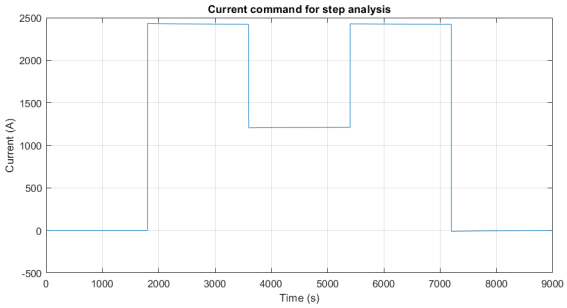

Figure 5.12: Current command for step analysis.

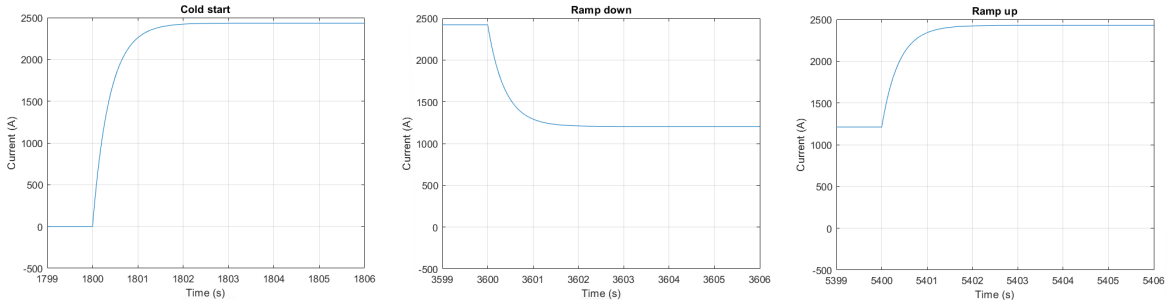

Figure 5.13: Current command for step analysis - Zoom.

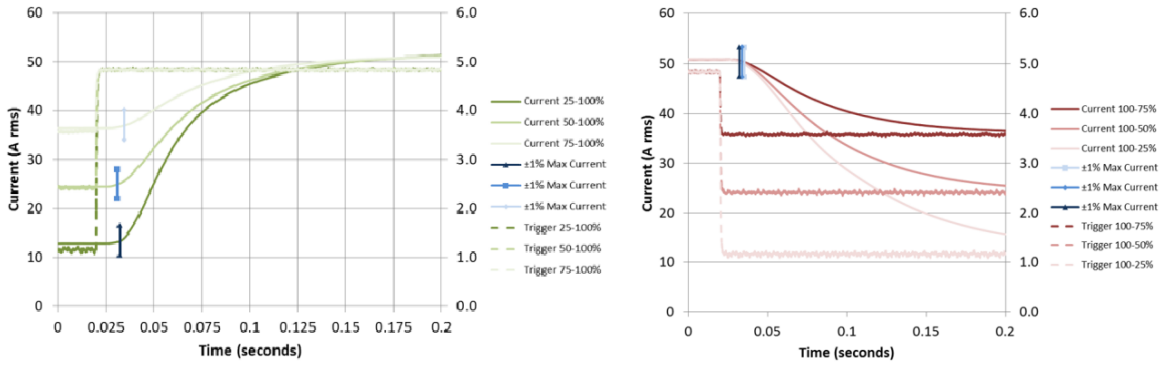

Figure 5.14: Ramp tests for PEM electrolyser. Taken from [24].

5.2.1 Cold start

Cold start occurs on the first execution of an inactive system. The electrolyser is powered from 0% to 100%. The stack temperature and pressure is considered equal to the ambient. Figure 5.15 is giving an overview of the cold start. We see the dynamic aspects. The higher power and voltage in the first seconds is due to the low temperature of the stack. The cell voltage stabilizes at 1.8V, the global power at 1060kW and the hydrogen

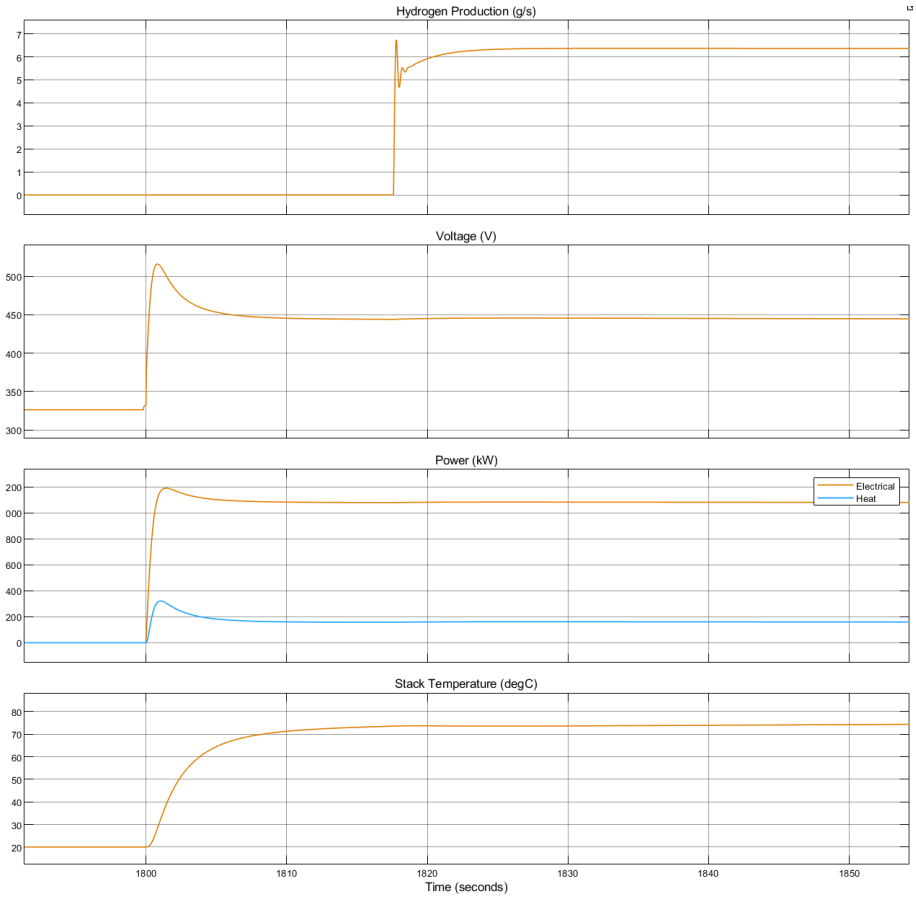

Figure 5.15: Cold start overview.

production around 6.3g/s. The temperature of the stack is regulated to prevent going above 80°C. The production energy for nominal power is 46,67kWh/kg or 4.2/Nm^3 so therefore it is about 71% for LHV efficiency.
We can see that there is a delay in the hydrogen production. This is due to the pressurization at the cathode side. Figure 5.16a shows the evolution of the pressure at the cathode. The increase is linear since the current and therefore the production is constant. When the cathode is at the wanted pressure, the pressure regulator starts to let pass the hydrogen gas to the output reservoir. We see a delay of 18 seconds before seeing hydrogen at the output. This delay is proportional to the volume of the pipes and may change in function of the design. The output gas is controlled by the PI controller that gives the particular response.

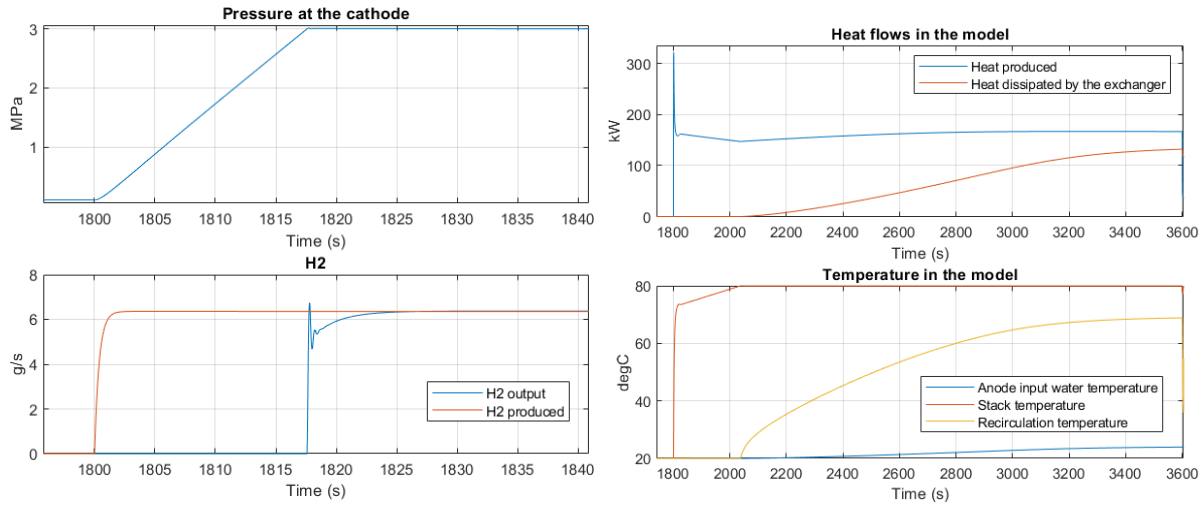

(a) Pneumatic analysis. (b) Thermal analysis.

Figure 5.16: Cold start analysis.

Figure 5.16b shows the heat flows and temperature in the electrolysis system. The water temperature in the recirculation circuit takes 30 minutes to reach its nominal value of 70°C. We see that the heat dissipation occurs proportionally to the recirculation temperature. The difference between the nominal produced heat and the nominal dissipated heat (at 3600s) is coming from the thermal flow of oxygen and hydrogen. The temperature difference between the anode input water temperature is the recirculation temperature is due to the heat exchanger and can be understood as the heat dissipated by the exchanger.

5.2.2 Ramp down

The ramp down goes from 100% of nominal power to 50%. We will see that the reactivity of the electrolysis design is really fast. Figure 5.17 presents an overview of the ramp down. We see that the temperature and the hydrogen output have a very fast reaction.

Figure 5.18 shows the cathode pressure, the hydrogen output and the different temperature. The response time of the pressure and the temperature of the recirculation water is lower than the output hydrogen and the stack temperature. But the pressure and recirculation water temperature deviations are low and do not represent a problem for the operating point. We can see the controllers dynamics in the hydrogen output and in the recirculation temperature.

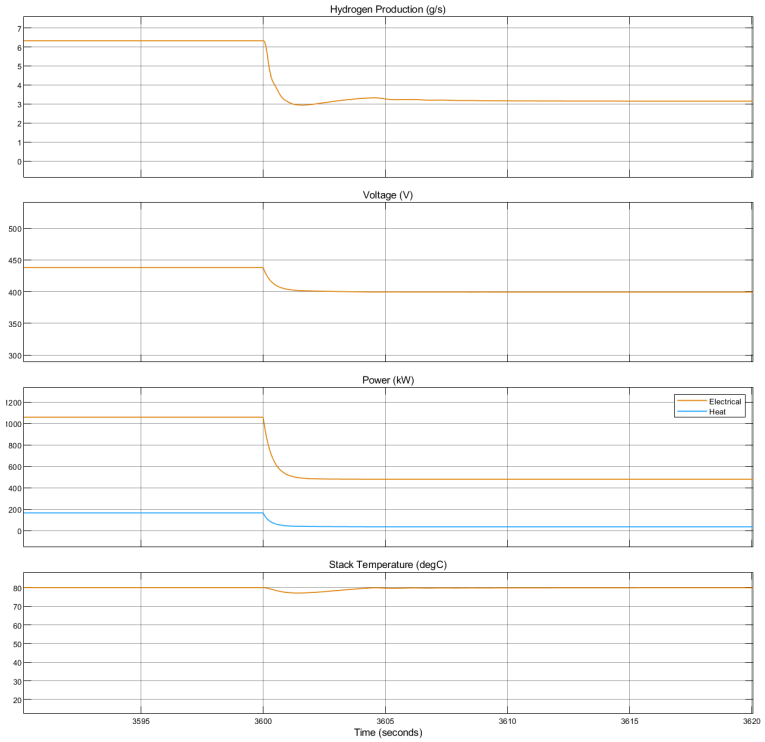

Figure 5.17: Ramp down overview.

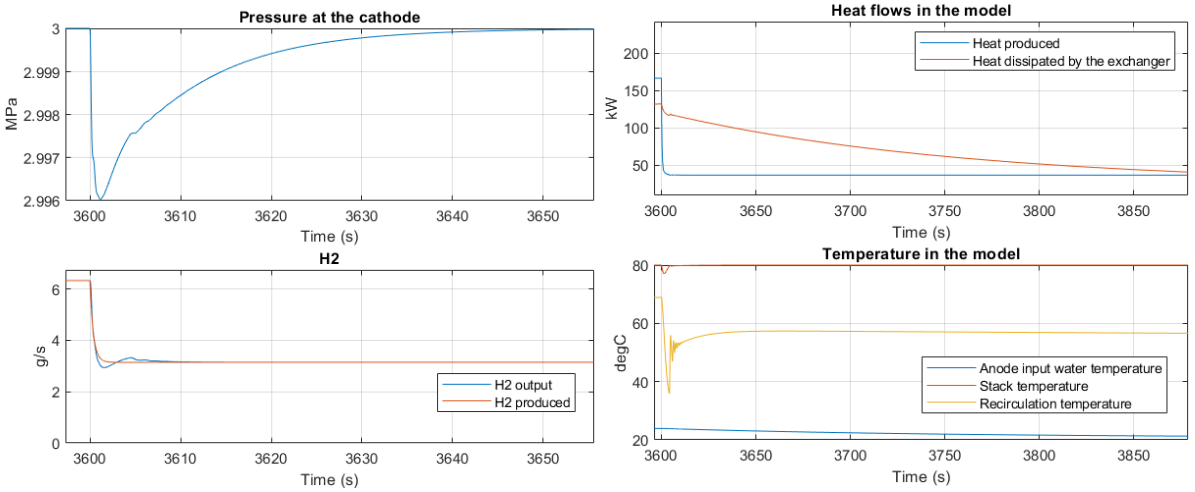

(a) Pneumatic analysis. (b) Thermal analysis.

Figure 5.18: Ramp down analysis.

5.2.3 Ramp up

The ramp up represents a rise in the power supplied to the electrolyser. Figure 5.19 is the overview of this increase of power. The situation is very similar to the ramp down.

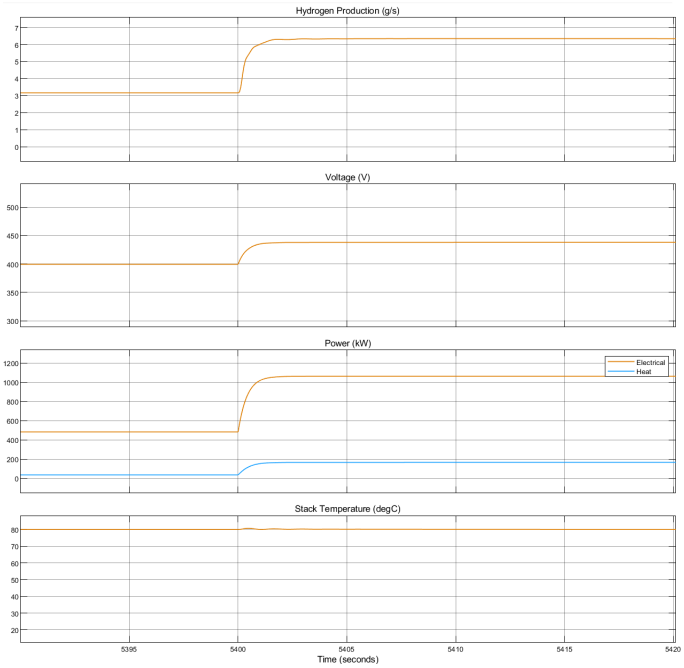

Figure 5.19: Ramp up overview.

Figure 5.20a shows the pressure and the hydrogen in the system and Figure 5.20b the temperature and the heat flows.

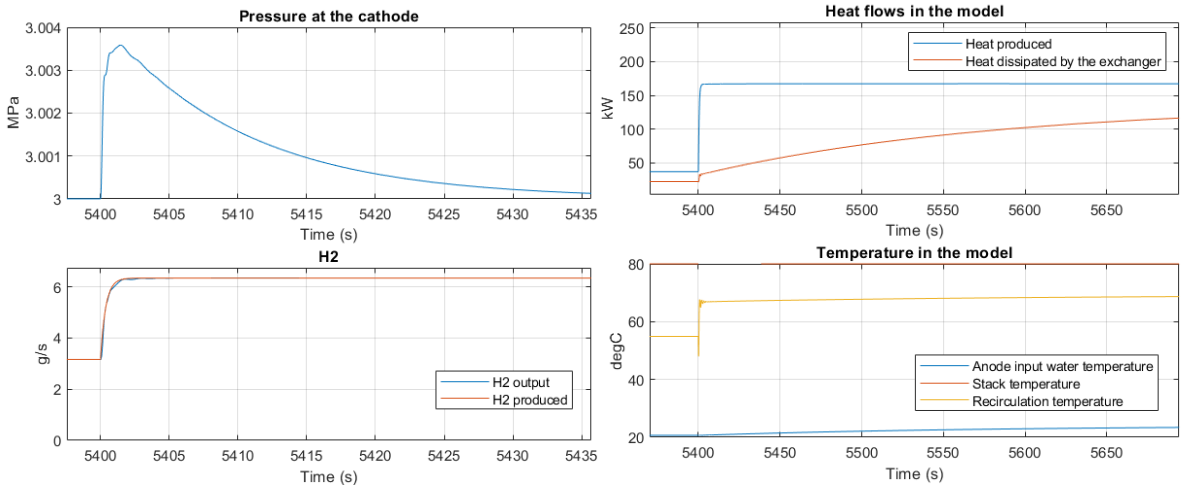

(a) Pneumatic analysis.

(b) Thermal analysis.

Figure 5.20: Ramp up analysis.

5.2.4 Time constants

Time constants are a fundamental issue in dynamic behaviour. To obtain them, we can for example analyze the step responses of the model. Table 5.2 shows the evaluated time constants.

Thermal

From the thermal perspective, we can evaluate the time constants of the stack and the heat exchanger. The stack time constant is evaluated with the thermal regulation. The heat exchanger time response is the response of the water circuit heating after a change in operating point.

Pneumatic

The pneumatics regulation is provided only by the pressure regulator and the parameters of the design. The response of the pressure regulator (hydrogen output) is quite fast and the pressure change at the cathode is slower. The time constant evaluated on the steps is 15 seconds.

Hydraulic

The biggest simplification is the purification of the cathode gas. The dehumidifier is constant[2] and instantaneous. This allows a continuous hydrogen flow at the output. On the anode side, there is no water recovery and since the anode gas is separated from the liquid water, there is no constraint on the gas release and therefore no time constants. For the water in the circulating circuit it is different. We can deduce two different time constants: the recirculation system and the water supply. Since the recirculation pump has to keep the temperature constant at the stack, it responds within the same time at the stack temperature. The recirculation time constant takes into account the heating of the water and the pump dynamics.

Electrical

The electrical and electrochemical time constants, i.e., and, are the very fast time constants. From the dynamic electric model, we find an electrochemical response lower than 0.5 second. The electrical converters making up the power supply are also fast with an electrochemical response lower than 0.1 second.

[2]implemented by an "Ideal Moisture Source", no dynamics

Definitions

- Heat exchanger: the thermal dynamic behaviour of the water in the recirculation circuit.
- Water supply: the water supply pump behaviour, commanded by its control chain.
- Recirculation water: the dynamic behaviour of the recirculation circuit water flow, including the thermal dynamic behaviour.
- Pressure at the cathode: the cathode pressure behaviour.
- Recirculation pump: the recirculation pump behaviour, commanded by its control chain.
- Thermal stack: the temperature of the stack, regulated with the recirculation circuit.
- Hydrogen output: the pressure regulator, commanded by its control chain.
- Dehumidifier: no dynamic behaviour for the purification and the dehumidification of the hydrogen. A static instantaneous module is used.
- Electric: the electric dynamic behaviour of the current source.
- Electrochemical: the electric stack behaviour.

Dynamic	**Evaluated time constant**
Heat exchanger	200s
Water supply	49s
Recirculation water	30s
Pressure at the cathode	15s
Recirculation pump	6s
Thermal stack	3s
Hydrogen output	1.2s
Dehumidifier	-
Electric	<0.1s
Electrochemical	<0.5s

Table 5.2: Time constants.

The biggest differences between Table 5.2 and Figure 5.21 is the method used. Pierre Olivier in [23] isolates the thermal time constant from the regulation system that implies longer timer constants. The operation of his electrolyser is very different since it needs compression "batches".

Dynamiques considérées		Constante de temps calculées ou évaluées (s)
Thermique	Stack	3000
	Séparateurs	3000
	Circuits recirculation	600
	Echangeur	75
	Circuit de froid	5
	Enceintes	400
Pneumatique	Séparateurs	3.55
	Colonne purification	25.82
Hydraulique Séparateurs		12.5
Electrique		Inférieur à 0.1 seconde
Electrochimique		Inférieur à 0.1 seconde

Figure 5.21: Time constant calculated or evaluated from the dynamics of the system. Taken from [23].

Chapter 6

Applying model to demand response

In the chapter below, we apply the electrolyser model to a real world problem. As mentioned in the title, the goal is to study the dynamic behaviour of large scale PEM electrolysers in a fast demand response perspective. So far we have a validated dynamic model. We will now test the model in a demand response perspective, for frequency services.
As we discussed in the introduction, this work is inspired by the techno-economic assessment work done by Arash E. Samani et al. in "Grid balancing with a large-scale electrolyser providing primary reserve". In the paper, 2017 data from the Belgian grid are used to provide FCR products. In this chapter we will apply these data to the model we have built.

6.1 One day in January 2017

Figure 6.1 represents the historical frequency data of the Belgian grid on 27/01/2017. The frequency tells us we have a mean under production of power but nothing surprising for the season.

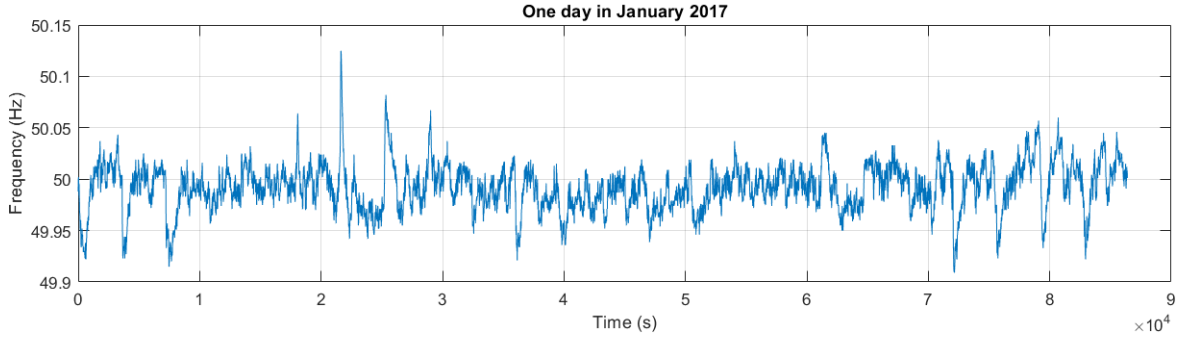

Figure 6.1: Belgian grid frequency during one day in January 2017.

Our electrolyser can help the grid by providing FCR. There are different FCR products

in Belgium. The 100 mHz product is the most profitable according to Arash E. Samani et al. [30]. Figure 6.2 shows the power–frequency chart of a symmetric 100 mHz product. The power input follows the frequency variation with the optimum baseload of 550kW with a reserve of 450kW. However, the primary reserve does not react within the first 10 mHz deviations from 50 Hz.

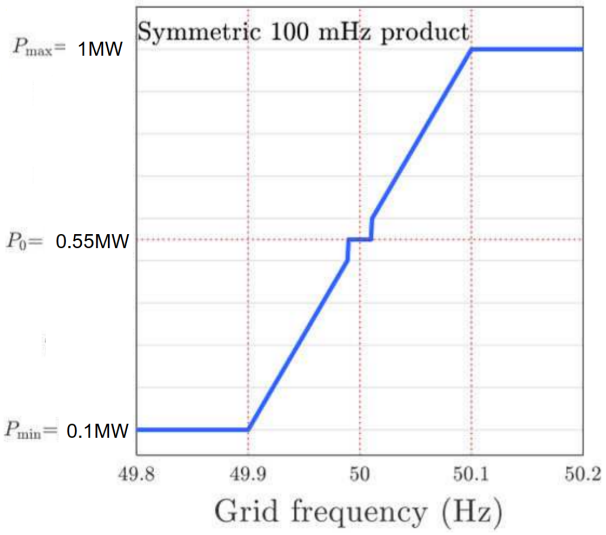

Figure 6.2: FCR symmetric 100 mHz product. Droop function.

If we apply the droop function to the frequency profile of the 27th of January we obtain Figure 6.3. We can see that the power command is limited to 1MW even if the frequency is above 50.1Hz and that there are stable frequency regions when the frequency is between 49.99Hz and 50.01Hz

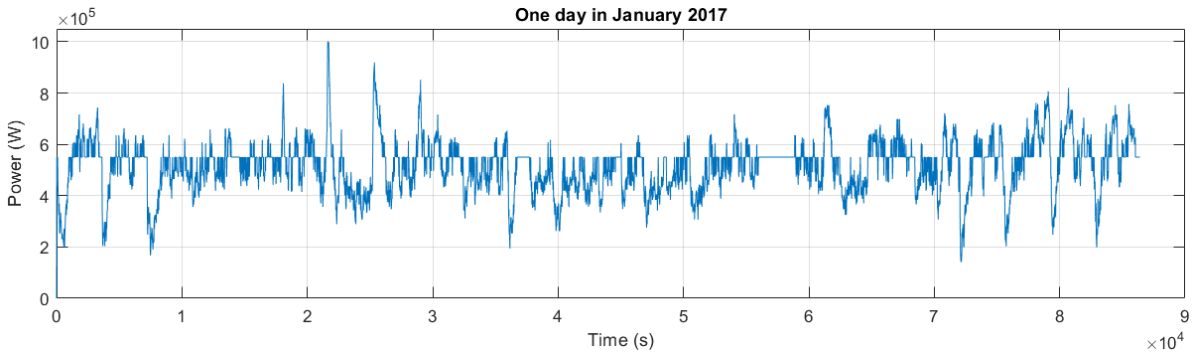

Figure 6.3: Power command providing FCR during one day in January 2017.

Figure 6.4 and 6.5 represent the histograms of the grid frequency and the electrolyser power. We can see that the median is below the 50Hz (or 550kW), about 49.99Hz (500kW). The mean consumption of the electrolyser is 503kW. We see that 20% of the time the electrolyser operates in the stability region at 550kW.

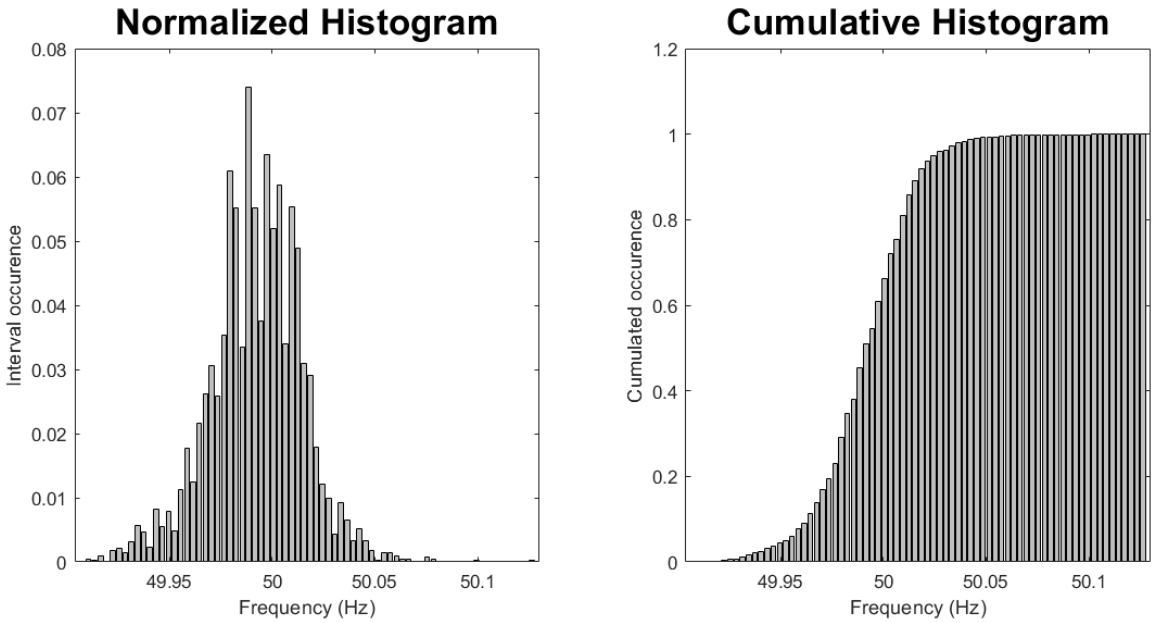

Figure 6.4: Histograms of the frequency.

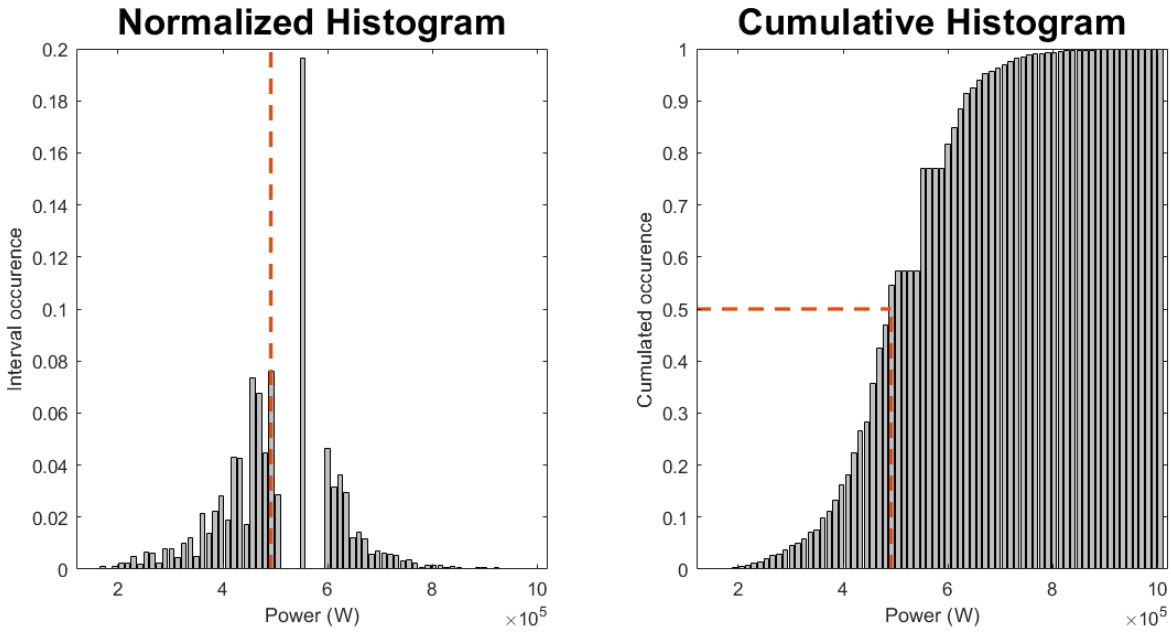

Figure 6.5: Histograms of the power associated to frequency.

6.2 Electrical power supply and control

In order to model the electrical supply of the system, we use another dynamic model. The chosen model is the one used by Arash E. Samani et al. and is represented on Figure 6.6 where the electrolyser subsystem is basically the equivalent circuit from Figure 4.15.

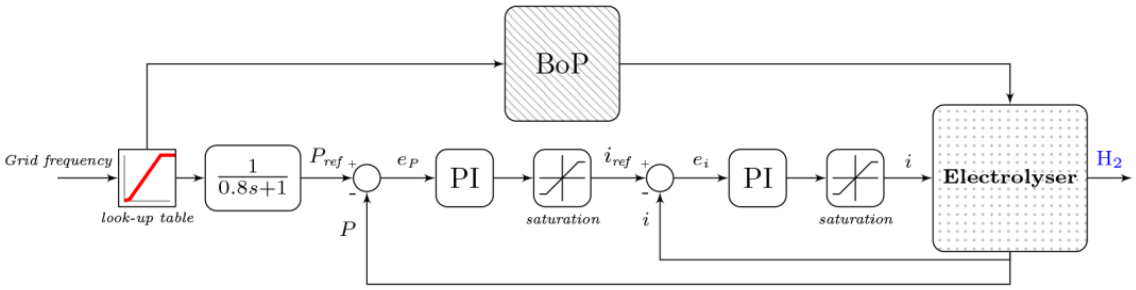

Figure 6.6: Control diagram of PEM electrolyser. Taken from [30].

This model has been implemented in Matlab Simulink by Cyril Cousein in Figure 6.7 and it provided inputs for the work. This model is used to produce the waveform of the current of the electrolyser according to section 4.3.

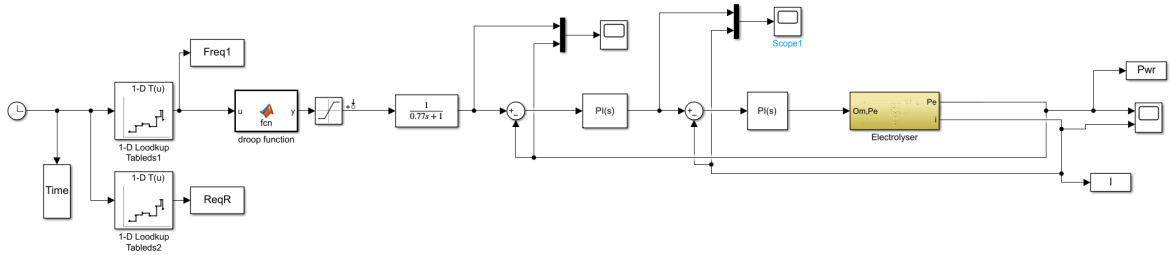

Figure 6.7: Cyril Cousein's simulink model from Samani control diagram.

The waveform of the current has been used as input for the current source of our model. There is no delay between the grid frequency change and the power change as there is no valid reason, after the dynamic analysis of the BoP, to delay the power command. The system will regulate itself in order to reach the closest possible point to the operating point.
The proportional and integral gains of the cascaded controller are a design choice explained by Arash E. Samani and resumed in Table 6.1.

Controller	Proportional gain (P)	Integral gain (I)
Power (outer loop)	20	10
Current (inner loop)	10	10

Table 6.1: Proportional and integral gains of the cascaded controller. From [30].

The droop function that transforms the frequency to the power command is represented in Figure 6.8. This function is completed by the saturation block in Figure 6.7 that restricts the power command to minimum 100kW and maximum 1MW. The power command to the electrolyser is set at 550kW when the grid is balanced i.e when the frequency is 50Hz.
The output of the model provides the current to apply to our electrolyser model. The power waveform of the commanded and response power of the electrical equivalent model are shown in Figure 6.9. We see that there is no delay and a rapid response of the electrolyser.

Own_Version_Arash ▸ droop function

```
1
2   function y = fcn(u)
3
4   Pb=550e3;
5   PwrR=450e3;
6   deltaf=0.1;
7   K=PwrR/deltaf;
8
9   if abs(u-50)>0.01
10  P=Pb+K*(u-50);
11  else
12  P=Pb;
13  end
14
15  y = P;
```

Figure 6.8: Droop function used in the model.

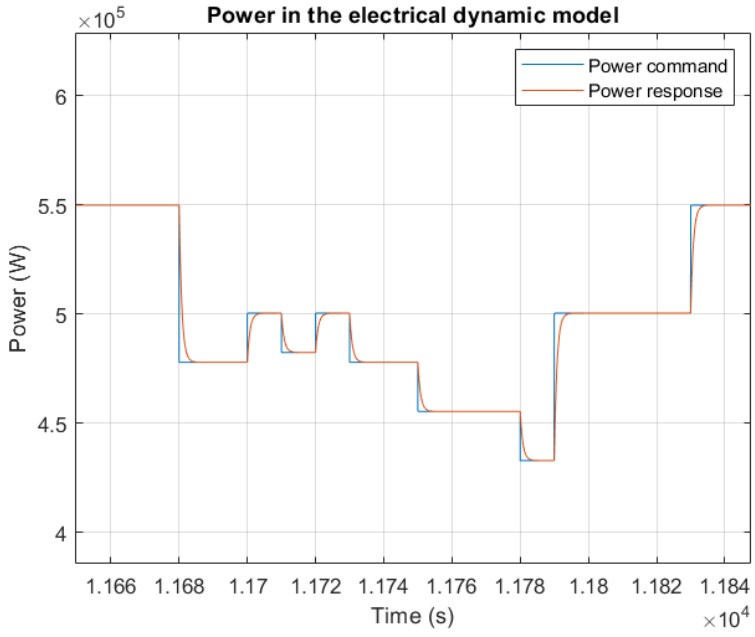

Figure 6.9: Power in the electrical dynamic model.

6.3 Providing FCR during 24h

We now apply the data above to our electrolyser to provide FCR. Figure 6.10 shows the overview of the simulation results of the electrolyser. Also we will focus on 3 time ranges

as shown in Figure 6.11. There is a peak, a rather stable period and a period of low power.

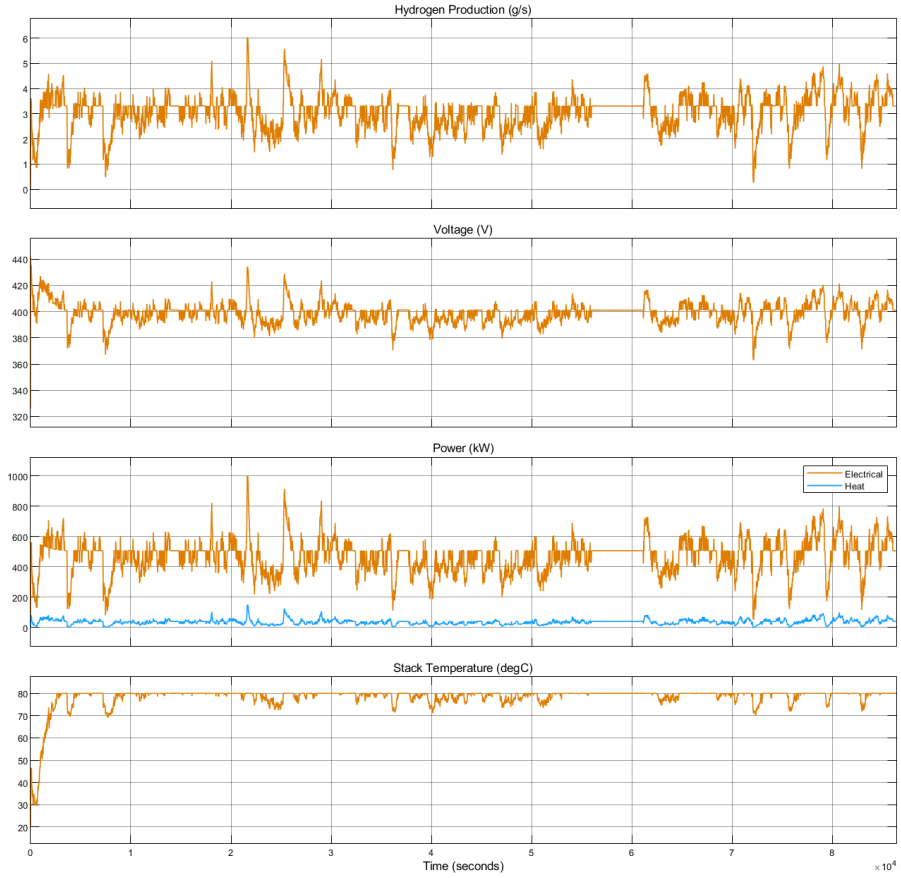

Figure 6.10: 24h providing FRC.

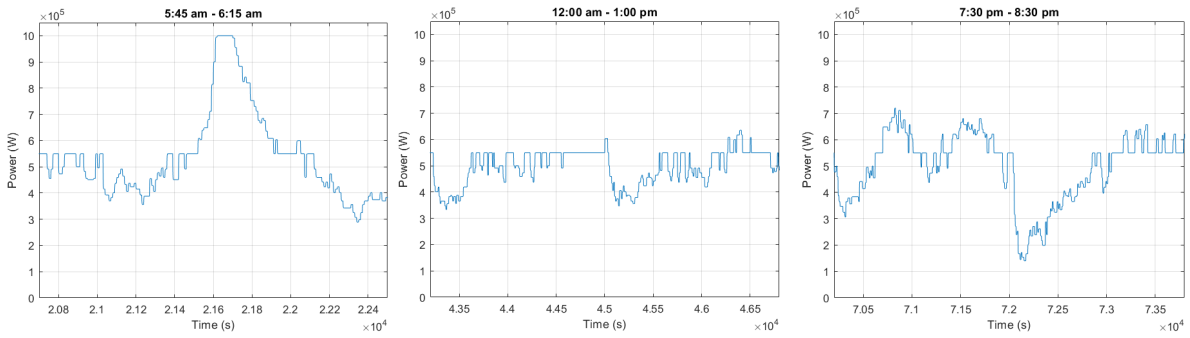

(a) Peak period. (b) Stable period. (c) Low power period.

Figure 6.11: The time period used for observations.

We will first look at the voltage and the pressure before looking at the 3 time periods. Figure 6.12 shows the composition of the cell voltage. The Nernst potential represents the minimum voltage when the activation and ohmic overpotential represent losses. We see that the Nernst potential is stable and varies a little bit with the temperature. The activation overpotential is almost a constant loss but decreases for low power and the ohmic overpotential is the linear loss from the power. For high power we will have more losses due to the ohmic effect and this will decrease the efficiency.

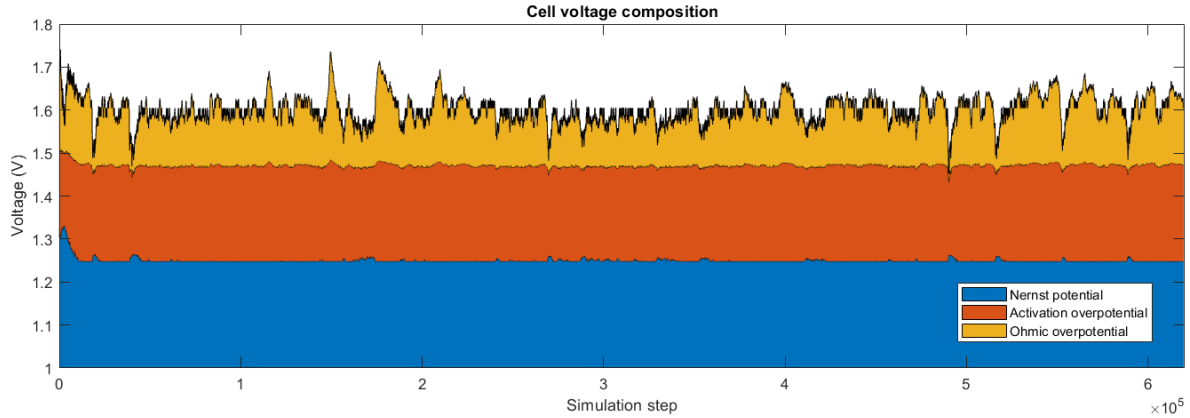

Figure 6.12: Cell voltage composition.

The pressure will not be part of this analysis since it remains rather stable with low variance. The pressure is available on Figure 6.13.

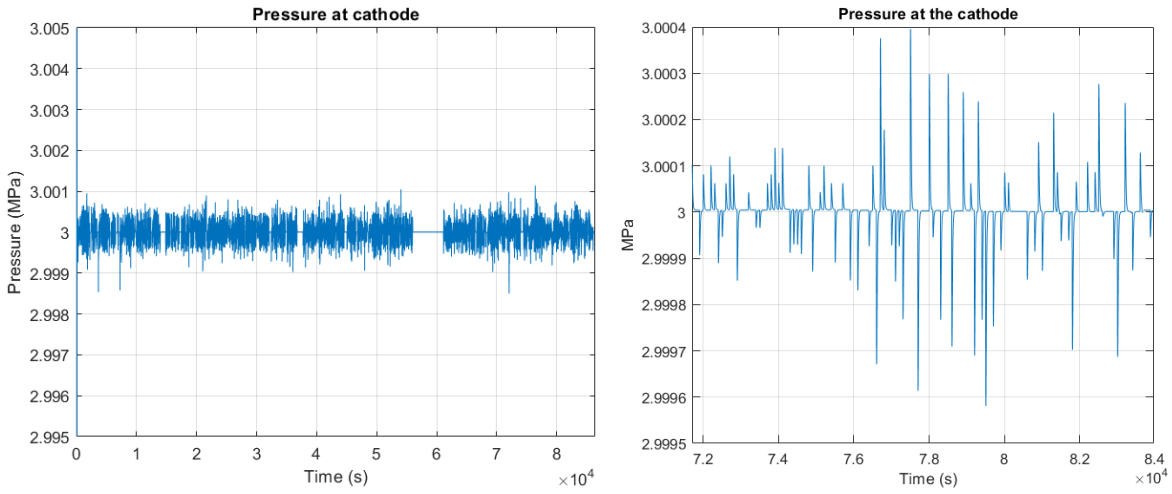

(a) Overview.

(b) Zoom.

Figure 6.13: Pressure at the cathode.

The analysis of the 3 time periods will be done in section 6.4. Annex D shows an overview of the day and three other time periods.

The first time range is around 6:00 am, available in Figure 6.14.

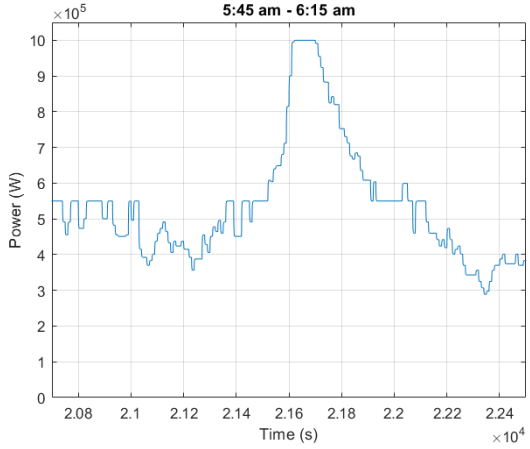

(a) Electrolyser power.

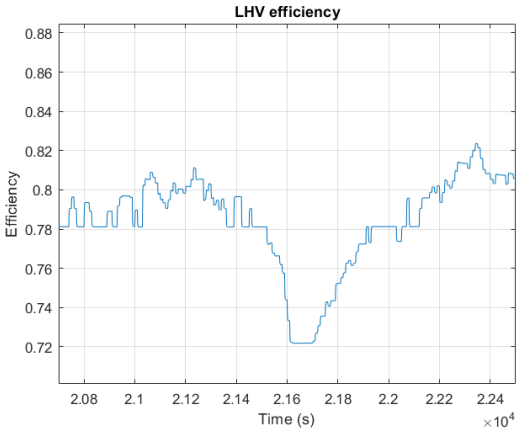

(b) Efficiency.

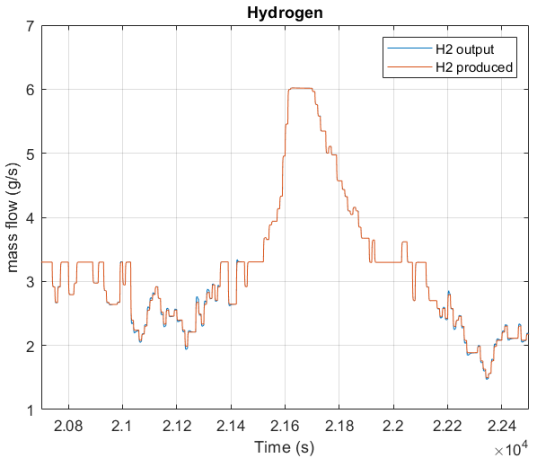

(c) Hydrogen.

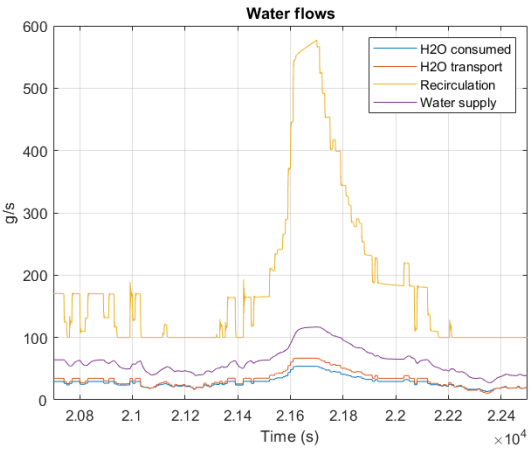

(d) Water flows.

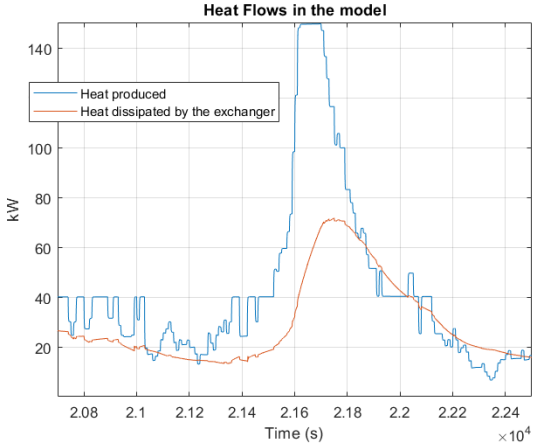

(e) Heat flows.

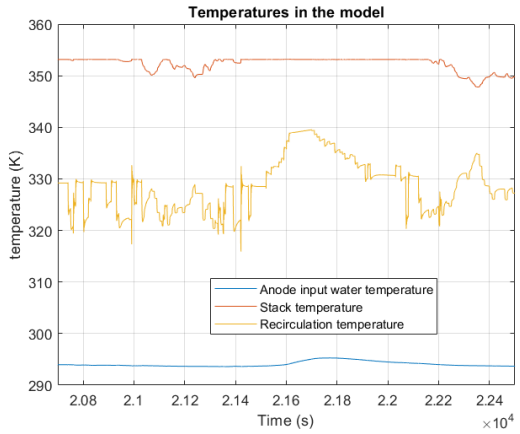

(f) Temperatures.

Figure 6.14: First time period - Peak load.

The second time range is from 12:00 am to 1:00pm, available in Figure 6.15.

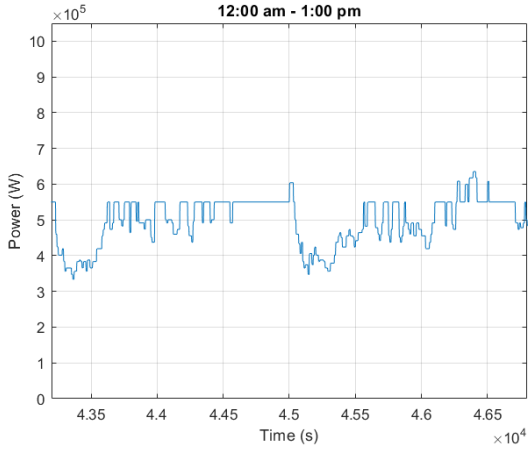

(a) Electrolyser power.

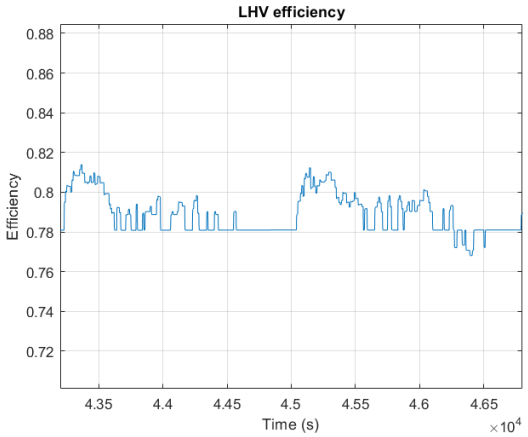

(b) Efficiency.

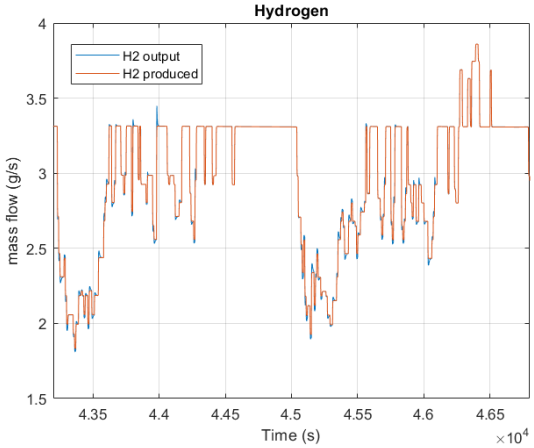

(c) Hydrogen.

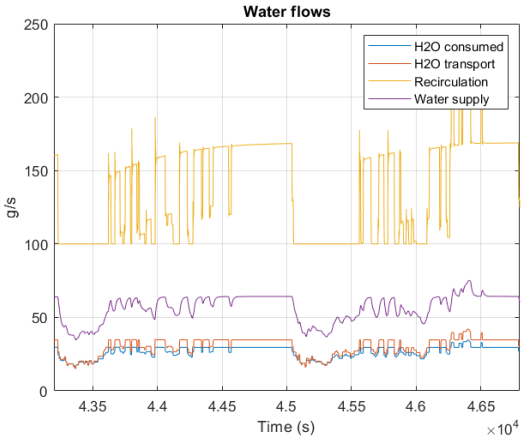

(d) Water flows.

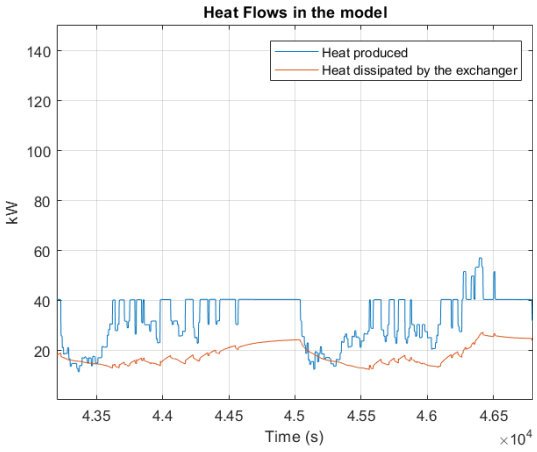

(e) Heat flows.

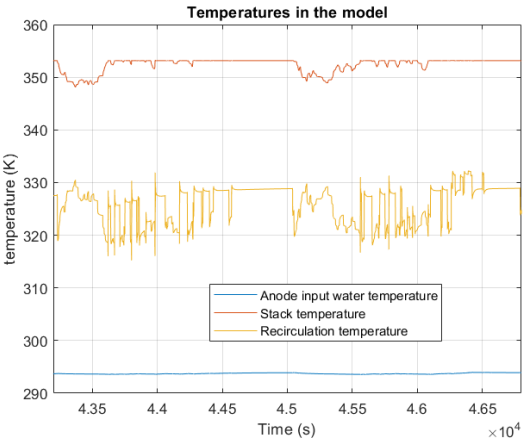

(f) Temperatures.

Figure 6.15: Second time period - Stable period.

The third time range is from 7:30 pm to 8:30pm, available in Figure 6.16.

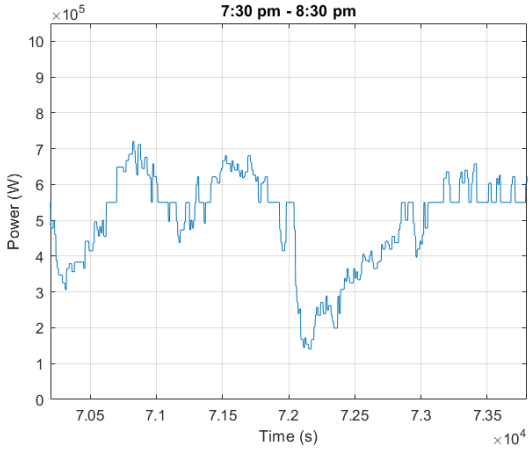

(a) Electrolyser power.

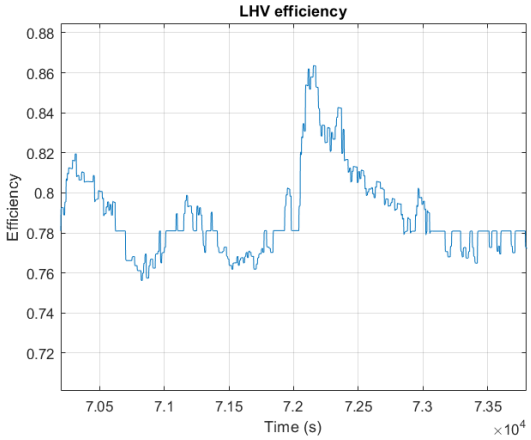

(b) Efficiency.

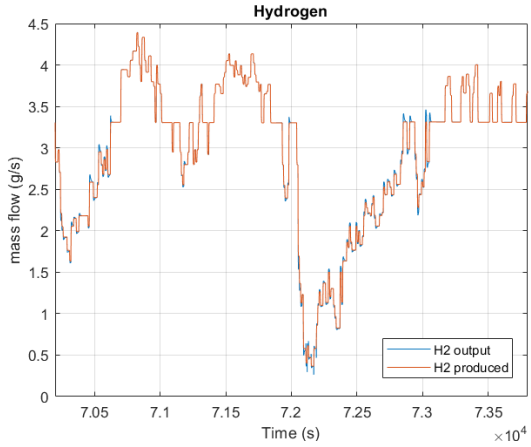

(c) Hydrogen.

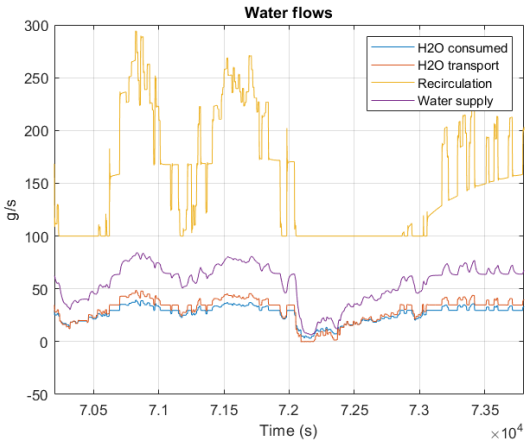

(d) Water flows.

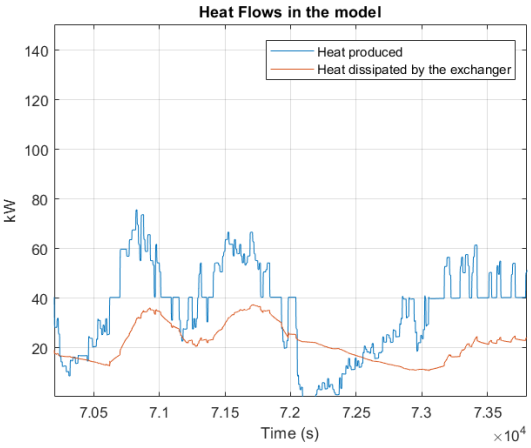

(e) Heat flows.

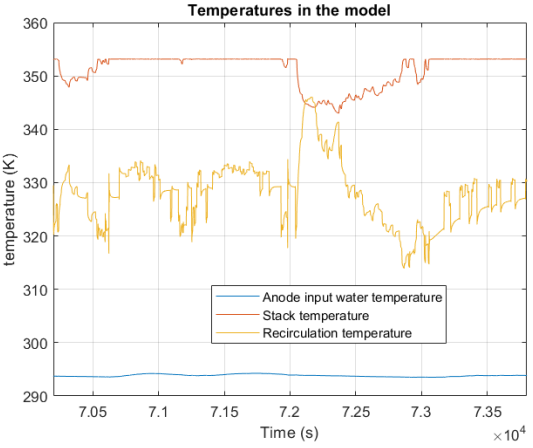

(f) Temperatures.

Figure 6.16: Third time period - Low load.

6.4 Observations and discussions

This section makes the observations about the dynamic behaviour of the model. We can see several things on the overview of the simulation in Figure 6.10. First, the model is able to provide FCR even when making a cold start[1]. Second, there is a frequency stable region between 3:30pm and 4:30pm that leads to constant production at 550kW. We also can see that the temperature is not always maintained at 80°C but goes below for low power. On the Figure 6.14, 6.15 and 6.16 we can make other observations.

Efficiency

The efficiency is obviously inversely proportional to the power since the ohmic losses are directly resulting from the current. The efficiency is rather high but do not take into account the losses from the AC-DC converters or the electrical consumption of the balance of plant. The efficiency during the simulated day is between 72% in Figure 6.14 and 86% in Figure 6.16.

Pressure at cathode

We see that the hydrogen circuit of the model does not represent high limitations. This can be due to the low pressure of the system and the simplifications made. On the other hand, there are very few papers addressing modelisation of purification and compression. The difference between the output and the production is due to the control chain ruling the pressure regulator.

Water in the MEA

We can see that for high density current (i.e. high power) we have more water transported across the membrane than consumed water from the reaction due to the electro-osmotic drag. This trend is reversed for low power as the pressure effect takes over.

Thermal regulation

On the thermal side, we can see that when the power decreases, the stack temperature decreases also despite the regulation of the recirculation circuit. This is due to the high efficiency of the heat exchanger and the floor flow of the recirculation pump. Therefore different solutions allow us to have better thermal regulation. First we have seen that the maximal thermal flow of the heat exchanger is about 2MW heat. This is never reached (Fig. 6.14e shows a maximum 150kW heat generation) so we can decrease the efficiency of the heat exchanger. If it is not sufficient, the control chain of the thermal regulation can be changed for example by lowering the floor water flow. It generates problems if the recirculation flow becomes lower than the consumed and transported

[1]The control chain does not take into account the additional power due to the low temperature at the beginning.

water. The minimal recirculation flow is 100g/s and can be decreased to approximately 70g/s without affecting the water flow across the membrane.

Running the model

For the final scenario the model ran in 26 minutes with 111000 input steps (current) and gave 650000 output steps without warnings. The challenge was to keep all steps in memory in order to provide the graphs. When running the model, Matlab was taking about 10GB RAM. Adding several Simulink scope blocks and modifying the MEA block to have access to certain states prevent keeping in memory all the state values for each step. Another solution is also to simulate shorter durations.

Global production

The mean power of the electrolyser is 500kW. On that day the system consumed 12MWh. This power consumption does not include the other losses. The losses from the electric supply rectifiers are not negligible (about 14%). On that day the system produced 259 kg of hydrogen thus 2882Nm^3 with an average energy of 46.3kWh/kg (4.16kWh/Nm^3).

Providing FCR

The observations of the electrolysis system operation confirm a good response to the dynamic needs. The results of this work support the conclusion of J. Eichman et al. resumed in Figure 6.17: electrolysers are able to respond within a second for high duration and with a rapid shutdown time.

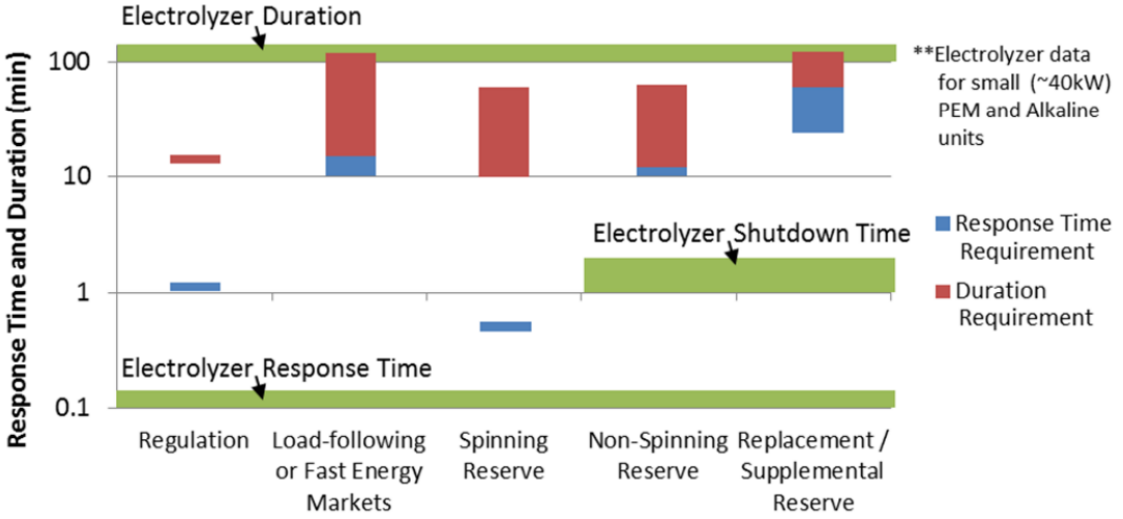

Figure 6.17: Summary of electrolyser flexibility compared to electricity market requirements. Taken from [24].

Some reflexions

- The minimum and maximum FCR demand on 27th of January 2017 was -41.85MW and 36.89MW. Therefore, in order to maintain the stability with only electrolysers, about 100 electrolysers like the one in this work should be installed. A pool of electrolysers for a total of 100MW represents a $100 \times \pm 450\text{kW} = \pm 45\text{MW}$ reserve.

- A realistic pool of electrolysers to reach 100MW could be 5 electrolysers of 20MW. The footprint of such installation, according to the HyLTZER®-5000-30 [82], is 2500m^2 (500m^2 each). It is a rather small footprint, equivalent to half of a soccer field.

Chapter 7

Conclusion

The focus of this master thesis was to develop a large scale electrolyser model able to study the dynamic behaviour in a demand response perspective to help the stability of the electrical power grid.

Firstly, we reviewed in the context leading to study the dynamic behaviour of large scale PEM electrolysers. Electrolysers are little explored today. Their number will most probably increase in the coming years due to the European strategy for decarbonisation. The electrolysers will therefore represent large loads for the electrical grid and there is an opportunity that they will contribute to the stability of the grid in an environment where this stability is decreasing.

The research on electrolyser and in particular on the PEM technology is in expansion. An analysis of the literature led to use several models. These models are from different physical approaches: electrochemical, thermal and mass models.

The Matlab model version 2022a from March 15th 2022 was found to be a good model to use for the study. It contains different physical components of the electrolyser. We improved the model with the results of the work. In particular, we brought the following modifications in order to get the conditions needed to answer the questions of the study:

- An electrical supply that integrates the electrical dynamic behaviour of the electrolyser.
- The voltage model modifications used by the electrolyser.
- A scale up of the model to reach 1MW.
- The modifications of the thermal and pneumatic behaviour of the Membrane Electrode Assembly.

For the simulation of the electrolyser, four control schemes were needed; one for the electrical supply and power to apply and three for the electrolyser regulation: one for the regulation of the pressure and the hydrogen outlet, another for the circulation of

water and thermal regulation and the last one to adjust the water level in the water circuit.

The model confirms the available results in the literature. In order to ensure the good application of the model, the theoretical validation confirmed identical behaviour to other models validated experimentally. The time constants are available in Table 5.2. The electrolyser responds in a stable manner within a few seconds. There is no issue in terms of electrical dynamic. Some dynamic behaviours can take longer but are compensated by controllers. The lack of real data and experimental installation did not allow us to fully validate the model.

We applied the improved model to the electrical grid situation of January 2017 as provided for the study. The dynamic response of a large scale electrolyser when it provides frequency reserve to the electrical grid was confirmed. Find here below the highlights:

- The electrical response time is <1s. The dynamic behaviour on electrical side depends on the current density.
- The balance of plant has to be well designed for dynamic behaviour, but does not represent intrinsic limitations for the electrolyser operation. The temperature remains under 80°C.
- The dynamic behaviour has an effect on efficiency since the temperature is not constant. Also the efficiency is driven by the current density so for low current the efficiency will be better.
- The pressure is the weak point of the model due to the ideal simplified purification part.

Technically electrolysers can resolve the lack of stability of the electrical grid. The study answers to the different questions of the research.

7.1 Further analysis

Find here below some reflection questions and proposals for further research.

- The use of electrolyser at Belgium level brings additional considerations. The hydrogen production as an electrical energy storage solution brings other questions in particular around the primary energy source in a high populated country which consumes a lot of energy and is not autonomous in terms of energy resources.
- The impact of electrolysers on the environment is an important topic. Hydrogen is a light gas that diffuses across pipeline walls and has a greenhouse effect.

- The impact of dynamic behaviour on degradation of the stack (mainly on the cell voltage) should be further studied. There is not much research on electrolyser. As PEM fuel cells are more developed, their degradation is already studied and could be a starting point for further research on the PEM electrolyser.

- The dynamic limits in the flexibility of the electrolyser power supply are dependent on the electrolyser design and should therefore be studied on a real installation.

- The electrochemical response is even faster for large currents. The current density will further increase over the years which will reduce the time response.

Annex A - Code custom block MEA: Electrolyzer.ssc

```
component (Propagation = blocks) electrolyzer_stack
% Electrolyzer
% This block models a stack of membrane electrode assemblies (MEA) ... for a
% proton exchange membrane (PEM) electrolyzer. Water is consumed ... from the
% connected anode flow channels. Oxygen and hydrogen are produced ... at the
% connected anode and cathode flow channels, respectively. Waste ... heat is
% dissipated to the connected thermal mass.

% Copyright 2021 The MathWorks, Inc.
% Modified by Martin Pasture in July 2022



%=============================================================================
% Simscape block creation
% This section give a shape to the simscape block by specifying the ... ports and the geometry

nodes
    % Electrodes
    p = foundation.electrical.electrical; % +
    n = foundation.electrical.electrical; % -
    % Moist air ports to obtain domain parameters and property ... tables for
    % the anode network and the cathode network only. There is no ... flow through ports A and C
    A = foundation.moist_air.moist_air; % A
    C = foundation.moist_air.moist_air; % C
    % Anode side thermal liquid port to remove water from channels
    H2O = foundation.thermal_liquid.thermal_liquid; % H2O
    % Anode side moist air source port to add oxygen to channels
    O2 = foundation.moist_air.moist_air_source; % O2
```

```
30      % Cathode side moist air source port to add hydrogen and water ...
            vapor to channels
31      H2 = foundation.moist_air.moist_air_source; % H2
32      % Thermal port for heat generation
33      H = foundation.thermal.thermal; % H
34      V_nernst_ = foundation.electrical.electrical;
35      V_ohm_ = foundation.electrical.electrical;
36      V_act_ = foundation.electrical.electrical;
37  end
38
39  inputs
40      % Input ports for the internal states of the cathode gas channels
41      FC = [101325; 293.15; 0.5; 0.01; 0.01; 0.01; 0.001; 0.001]; % FC
42  end
43
44  annotations
45      [p, n]       : Side = top;
46      [A, H2O, O2] : Side = left;
47      [C, H2, FC]  : Side = right;
48      [H, V_nernst_, V_ohm_, V_act_] : Side = bottom;
49  end
50
51
52
53
54  %=========================================================================
55  % Parameters of the MEA and the electrolyzer
56  %
57  parameters
58      N_cell       = {50,    '1'      }; % Number of cells in stack
59      area_cell    = {280,   'cm^2'   }; % Cell area
60      t_membrane   = {125,   'um'     }; % Membrane thickness
61      t_gdl_A      = {25,    'um'     }; % Anode gas diffusion layer ...
            (GDL) thickness
62      t_gdl_C      = {250,   'um'     }; % Cathode gas diffusion layer ...
            (GDL) thickness
63      io           = {8e-05, 'A/cm^2' }; % Exchange current density
64      alpha        = {0.5,   '1'      }; % Charge transfer coefficient
65      D_H2O_gdl_A  = {0.07,  'cm^2/s' }; % Water diffusivity in anode GDL
66      D_H2O_gdl_C  = {0.07,  'cm^2/s' }; % Water diffusivity in ...
            cathode GDL
67      rho_membrane = {2000,  'kg/m^3' }; % Density of dry membrane
68      M_membrane   = {1.1,   'kg/mol' }; % Equivalent weight of dry ...
            membrane
69  end
70
71  % Parameter checks
72  equations
73      assert(N_cell > 0)
74      assert(area_cell > 0)
75      assert(t_membrane > 0)
76      assert(t_gdl_A > 0)
```

```
77      assert(t_gdl_C > 0)
78      assert(io > 0)
79      assert(alpha > 0)
80      assert(D_H2O_gdl_A > 0)
81      assert(D_H2O_gdl_C > 0)
82      assert(rho_membrane > 0)
83      assert(M_membrane > 0)
84  end
85
86  %=========================================================================
87  % Internal parameters
88  %
89
90  parameters (Access = protected)
91      % Constants
92      R_u    = {8.31446261815324, 'J/K/mol'}; % Universal gas constant
93      F      = {96485.33212,      'C/mol'  }; % Faraday constant
94      G_H2O  = {-237.14,          'kJ/mol' }; % Gibbs free energy of ...
            water
95      HHV_H2 = {285.8,            'kJ/mol' }; % Higher heating value ...
            of hydrogen
96      LHV_H2 = HHV_H2 - MW_H2O * hfg_H2O_std; % Lower heating value ...
            of hydrogen
97      T_std  = {25,               'degC'   }; % Standard temperature
98      p_std  = {1,                'atm'    }; % Standard pressure
99
100     % Standard cell potential
101     %E_cell = G_H2O/(-2*F); = 1.2289 has been redifined at line 252
102
103
104     % Membrane permeability to water
105     K_darcy = {1.58e-14, 'cm^2'};
106
107     % Compute molar masses from specific gas constants
108     MW_H2O = R_u/A.R_w;
109     MW_O2  = R_u/A.R_g;
110     MW_H2  = R_u/C.R_g;
111
112     % Species specific enthalpy at standard temperature
113     h_H2O_std   = tablelookup(A.T_TLU, A.h_w_TLU,     T_std, ...
            interpolation = linear, extrapolation = linear);
114     hfg_H2O_std = tablelookup(A.T_TLU, A.h_w_vap_TLU, T_std, ...
            interpolation = linear, extrapolation = linear);
115     h_O2_std    = tablelookup(A.T_TLU, A.h_g_TLU,     T_std, ...
            interpolation = linear, extrapolation = linear);
116     h_H2_std    = tablelookup(C.T_TLU, C.h_g_TLU,     T_std, ...
            interpolation = linear, extrapolation = linear);
117
118
119     i_lim = 9.4 % from fontes2005modelisation
120
121     %RC for electrochemical equivalent circuit
```

```
122     R_a = {0.015*0.888/0.11, 'Ohm'};
123     C_a = {4400*0.36/0.11, 'F'};
124     R_c = {0.015*0.097/0.11, 'Ohm'};
125     C_c = {4400*0.027/0.11, 'F'};
126     R_ohm2 = {0.042/0.11, 'Ohm'};
127     E_cell2 = {1.4*5000, 'V'};
128 end
129
130 %=========================================================================
131 % Variables of the MEA and the electrolyzer
132 %
133 variables (ExternalAccess = observe)
134     i = {0, 'A' }; % Current (positive in)
135     Q = {0, 'kW'}; % Heat flow rate (positive in)
136     %v = {0, 'V' };  % Voltage
137
138     RH_acl = {0.5, '1'}; % Relative humidity at anode catalyst ...
            layer (ACL)
139     RH_ccl = {0.5, '1'}; % Relative humidity at cathode catalyst ...
            layer (CC)
140 end
141
142 variables (ExternalAccess = none)
143     % Through variables for thermal liquid port
144     mdot_H2O = {0, 'kg/s'}; % TL mass flow rate into port H2O
145     Phi_H2O  = {0, 'kW'  }; % TL energy flow rate into port H2O
146 end
147
148
149 %=========================================================================
150 % Branches establish relationship between component Through ...
       variables and nodes
151 %
152
153 branches
154     i : p.i -> n.i;
155     Q : H.Q -> *;
156
157     mdot_H2O : H2O.mdot -> *
158     Phi_H2O  : H2O.Phi  -> *
159 end
160
161
162
163 %=========================================================================
164 % Define intermediate terms for use in equations
165 %
166
167 % For logging
168 intermediates
169     v = p.v - n.v; % Voltage
170     vnernst = V_nernst_.v - p.v;
```

```
171     vohm = V_ohm_.v - p.v;
172     vact = V_act_.v - p.v;
173     i_cell = if ge(i, 0), i/area_cell else 0 end; % Cell current ...
            density
174     v_cell = v_nernst + v_ohm + v_act_diff ; % Cell voltage
175     R_ohm = t_membrane / sigma; % Membrane resistance
176     %{
177     v_stack = v;
178     v_cell = v_stack/N_cell
179     i_cell = i/area_cell;
180     %}
181     power_elec = N_cell * v_cell * i_cell * area_cell; % Electrical ...
            power consumed
182     power_dissipated = power_elec - power_net; % Power dissipated
183     efficiency_HHV = simscape.function.limit(HHV_H2/(2*F) / v_cell, ...
            0, 1, false); % Thermal efficiency based on HHV
184     efficiency_LHV = simscape.function.limit(LHV_H2/(2*F) / v_cell, ...
            0, 1, false); % Thermal efficiency based on LHV
185
186     H2O_consumed = N_cell * MW_H2O * area_cell * i_cell/(2*F); % ...
            Water consumed
187     O2_produced  = N_cell * MW_O2  * area_cell * i_cell/(4*F); % ...
            Oxygen produced
188     H2_produced  = N_cell * MW_H2  * area_cell * i_cell/(2*F); % ...
            Hydrogen produced
189
190     H2O_transport = (nflux_H2O_diff + nflux_H2O_drag + ...
            nflux_H2O_hydraulic) * MW_H2O * area_cell * N_cell; % Net ...
            water transport from anode to cathode
191     %H2O_transport = (nflux_H2O_diff + nflux_H2O_drag) * MW_H2O * ...
            area_cell * N_cell; % Net water transport from anode to cathode
192 end
193 %{
194 components (ExternalAccess = none)
195     r_ohm = foundation.electrical.elements.resistor(R=N_cell*R_ohm2);
196     r_acta = foundation.electrical.elements.resistor(R=N_cell*R_a);
197     r_actc = foundation.electrical.elements.resistor(R=N_cell*R_c);
198     c_acta = foundation.electrical.elements.capacitor(c=N_cell*C_a);
199     c_actc = foundation.electrical.elements.capacitor(c=N_cell*C_c);
200     v_rev = ...
            foundation.electrical.sources.dc_voltage(v0=N_cell*E_cell2);
201 end
202
203 connections
204     connect(c_acta.n,r_ohm.p);
205     connect(c_acta.n,r_acta.n);
206     connect(c_acta.p,r_acta.p);
207     connect(c_acta.p,p);
208     connect(c_actc.n,r_actc.n);
209     connect(c_actc.p,r_actc.p);
210     connect(c_actc.p,v_rev.n);
211     connect(c_actc.n,n);
```

```
212     connect(v_rev.p,r_ohm.n);
213 end
214 %}
215 annotations
216     [v, v_cell]                                                    : ...
        LoggingUnit = 'V';
217     i_cell                                                         : ...
        LoggingUnit = 'A/cm^2';
218     R_ohm                                                          : ...
        LoggingUnit = 'Ohm*cm^2';
219     [power_elec, power_dissipated]                                 : ...
        LoggingUnit = 'kW';
220     [efficiency_HHV, efficiency_LHV]                               : ...
        LoggingUnit = '1';
221     [H2O_consumed, O2_produced, H2_produced, H2O_transport] : ...
        LoggingUnit = 'g/s';
222 end
223
224 intermediates (ExternalAccess = none)
225     % Extract cathode gas states from input FC
226     % Note: Can also connect Measurement Select (MA) block to ...
        choose values
227     p_C     = {FC(1), 'Pa'}; % Pressure
228     y_H2O_C = FC(5);         % Water vapor mole fraction
229     y_H2_C  = FC(8);         % Hydrogen mole fraction
230
231     % Anode pressure and temperature
232     p_A = H2O.p;
233     T_A = H2O.T;
234
235     % Mole fractions at anode
236     % Assume saturated water vapor at stack temperature
237     y_H2O_A = if ge(p_ws_ratio_A, 1), 1/p_ws_ratio_A else 1 end;
238     y_O2_A  = 1 - y_H2O_A;
239
240     % Stack temperature
241     T_stack = H.T;
242
243     % Ratio of pressure to water vapor saturation pressure
244     p_ws_ratio_A = exp(log(value(p_A, 'Pa')) - tablelookup(A.T_TLU, ...
        A.log_p_ws_TLU, T_stack, interpolation = linear, ...
        extrapolation = linear));
245     p_ws_ratio_C = exp(log(value(p_C, 'Pa')) - tablelookup(C.T_TLU, ...
        C.log_p_ws_TLU, T_stack, interpolation = linear, ...
        extrapolation = linear));
246
247     % Activities
248     a_H2O_A_ = y_H2O_A * p_ws_ratio_A;
249     a_O2_A_  = y_O2_A  * p_A / p_std;
250     a_H2_C_  = y_H2_C  * p_C / p_std;
251     a_H2O_A  = if ge(a_H2O_A_, 1e-9), a_H2O_A_ else 1e-6 end;
252     a_O2_A   = if ge(a_O2_A_,  1e-9), a_O2_A_  else 1e-6 end;
```

```
253     a_H2_C    = if ge(a_H2_C_,  1e-9), a_H2_C_  else 1e-6 end;
254
255     % Nernst voltage
256     E_cell = G_H2O/(-2*F) - {0.0009, 'V/K'}*(T_stack-{298,'K'})
257     % ORIGINAL VERSION
258     %v_nernst = E_cell + R_u*T_stack/(2*F) * log((a_H2_C * ...
            a_O2_A^0.5) / a_H2O_A);
259     % MODIFIED VERSION
260     v_nernst = E_cell + R_u*T_stack/(2*F) * log((p_ws_ratio_C * ...
            p_ws_ratio_A^0.5)/ a_H2O_A);
261
262     % Activation losses from Tafel equation + diffusion overvoltage
263     b = R_u * T_stack / (2 * alpha * F);
264     % ORIGINAL VERSION
265     %v_act = if ge(i_cell, io), b*log(i_cell/io) else 0 end;
266     % MODIFIED VERSION
267     v_act_diff = if ge(i_cell, io), ...
            b*log((i_cell/io)/(1-(1/i_lim))+sqrt(1+((i_cell/io)/(1-(1/i_lim)))^2)) ...
            else 0 end;
268
269     % Water content
270     lambda_acl = membrane_water(RH_acl);
271     lambda_ccl = membrane_water(RH_ccl);
272     lambda_membrane = (lambda_acl + lambda_ccl)/2;
273
274     % Membrane conductivity
275     sigma_30 = {if ge(lambda_membrane, 1), 0.005139*lambda_membrane ...
            - 0.00326 else 0.005139 - 0.00326 end, '1/(Ohm*cm)'};
276     sigma = sigma_30 * exp(1268*(1/303.15 - 1/value(T_stack, 'K')));
277
278     % Resistive voltage loss
279     v_ohm = R_ohm * i_cell; % ORIGINAL VERSION
280
281     % Water diffusion coefficient across membrane
282     D_H2O_membrane = {1.25e-10, 'm^2/s'} * exp(2416*(1/303.15 - ...
            1/value(T_stack, 'K')));
283     %D_H2O_membrane = {1.25e-6, 'm^2/s'} * exp(2416*(1/303.15 - ...
            1/value(T_stack, 'K')));
284
285     % Water concentrations at anode and cathode catalyst layers
286     Conc_H2O_acl = rho_membrane / M_membrane * lambda_acl;
287     Conc_H2O_ccl = rho_membrane / M_membrane * lambda_ccl;
288
289     % Molar flux of water across membrane due to diffusion
290     nflux_H2O_diff = D_H2O_membrane*(Conc_H2O_acl - ...
            Conc_H2O_ccl)/t_membrane;
291
292     % Water electro-osmotic drag coefficient
293     nd_H2O_membrane = ...
294         if ge(lambda_acl, 0), ...
295             0.0029*lambda_acl^2 + 0.05*lambda_acl - 3.4e-19 ...
296         else ...
```

```
297             0.05*lambda_acl - 3.4e-19 ...
298         end;
299
300     % Molar flux of water across membrane due to electro-osmotic drag
301     nflux_H2O_drag = nd_H2O_membrane * i_cell / F;
302
303     % Water vapor mole fraction at anode and cathode catalyst layers
304     y_H2O_acl = RH_acl/p_ws_ratio_A;
305     y_H2O_ccl = RH_ccl/p_ws_ratio_C
306
307     % Molar flux of water across anode and cathode diffusion layers
308     nflux_H2O_A = p_A*D_H2O_gdl_A/(R_u*T_stack) * (y_H2O_A - ...
            y_H2O_acl)/t_gdl_A;
309     nflux_H2O_C = p_C*D_H2O_gdl_C/(R_u*T_stack) * (y_H2O_ccl - ...
            y_H2O_C)/t_gdl_C;
310
311     % Molar flux of water across membrane due to hydraulic pressure ...
            difference based on Darcy's law
312     mu_H2O = tablelookup(A.T_TLU, A.mu_w_TLU, T_stack, ...
            interpolation = linear, extrapolation = nearest);
313     nflux_H2O_hydraulic = ...
314         if gt(p_A, p_C), ...
315             (p_A - p_C) * K_darcy * p_A * y_H2O_acl / (R_u * ...
                    T_stack * mu_H2O * t_membrane) ...
316         else...
317             (p_A - p_C) * K_darcy * p_C * y_H2O_ccl / (R_u * ...
                    T_stack * mu_H2O * t_membrane) ...
318         end
319
320     % Specific enthalpy of water at port H2O
321     % based on fluid properties of thermal liquid network
322     u_H2O   = tablelookup(H2O.T_TLU, H2O.p_TLU, H2O.u_TLU,   T_A, ...
            p_A, interpolation = linear, extrapolation = linear);
323     rho_H2O = tablelookup(H2O.T_TLU, H2O.p_TLU, H2O.rho_TLU, T_A, ...
            p_A, interpolation = linear, extrapolation = linear);
324     h_H2O   = u_H2O + p_A/rho_H2O;
325
326     % Specific enthalpy of water at anode
327     % based on fluid properties of moist air network
328     h_H2O_A   = tablelookup(A.T_TLU, A.h_w_TLU,     T_A, ...
            interpolation = linear, extrapolation = linear);
329     hfg_H2O_A = tablelookup(A.T_TLU, A.h_w_vap_TLU, T_A, ...
            interpolation = linear, extrapolation = linear);
330
331     % Energy consumed by reaction at standard temperature
332     power_rxn = HHV_H2 * H2_produced / MW_H2;
333
334     % Energy gain in membrane due to bringing reactants and ...
            products to standard temperature
335     power_Δ_std = H2O_consumed*(h_H2O_A - hfg_H2O_A) - ...
            H2O_consumed*(h_H2O_std - hfg_H2O_std) ...
336         + (source_O2_A.Phi_S - source_O2_A.mdot_g_S*h_O2_std) ...
```

```
337         + (source_H2_C.Phi_S - source_H2_C.mdot_g_S*h_H2_std);
338
339     % Energy gain in membrane due to water transport
340     power_trans = H2O_transport*(h_H2O_A - hfg_H2O_A) + ...
            transport_H2O_C.Phi_S;
341
342     % Net energy consumption in stack
343     power_net = power_rxn - power_Δ_std - power_trans;
344 end
345
346
347
348 %=============================================================================
349 % Equations
350 %
351 equations
352
353     % Stack voltage
354     v == N_cell * (v_nernst + v_ohm + v_act_diff);
355
356
357     % Heat generated
358     -Q ==  power_dissipated; % ORIGINAL VERSION
359     %-Q == N_cell*(v_nernst + v_ohm + v_act_diff - E_cell)*i_cell * ...
            area_cell % MODIFIED VERSION
360
361     % Equate water vapor mass flow rates at GDL and membrane
362     % to solve for relative humidity at ACL and CCL
363     nflux_H2O_A * MW_H2O * area_cell * N_cell == H2O_transport + ...
            H2O_consumed;
364     nflux_H2O_C * MW_H2O * area_cell * N_cell == H2O_transport;
365
366     % Through variables for removal of water at port H2O
367     mdot_H2O == H2O_consumed + H2O_transport;
368     Phi_H2O == mdot_H2O*h_H2O;
369
370     % Assign mass flow rate to internal trace gas source and ...
            moisture source blocks
371     % to model mass consumption/generation due to reaction and ...
            water transport
372     source_O2_A.M     == O2_produced;
373     source_H2_C.M     == H2_produced;
374     transport_H2O_C.M == H2O_transport;
375
376     source_O2_A.T     == T_stack;
377     source_H2_C.T     == T_stack;
378     transport_H2O_C.T == T_stack;
379
380     vnernst == v_nernst;
381     vohm == v_ohm;
382     vact == v_act_diff;
383 end
```

```
384
385 % Internal components to add or remove mass at the anode and cathode
386 components (ExternalAccess = none)
387     % Anode trace gas source block for oxygen production
388     source_O2_A = ...
            foundation.moist_air.sources.moisture_trace_gas.controlled_trace_gas_source;
389     % Cathode trace gas source and moisture source blocks for ...
            hydrogen production and water transport
390     source_H2_C = ...
            foundation.moist_air.sources.moisture_trace_gas.controlled_trace_gas_source;
391     transport_H2O_C = ...
            foundation.moist_air.sources.moisture_trace_gas.controlled_moisture_source( ...
            ...
392          moisture_source_spec = ...
                foundation.enum.moisture_source_spec.liquid);
393 end
394
395 connections
396     connect(O2, source_O2_A.S)
397     connect(H2, source_H2_C.S, transport_H2O_C.S)
398 end
399
400 end
401
402
403
404 function lambda = membrane_water(a)
405 % Compute the water content of the membrane as a function of the water
406 % activity, assumed to be equal to the relative humidity. This ...
        function is
407 % based on fits to FEA simulations.
408 %
409 % See: Dutta, et.al., Numerical prediction of mass-exchange between
410 % cathode and anode channels in a PEM fuel cell. (Equation 16)
411
412 definitions
413     lambda = ...
414         if lt(a, 0), ...
415             0.043 + 17.81*a ...
416         elseif le(a, 1), ...
417             0.043 + 17.81*a - 39.85*a^2 + 36*a^3 ...
418         else ...
419             14.003 + 1.4*(a - 1) ...
420         end;
421 end
422
423 end
```

Annex B - Parameters of the MATLAB Simulink model

```
%% Code to define parameters for ssc_electrolyzer
% Open Model Workspace in the Model Explorer to view and modify ...
    parameter
% values. Click 'Reinitialize from Source' to reset to the ...
    parameter values
% in this script.

% Copyright 2021 The MathWorks, Inc.

% Environment conditions
env_p = 0.101325; % [MPa] Pressure
env_T = 20; % [degC] Temperature

% Example solar power profile over 24 hr
solar_profile_time = (0:23)' * 3600; % s
solar_profile_power = [0 0 0 0 0 0 0.572 13.1 44.9 74.5 96.4 100 ...
    97.5 89.5 65.8 34.0 7.61 0 0 0 0 0 0 0]'; % kW

% Fuel cell stack
stack_num_cells = 50*5; % [-] Number cells
stack_area = 1000; % [cm^2] Cell area
stack_t_membrane = 125; % [um] Membrane thickness
stack_t_gdl_A = 25; % [um] Anode gas diffusion layer thickness
stack_t_gdl_C = 250; % [um] Cathode gas diffusion layer thickness
stack_t_CL = 2000; %[um] bipolar plate --------------- ADDITION
stack_w_channels = 2; % [cm] Gas channel width and height
stack_num_channels = 8*2; % [-] Number of gas channels per cell
stack_io = 1e-04; % [A/cm^2] Exchange current density
stack_alpha = 0.7; % [-] Charge transfer coefficient
stack_D_gdl_A = 0.07; % [cm^2/s] Water diffusivity in anode GDL
stack_D_gdl_C = 0.07; % [cm^2/s] Water diffusivity in cathode GDL
stack_membrane_rho = 2000; % [kg/m^3] Density of dry membrane
stack_membrane_MW = 1.1; % [kg/mol] Equivalent weight of dry membrane
stack_mea_rho = 1051; % [kg/s] MODIFIED Overall density of membrane ...
    electrode assembly (1980*125+1000*(25+250+2000))/(125+25+250+2000)
stack_mea_cp = 1552; % [J/(kg*K)] Overall specific heat of membrane ...
    electrode assembly ...
```

```
    (833*125*1980+2000*275*1000+1580*2000*1000)/((125+25+250+2000)*1051)

water_pipe_D = 0.1; % m
gas_pipe_D = 0.1; % m

% Heat exchanger dimensions
exchanger_L = 1; % [m] Overall radiator length
exchanger_W = 0.3; % [m] Overall radiator width
exchanger_H = 0.5; % [m] Overal radiator height
exchanger_N_tubes = 25; % [-] Number of coolant tubes
exchanger_tube_H = 0.0015; % [m] Height of each coolant tube
exchanger_fin_spacing = 0.002; % [-] Fin spacing
exchanger_eta_fin = 0.7; % [-] Fin efficiency

exchanger_gap_H = (exchanger_H - ...
    exchanger_N_tubes*exchanger_tube_H) / (exchanger_N_tubes - 1); % ...
    [m] Height between coolant tubes
exchanger_air_area_primary = 2 * (exchanger_N_tubes - 1) * ...
    exchanger_W * (exchanger_L + exchanger_gap_H); % [m^2] Primary ...
    air heat transfer surface area
exchanger_N_fins = (exchanger_N_tubes - 1) * exchanger_L / ...
    exchanger_fin_spacing; % [-] Total number of fins
exchanger_air_area_fins = 2 * exchanger_N_fins * exchanger_W * ...
    exchanger_gap_H; % [m^2] Total fin surface area
exchanger_tube_Leq = 2*(exchanger_H + ...
    20*exchanger_tube_H*exchanger_N_tubes); % [m] Additional ...
    equivalent tube length for losses due to manifold and splits

% Hydrogen property tables
H2_R = 4124.48151675695; % [J/(kg*K)] Specific gas constant
H2_T = [-56.55, -50:10:-10, -5:1:5, 10:10:350]; % [degC] ...
    Temperature vector
H2_h = [2783.66044045879, 2873.94181645932, 3012.62601981068, ...
    3152.22537301871, 3292.62486344326, 3433.72138359680, ...
    3504.50184295996, 3518.67512520997, 3532.85394543712, ...
    3547.03822323045, 3561.22787913325, 3575.42283463482, ...
    3589.62301216223, 3603.82833507219, 3618.03872764290, ...
    3632.25411506595, 3646.47442343830, 3717.64725530348, ...
    3860.32198734890, 4003.38288163040, 4146.77354613486, ...
    4290.44463593559, 4434.35318483605, 4578.46197843019, ...
    4722.73896833090, 4867.15672726297, 5011.69194456718, ...
    5156.32496143709, 5301.03934494342, 5445.82149962224, ...
    5590.66031514150, 5735.54684833147, 5880.47403768083, ...
    6025.43644826542, 6170.43004499140, 6315.45199199528, ...
    6460.50047604533, 6605.57455182556, 6750.67400704912, ...
    6895.79924543541, 7040.95118568927, 7186.13117473630, ...
    7331.34091359044, 7476.58239435534, 7621.85784698693, ...
    7767.16969456766, 7912.52051596217, 8057.91301483815, ...
    8203.34999414341, 8348.83433523064, 8494.36898091475, ...
    8639.95692183309]; % [kJ/kg] Specific enthalpy vector
H2_mu = [7.13280985169147, 7.28192581803172, 7.50683010986396, ...
    7.72860158311813, 7.94743907374985, 8.16352107178216, ...
```

```
      8.27057966039486, 8.29191522386247, 8.31322574339419, ...
      8.33451136221049, 8.35577222214406, 8.37700846365822, ...
      8.39822022586488, 8.41940764654233, 8.44057086215268, ...
      8.46171000785900, 8.48282521754219, 8.58804682376172, ...
      8.79676834158601, 9.00329345223078, 9.20773222364170, ...
      9.41018554308578, 9.61074613691738, 9.80949945111700, ...
      10.0065244149257, 10.2018941058184, 10.3956763308132, ...
      10.5879341365094, 10.7787262581519, 10.9681075163184, ...
      11.1561291684380, 11.3428392212160, 11.5282827091027, ...
      11.7125019431712, 11.8955367341236, 12.0774245926121, ...
      12.2582009096067, 12.4378991191677, 12.6165508456572, ...
      12.7941860371557, 12.9708330866186, 13.1465189421111, ...
      13.3212692072909, 13.4951082331655, 13.6680592020247, ...
      13.8401442043429, 14.0113843093520, 14.1817996299056, ...
      14.3514093821846, 14.5202319407340, 14.6882848892642, ...
      14.8555850676093]; % [uPa*s] Dynamic viscosity vector
H2_k = [142.834673487453, 146.602208511061, 152.236222042957, ...
      157.732550941948, 163.097652939664, 168.338595936873, ...
      170.914793442425, 171.426608923333, 171.937300226766, ...
      172.446874689218, 172.955339634979, 173.462702374715, ...
      173.968970204106, 174.474150402550, 174.978250231913, ...
      175.481276935350, 175.983237736166, 178.477304495221, ...
      183.389581255575, 188.206454189023, 192.934525090876, ...
      197.580042887656, 202.148890500710, 206.646585109232, ...
      211.078287130673, 215.448814629342, 219.762660868078, ...
      224.024013435935, 228.236773894856, 232.404577248187, ...
      236.530810785993, 240.618632037420, 244.670985680918, ...
      248.690619345047, 252.680098287219, 256.641818973249, ...
      260.578021602720, 264.490801638200, 268.382120402950, ...
      272.253814814231, 276.107606318911, 279.945109095949, ...
      283.767837587053, 287.577213413001, 291.374571728986, ...
      295.161167068166, 298.938178718576, 302.706715674597, ...
      306.467821200562, 310.222477040649, 313.971607306067, ...
      317.716082067666]; % [mW/(m*K)] Thermal conductivity vector
H2_D = 74; % [mm^2/s] Diffusivity

% Oxygen property tables
O2_R = 259.836612622973; % [J/(kg*K)] Specific gas constant
O2_T = [-56.55, -50:10:-10, -5:1:5, 10:10:350]; % [degC] ...
      Temperature vector
O2_h = [196.314045635230, 202.302438242727, 211.445560194021, ...
      220.590899228792, 229.740231593225, 238.895348952500, ...
      243.475641264001, 244.391947430149, 245.308340402054, ...
      246.224821996439, 247.141394030059, 248.058058319568, ...
      248.974816681386, 249.891670931563, 250.808622885637, ...
      251.725674358497, 252.642827164235, 257.230174605453, ...
      266.413508632715, 275.609852765421, 284.820965750972, ...
      294.048557917965, 303.294277512928, 312.559698673577, ...
      321.846311315623, 331.155513043735, 340.488603075706, ...
      349.846778083808, 359.231129801281, 368.642644208585, ...
      378.082202097877, 387.550580810768, 397.048456949970, ...
      406.576409877154, 416.134925824813, 425.724402467528, ...
```

```
      435.345153816409, 444.997415318718, 454.681349062211, ...
      464.397049000008, 474.144546126762, 483.923813550211, ...
      493.734771414086, 503.577291638585, 513.451202453549, ...
      523.356292706982, 533.292315937896, 543.258994207727, ...
      553.256021688858, 563.283068012223, 573.339781378746, ...
      583.425791441447]; % [kJ/kg] Specific enthalpy vectdor
64 O2_mu = [15.7665575307288, 16.1727626078850, 16.7849249433608, ...
      17.3877315055497, 17.9815180942032, 18.5666055809413, ...
      18.8559834763191, 18.9136105724852, 18.9711555251620, ...
      19.0286186248432, 19.0860001606775, 19.1433004204737, ...
      19.2005196907073, 19.2576582565260, 19.3147164017561, ...
      19.3716944089079, 19.4285925591820, 19.7118952084836, ...
      20.2726692662067, 20.8258892364295, 21.3718096794610, ...
      21.9106736606882, 22.4427133237112, 22.9681504449081, ...
      23.4871969666892, 24.0000555077772, 24.5069198496509, ...
      25.0079753988870, 25.5033996255713, 25.9933624782616, ...
      26.4780267762054, 26.9575485796604, 27.4320775392600, ...
      27.9017572254189, 28.3667254387956, 28.8271145028300, ...
      29.2830515393565, 29.7346587282699, 30.1820535521826, ...
      30.6253490269743, 31.0646539190931, 31.5000729504200, ...
      31.9317069914666, 32.3596532436319, 32.7840054111974, ...
      33.2048538637040, 33.6222857893065, 34.0363853396718, ...
      34.4472337669430, 34.8549095532629, 35.2594885333161, ...
      35.6610440103170]; % [uPa*s] Dynamic viscosity vector
65 O2_k = [19.6661951881093, 20.2224765128182, 21.0645207724504, ...
      21.8980296960484, 22.7232456337983, 23.5404090717681, ...
      23.9460452976483, 24.0269406552993, 24.1077592592045, ...
      24.1885013406030, 24.2691671301751, 24.3497568580346, ...
      24.4302707537208, 24.5107090461917, 24.5910719638169, ...
      24.6713597343701, 24.7515725850235, 25.1515209478718, ...
      25.9459275198455, 26.7331962712293, 27.5135401678269, ...
      28.2871691203210, 29.0542797087419, 29.8150645640764, ...
      30.5697094830221, 31.3183935589296, 32.0612893462030, ...
      32.7985630478626, 33.5303747183955, 34.2568784758844, ...
      34.9782227188418, 35.6945503442869, 36.4059989644644, ...
      37.1127011202719, 37.8147844899821, 38.5123720922485, ...
      39.2055824826964, 39.8945299436419, 40.5793246666704, ...
      41.2600729279479, 41.9368772562485, 42.6098365937651, ...
      43.2790464498297, 43.9445990477190, 44.6065834647486, ...
      45.2650857658856, 45.9201891311213, 46.5719739768538, ...
      47.2205180715361, 47.8658966458414, 48.5081824975986, ...
      49.1474460917422]; % [mW/(m*K)] Thermal conductivity vector
66 O2_D = 18; % [mm^2/s] Diffusivity
67
68 % Nitrogen property tables
69 N2_R = 296.802103844292; % [J/(kg*K)] Specific gas constant
70 N2_T = [-56.55, -50:10:-10, -5:1:5, 10:10:350]; % [degC] ...
      Temperature vector
71 N2_h = [224.312019475783, 231.141016528663, 241.564116974996, ...
      251.984329606098, 262.402210767198, 272.818266126753, ...
      278.025759131002, 279.067222480148, 280.108675169779, ...
      281.150117667373, 282.191550440608, 283.232973957487, ...
```

```
      284.274388686473, 285.315795096618, 286.357193657682, ...
      287.398584840260, 288.439969115894, 293.646803474573, ...
      304.060229225710, 314.473742203777, 324.887858161051, ...
      335.303123493654, 345.720119003427, 356.139461810715, ...
      366.561805672305, 376.987839945795, 387.418287430292, ...
      397.853901301030, 408.295461341278, 418.743769658649, ...
      429.199646054884, 439.663923199077, 450.137441734658, ...
      460.621045430963, 471.115576471389, 481.621870952319, ...
      492.140754650669, 502.673039103050, 513.219518026408, ...
      523.780964098585, 534.358126107445, 544.951726469054, ...
      555.562459108678, 566.190987693008, 576.837944197865, ...
      587.503927792527, 598.189504019663, 608.895204248440, ...
      619.621525377624, 630.368929765337, 641.137845362314, ...
      651.928666026144]; % [kJ/kg] Specific enthalpy vector
72 N2_mu = [13.7948920665312, 14.1367187351510, 14.6513506072199, ...
      15.1575394445859, 15.6556177860831, 16.1459023391225, ...
      16.3882166949119, 16.4364580271216, 16.4846261830610, ...
      16.5327214469937, 16.5807441017456, 16.6286944287114, ...
      16.6765727078615, 16.7243792177482, 16.7721142355126, ...
      16.8197780368914, 16.8673708962236, 17.1042805670559, ...
      17.5729330929829, 18.0349108462106, 18.4904598524977, ...
      18.9398140034241, 19.3831957199835, 19.8208165930053, ...
      20.2528779961256, 20.6795716689317, 21.1010802692360, ...
      21.5175778943589, 21.9292305719283, 22.3361967211248, ...
      22.7386275855675, 23.1366676391963, 23.5304549665897, ...
      23.9201216191847, 24.3057939488592, 24.6875929202991, ...
      25.0656344035241, 25.4400294478834, 25.8108845387614, ...
      26.1783018381670, 26.5423794103038, 26.9032114331518, ...
      27.2608883970194, 27.6154972909606, 27.9671217778900, ...
      28.3158423591670, 28.6617365293689, 29.0048789219164, ...
      29.3453414461711, 29.6831934165754, 30.0185016743671, ...
      30.3513307023604]; % [uPa*s] Dynamic viscosity vector
73 N2_k = [19.6296532607374, 20.1533289725195, 20.9436243615696, ...
      21.7231523445233, 22.4923063139090, 23.2514823266989, ...
      23.6274403302585, 23.7023472871786, 23.7771601872884, ...
      23.8518793809024, 23.9265052168265, 24.0010380423605, ...
      24.0754782033001, 24.1498260439393, 24.2240819070729, ...
      24.2982461339996, 24.3723190645241, 24.7413260601341, ...
      25.4726839899413, 26.1954347636057, 26.9098870600572, ...
      27.6163358040134, 28.3150627088262, 29.0063368423447, ...
      29.6904152006066, 30.3675432785589, 31.0379556302294, ...
      31.7018764131555, 32.3595199136277, 33.0110910505971, ...
      33.6567858570436, 34.2967919382928, 34.9312889072676, ...
      35.5604487970156, 36.1844364511046, 36.8034098926428, ...
      37.4175206727930, 38.0269141997105, 38.6317300488700, ...
      39.2321022557508, 39.8281595918420, 40.4200258249072, ...
      41.0078199644172, 41.5916564930240, 42.1716455849090, ...
      42.7478933117983, 43.3205018373934, 43.8895696009277, ...
      44.4551914905138, 45.0174590069098, 45.5764604182929, ...
      46.1322809065919]; % [mW/(m*K)] Thermal conductivity vector
```

Annex C - Rough analyses of 5.2 Dynamic analysis

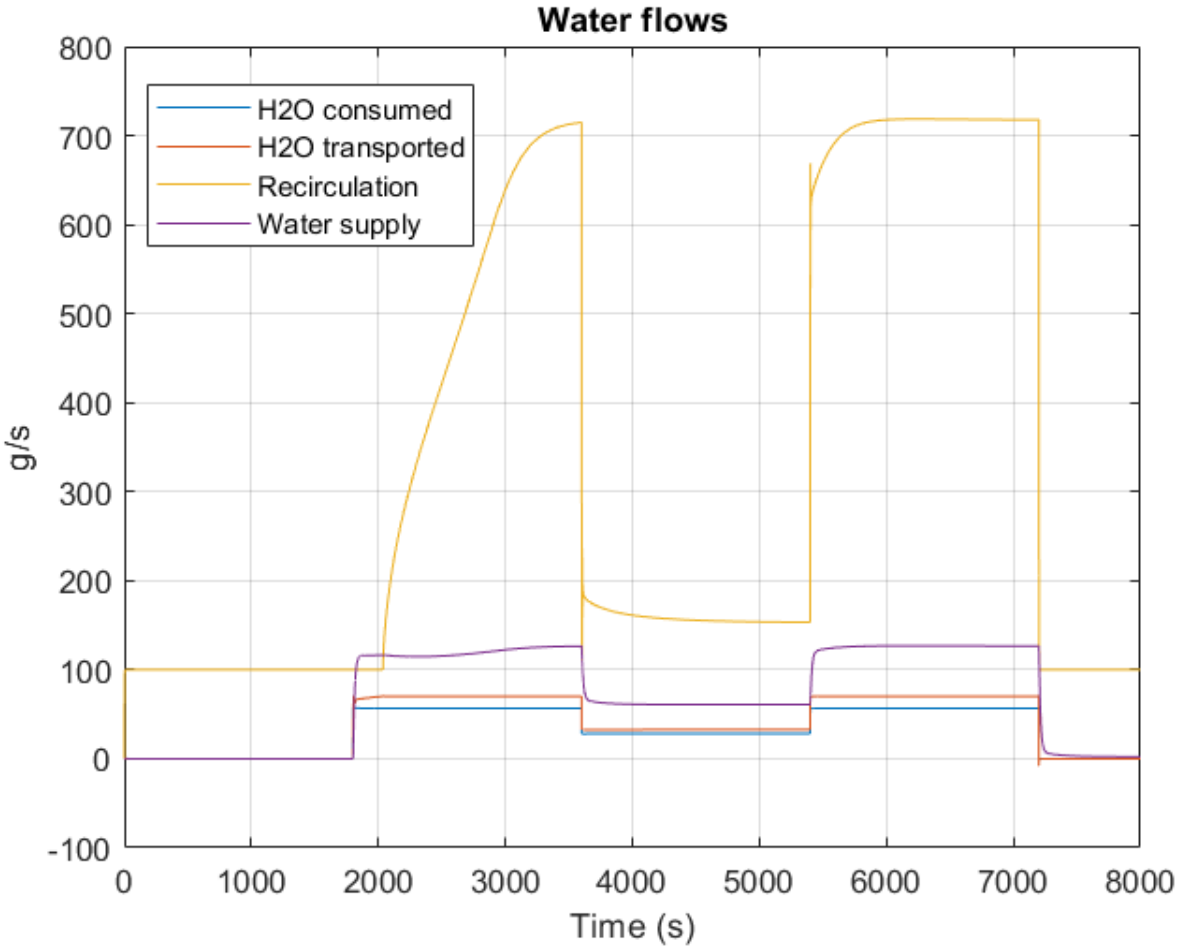

Figure 7.1: Water analysis. From model.

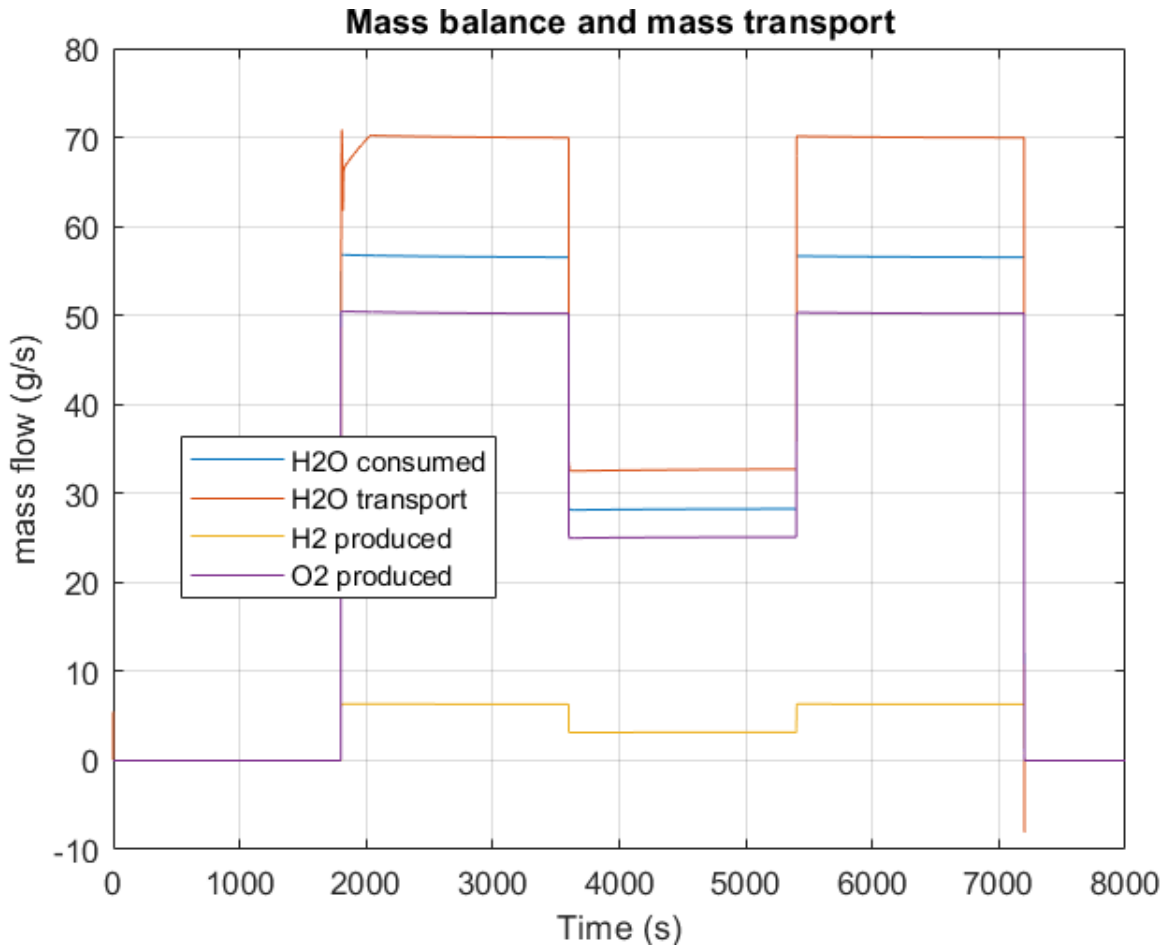

Figure 7.2: Mass analysis. From model.

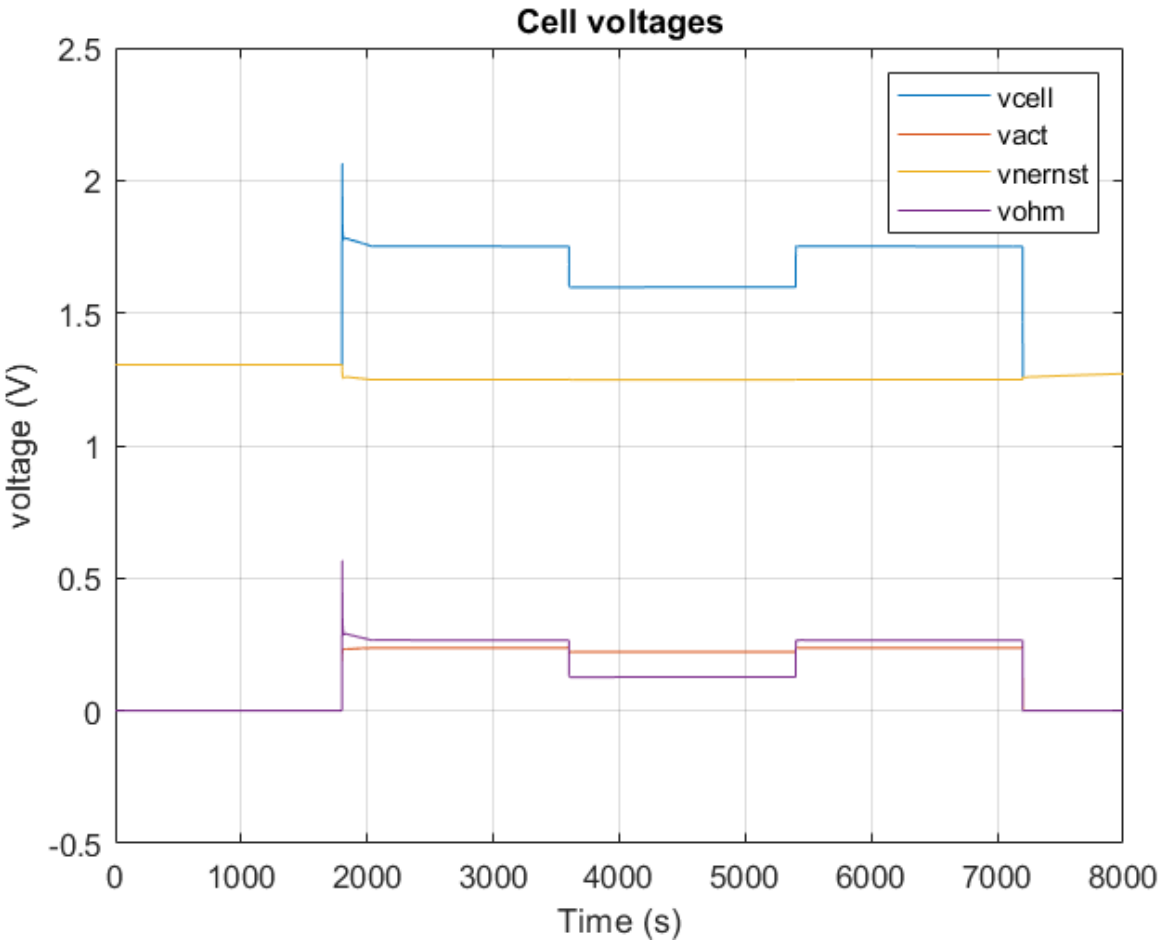

Figure 7.3: Voltage analysis. From model.

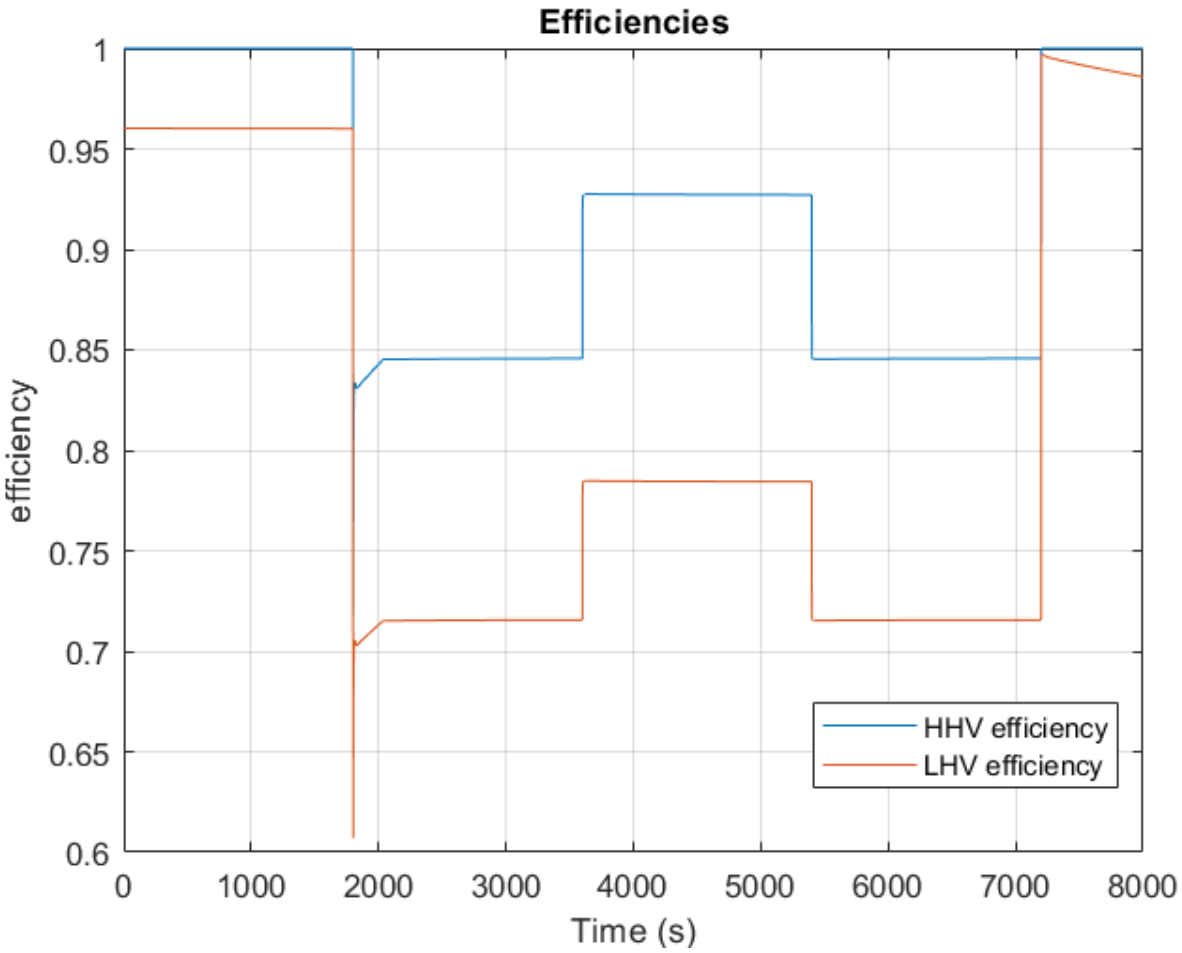

Figure 7.4: Efficiency analysis. From model.

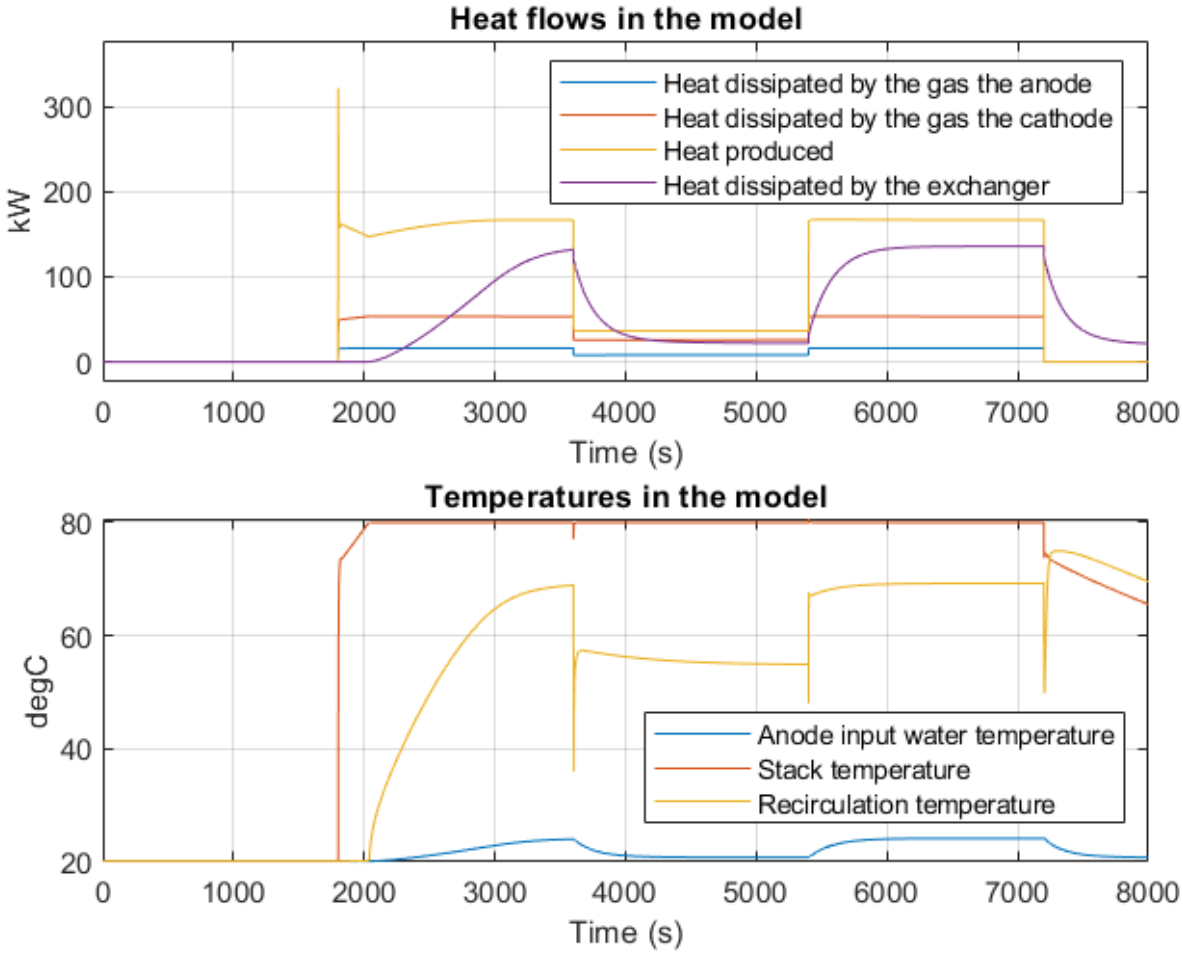

Figure 7.5: Heat analysis. From model.

Annex D - Other analyses of the supply of FCR

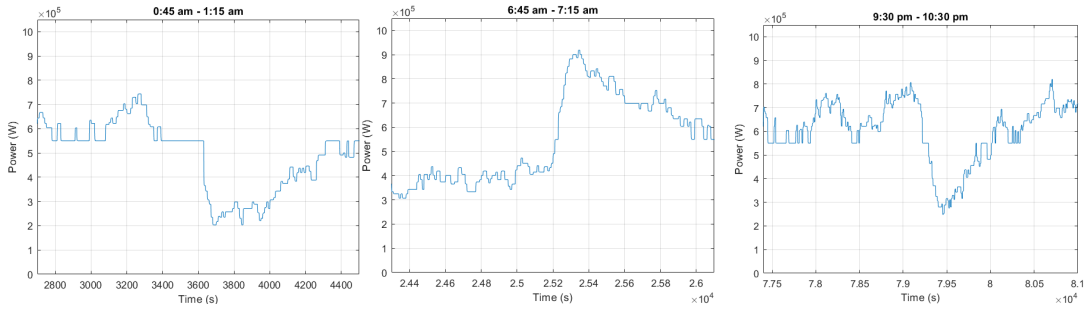

(a) (b) (c)

Figure 7.6: Three other time periods.

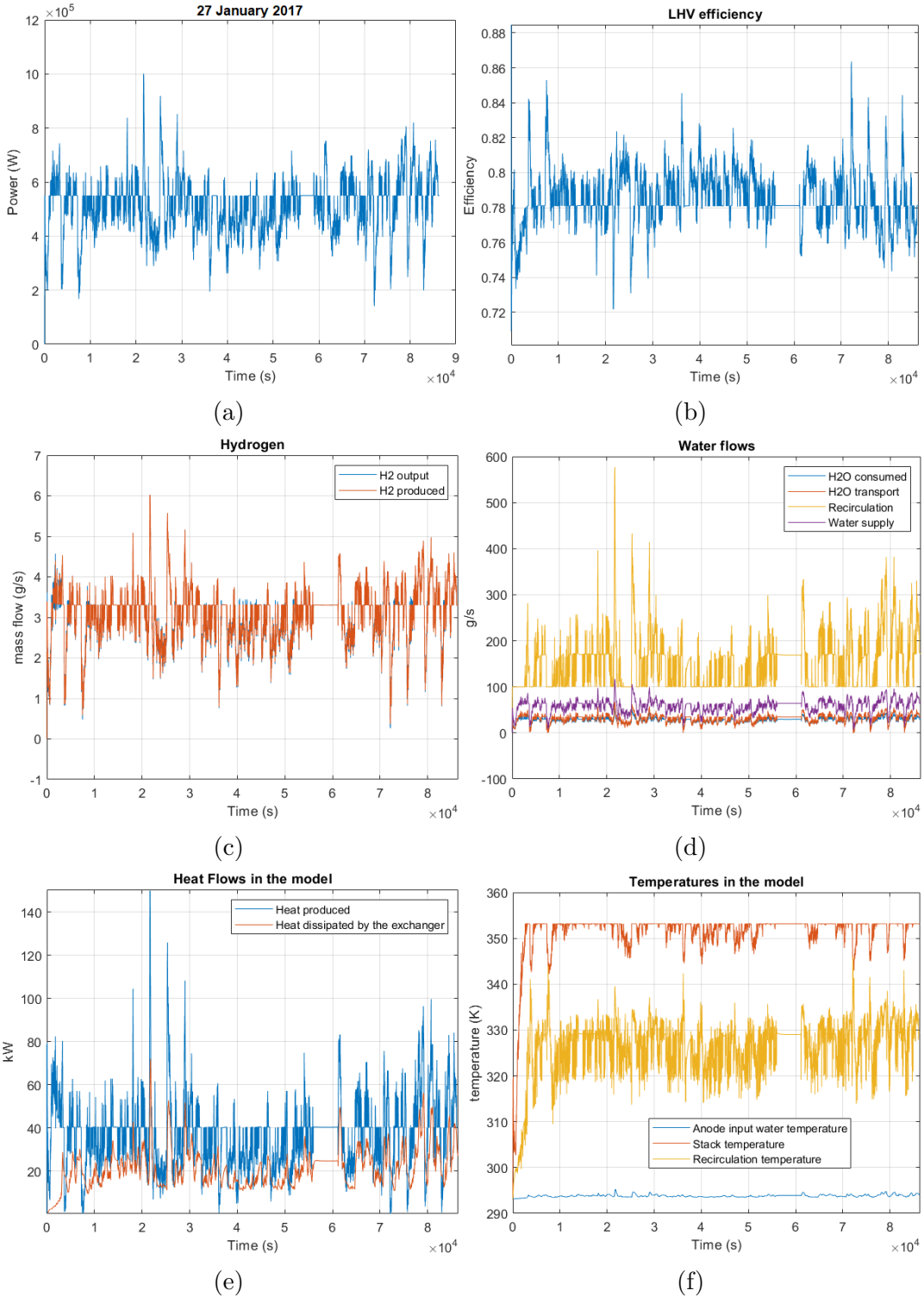

Figure 7.7: Global analysis of the day providing FCR.

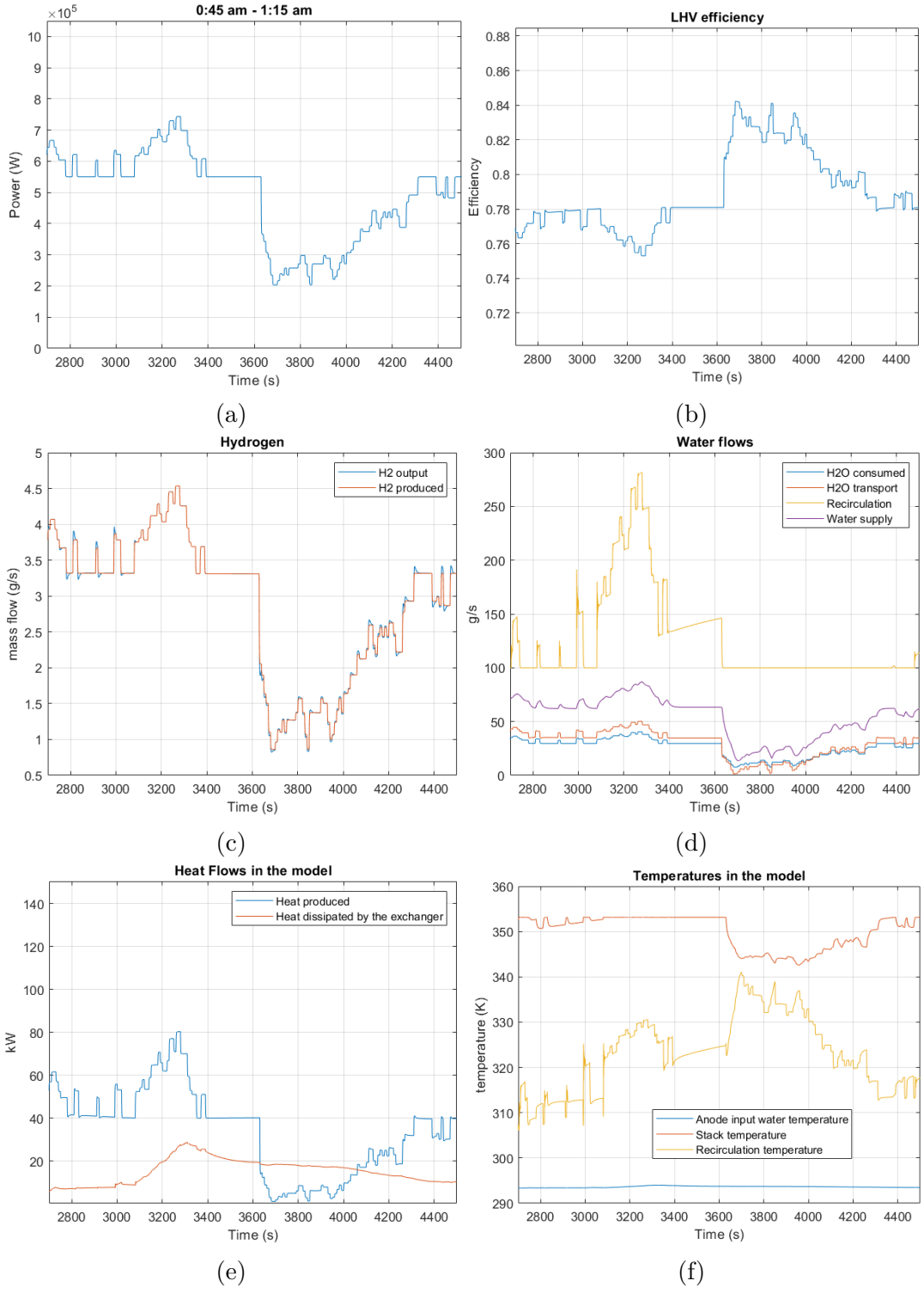

Figure 7.8: First annex time period.

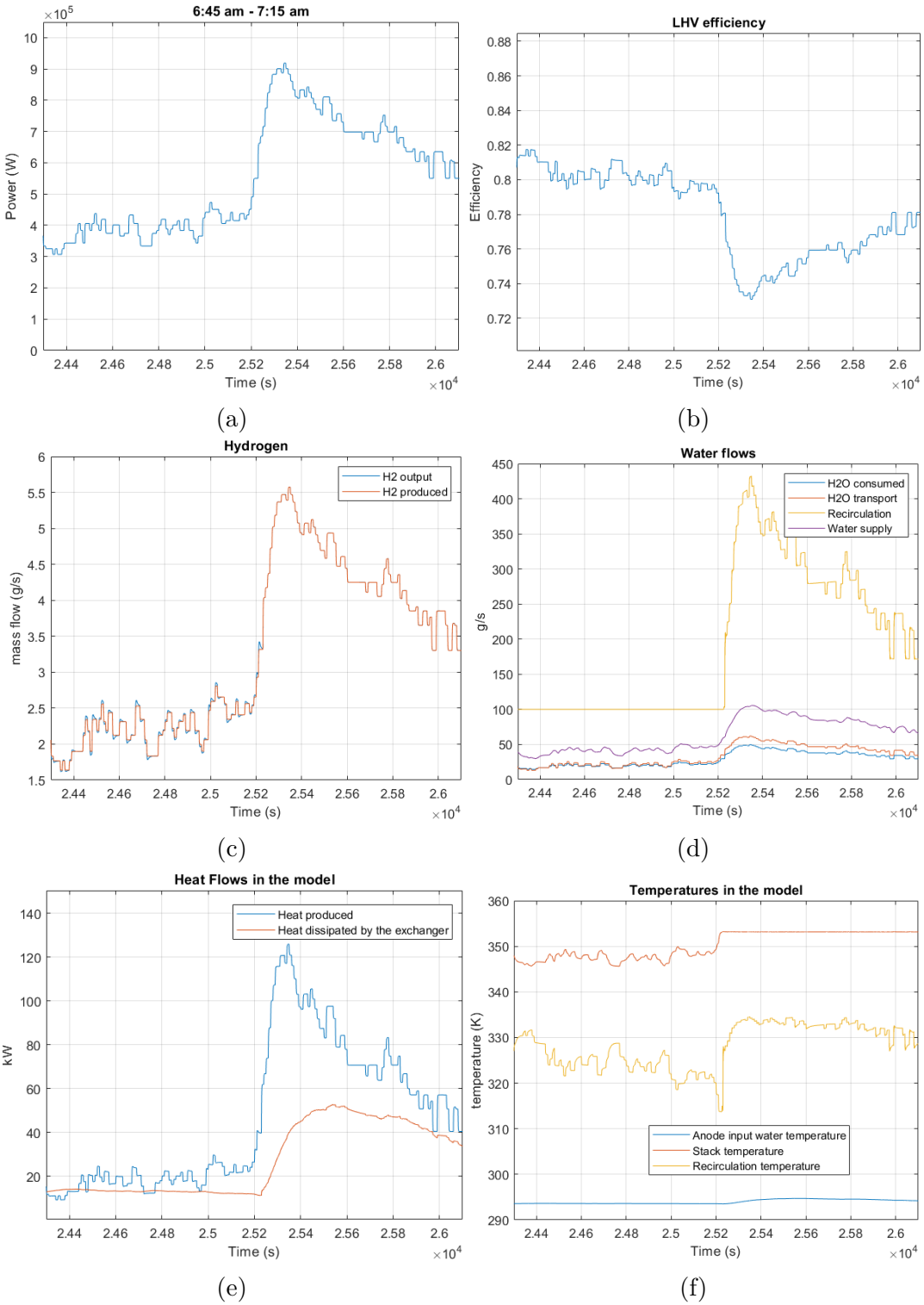

Figure 7.9: Second annex time period.

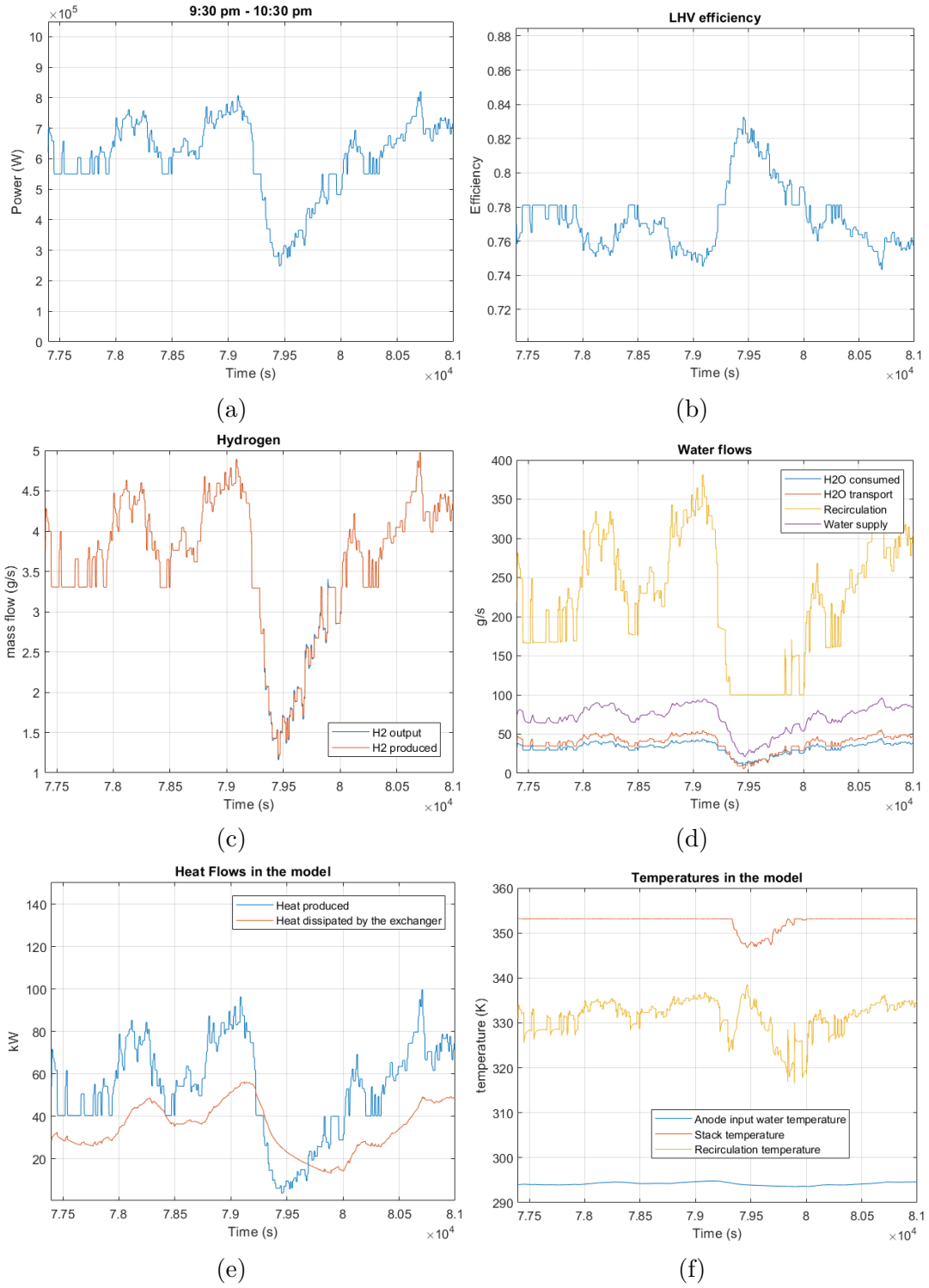

Figure 7.10: Third annex time period.

Bibliography

[1] Grzegorz Pawelec, Matus Muron, Johan Bracht, Bastien Bonnet-Cantalloube, Alexandru Floristean, and Nicolas Brahy. Clean hydrogen monitor. 2020.

[2] Aurora. Enabling the european hydrogen economy - report, May 2021.

[3] Grzegorz Pawelec, Matus Muron, Joana Fonseca, and Alexandru Floristean. Clean hydrogen monitor. 2021.

[4] European commission. Communication from the commission to the european parliament, the european council, the council, the european economic and social committee and the committee of the regions - repowereu plan, 18 May 2022.

[5] Wikipedia. Polymer electrolyte membrane electrolysis. `http://en.wikipedia.org/w/index.php?title=Polymer\%20electrolyte\%20membrane\%20electrolysis&oldid=1103230260`, 2022.

[6] S Shiva Kumar and V Himabindu. Hydrogen production by pem water electrolysis–a review. *Materials Science for Energy Technologies*, 2(3):442–454, 2019.

[7] Emmanuel De Jaeger. Lelec2595 - electrical power systems dynamics, 2022.

[8] ENTSO-E WGAS. Annual report 2020 edition. `https://annualreport2020.entsoe.eu/wp-content/uploads/2021/07/entso-e_AR2020.pdf`, 2020.

[9] Pieter Tielens and Dirk Van Hertem. The relevance of inertia in power systems. *Renewable and Sustainable Energy Reviews*, 55:999–1009, 2016.

[10] L Allidières, A Brisse, P Millet, S Valentin, and M Zeller. On the ability of pem water electrolysers to provide power grid services. *International Journal of Hydrogen Energy*, 44(20):9690–9700, 2019.

[11] Denis THOMAS. State of play and developments of power-to-hydrogen technologies. `https://etipwind.eu/wp-content/uploads/A2-Hydrogenics_v2.pdf`, 2019.

[12] Ángel Hernández-Gómez, Victor Ramirez, and Damien Guilbert. Investigation of pem electrolyzer modeling: Electrical domain, efficiency, and specific energy consumption. *International Journal of Hydrogen Energy*, 45(29):14625–14639, 2020.

[13] Øystein Ulleberg. Stand-alone power systems for the future: optimal design, operation and control of solar-hydrogen energy systems. 1998.

[14] Bart W Tuinema, Ebrahim Adabi, Patrick KS Ayivor, Víctor García Suárez, Lian Liu, Arcadio Perilla, Zameer Ahmad, José Luis Rueda Torres, Mart AMM van der Meijden, and Peter Palensky. Modelling of large-sized electrolysers for real-time simulation and study of the possibility of frequency support by electrolysers. *IET Generation, Transmission & Distribution*, 14(10):1985–1992, 2020.

[15] Damien Guilbert and Gianpaolo Vitale. Dynamic emulation of a pem electrolyzer by time constant based exponential model. *Energies*, 12(4):750, 2019.

[16] Simon Bourne. Itm power 100mw electrolyser. `https://www.youtube.com/watch?v=eku0GuSKiIc&t=612s&ab_channel=H2FCHannover`, 2017.

[17] M Maier, K Smith, J Dodwell, G Hinds, PR Shearing, and DJL Brett. Mass transport in pem water electrolysers: A review. *International Journal of Hydrogen Energy*, 2021.

[18] Francesco Marangio, Massimo Santarelli, and Michele Calì. Theoretical model and experimental analysis of a high pressure pem water electrolyser for hydrogen production. *International journal of hydrogen energy*, 34(3):1143–1158, 2009.

[19] Nel Hydrogen. The world's most efficient and reliable electrolysers. `https://nelhydrogen.com/wp-content/uploads/2020/03/Electrolysers-Brochure-Rev-D.pdf`, 2021.

[20] Vincenzo Liso, Giorgio Savoia, Samuel Simon Araya, Giovanni Cinti, and Soren Knudsen Kaer. Modelling and experimental analysis of a polymer electrolyte membrane water electrolysis cell at different operating temperatures. *Energies*, 11(12):3273, 2018.

[21] Manuel Espinosa-López, Christophe Darras, Philippe Poggi, Raynal Glises, Philippe Baucour, André Rakotondrainibe, Serge Besse, and Pierre Serre-Combe. Modelling and experimental validation of a 46 kw pem high pressure water electrolyzer. *Renewable energy*, 119:160–173, 2018.

[22] Alexander Buttler and Hartmut Spliethoff. Current status of water electrolysis for energy storage, grid balancing and sector coupling via power-to-gas and power-to-liquids: A review. *Renewable and Sustainable Energy Reviews*, 82:2440–2454, 2018.

[23] Pierre Olivier. *Modélisation et analyse du comportement dynamique d'un système d'électrolyse PEM soumis à des sollicitations intermittentes: Approche Bond Graph.* PhD thesis, Lille 1, 2016.

[24] J Eichman, K Harrison, and Michael Peters. Novel electrolyzer applications: providing more than just hydrogen. Technical report, National Renewable Energy Lab.(NREL), Golden, CO (United States), 2014.

[25] Fuel Cells and Hydrogen Joint Undertaking. State-of-the-art and future targets (kpis). `https://www.fch.europa.eu/soa-and-targets`, 2017.

[26] Hydrogen Joint Undertaking. Multi-annual work plan. *Integration*, 1(2):35, 2014.

[27] Marcelo Carmo, David L Fritz, Jürgen Mergel, and Detlef Stolten. A comprehensive review on pem water electrolysis. *International journal of hydrogen energy*, 38(12):4901–4934, 2013.

[28] Ángel Hernández-Gómez, Victor Ramirez, Damien Guilbert, and Belem Saldivar. Cell voltage static-dynamic modeling of a pem electrolyzer based on adaptive parameters: Development and experimental validation. *Renewable Energy*, 163:1508–1522, 2021.

[29] Zainul Abdin, Ali Zafaranloo, Ahmad Rafiee, Walter Mérida, Wojciech Lipiński, and Kaveh R Khalilpour. Hydrogen as an energy vector. *Renewable and sustainable energy reviews*, 120:109620, 2020.

[30] Arash E Samani, Anna D'Amicis, Jeroen DM De Kooning, Dimitar Bozalakov, Paolo Silva, and Lieven Vandevelde. Grid balancing with a large-scale electrolyser providing primary reserve. *IET Renewable Power Generation*, 14(16):3070–3078, 2020.

[31] FRC ENTSO-e. Frequency containment reserves (fcr), 2017.

[32] Mohamed H Albadi and Ehab F El-Saadany. A summary of demand response in electricity markets. *Electric power systems research*, 78(11):1989–1996, 2008.

[33] Víctor García Suárez, Patrick Ayivor, Jose Rueda Torres, and Mart van der Meijden. Demand side response in multi-energy sustainable systems to support power system stability. In *16th Wind Integration Workshop*, pages 1–6. Energynautics GmbH, 2017.

[34] Freedonia Group. World hydrogen – industry study with forecasts for 2018 and 2023, study 3165, 2014.

[35] National Research Council et al. *The hydrogen economy: opportunities, costs, barriers, and R&D needs*. National Academies Press, 2004.

[36] European commission. Crepowereu: A plan to rapidly reduce dependence on russian fossil fuels and fast forward the green transition, 18 May 2022.

[37] Rodney L LeRoy, Christopher T Bowen, and Donald J LeRoy. The thermodynamics of aqueous water electrolysis. *Journal of the Electrochemical Society*, 127(9):1954, 1980.

[38] DS Falcão and AMFR Pinto. A review on pem electrolyzer modelling: Guidelines for beginners. *Journal of Cleaner Production*, 261:121184, 2020.

[39] Caroline Rozain. *Développement de nouveaux matériaux d'électrodes pour la production d'hydrogène par électrolyse de l'eau*. PhD thesis, Paris 11, 2013.

[40] Amin Mohammadi and Mehdi Mehrpooya. A comprehensive review on coupling different types of electrolyzer to renewable energy sources. *Energy*, 158:632–655, 2018.

[41] Fuel Cells and Hydrogen Joint Undertaking. Cost reduction and performance increase of pem electrolysers. `https://www.fch.europa.eu/sites/default/files/Nov22_Session3_Panel%205_Slot%202_NOVEL-MEGASTACK_Thomassen%20%28ID%202891376%29.pdf`, 2016.

[42] ENTSO-E WGAS. Survey on ancillary services procurement, balancing market design 2017. `https://docstore.entsoe.eu/Documents/Publications/Market%20Committee%20publications/ENTSO-E_AS_survey_2017.pdf`, 2018.

[43] Inertia entsoe. The inertia challenge in europe – present and long-term perspective insight report, January 2021.

[44] Frans Van Hulle, Iván Pineda, and Paul Wilczek. Economic grid support services by wind and solar pv, September 2014.

[45] Jan Machowski, Zbigniew Lubosny, Janusz W Bialek, and James R Bumby. *Power system dynamics: stability and control*. John Wiley & Sons, 2020.

[46] Pierluigi Mancarella, S Puschel, L Zhang, H Wang, M Brear, T Jones, M Jeppesen, R Batterham, R Evans, and I Mareels. Power system security assessment of the future national electricity market. *University of Melbourne*, 2017.

[47] Robert Eriksson, Niklas Modig, and Katherine Elkington. Synthetic inertia versus fast frequency response: a definition. *IET Renewable Power Generation*, 12(5):507–514, 2018.

[48] Pierre Olivier, Cyril Bourasseau, and Pr Belkacem Bouamama. Low-temperature electrolysis system modelling: A review. *Renewable and Sustainable Energy Reviews*, 78:280–300, 2017.

[49] Burin Yodwong, Damien Guilbert, Melika Hinaje, Matheepot Phattanasak, Wattana Kaewmanee, and Gianpaolo Vitale. Proton exchange membrane electrolyzer emulator for power electronics testing applications. *Processes*, 9(3):498, 2021.

[50] Øystein Ulleberg. Modeling of advanced alkaline electrolyzers: a system simulation approach. *International journal of hydrogen energy*, 28(1):21–33, 2003.

[51] NV Dale, MD Mann, and H Salehfar. Semiempirical model based on thermodynamic principles for determining 6 kw proton exchange membrane electrolyzer stack characteristics. *Journal of Power Sources*, 185(2):1348–1353, 2008.

[52] CY Biaku, NV Dale, MD Mann, H Salehfar, AJ Peters, and T Han. A semiempirical study of the temperature dependence of the anode charge transfer coefficient of a 6 kw pem electrolyzer. *International journal of hydrogen energy*, 33(16):4247–4254, 2008.

[53] Kevin W Harrison, Eduardo Hernández-Pacheco, Michael Mann, and Hossein Salehfar. Semiempirical model for determining pem electrolyzer stack characteristics. 2006.

[54] Amitava Roy, Simon Watson, and David Infield. Comparison of electrical energy efficiency of atmospheric and high-pressure electrolysers. *International Journal of Hydrogen Energy*, 31(14):1964–1979, 2006.

[55] Guillaume Fontès. *Modélisation et caractérisation de la pile PEM pour l'étude des interactions avec les convertisseurs statiques*. PhD thesis, 2005.

[56] Thomas E Springer, TA Zawodzinski, and Shimshon Gottesfeld. Polymer electrolyte fuel cell model. *Journal of the electrochemical society*, 138(8):2334, 1991.

[57] Amin Nouri-Khorasani, Emile Tabu Ojong, Tom Smolinka, and David P Wilkinson. Model of oxygen bubbles and performance impact in the porous transport layer of pem water electrolysis cells. *International journal of hydrogen energy*, 42(48):28665–28680, 2017.

[58] Monica Sanchez, Ernesto Amores, Lourdes Rodriguez, and Carmen Clemente-Jul. Semi-empirical model and experimental validation for the performance evaluation of a 15 kw alkaline water electrolyzer. *International Journal of Hydrogen Energy*, 43(45):20332–20345, 2018.

[59] P Ayivor, J Torres, MAMM van der Meijden, R van der Pluijm, and B Stouwie. Modelling of large size electrolyzer for electrical grid stability studies in real time digital simulation. In *Proceedings of the 3rd International Hybrid Power Systems Workshop, Tenerife, Spain*, pages 8–9, 2018.

[60] Damien Guilbert and Gianpaolo Vitale. Improved hydrogen-production-based power management control of a wind turbine conversion system coupled with multistack proton exchange membrane electrolyzers. *Energies*, 13(5):1239, 2020.

[61] Burin Yodwong, Damien Guilbert, Matheepot Phattanasak, Wattana Kaewmanee, Melika Hinaje, and Gianpaolo Vitale. Ac-dc converters for electrolyzer applications: State of the art and future challenges. *Electronics*, 9(6):912, 2020.

[62] José Luis Monroy-Morales, Máximo Hernández-Angeles, David Campos-Gaona, Rafael Pena-Alzola, Martin Ordonez, and Walter Mérida. Modeling and control design of a vienna rectifier based electrolyzer. In *2016 IEEE 7th International Symposium on Power Electronics for Distributed Generation Systems (PEDG)*, pages 1–8. IEEE, 2016.

[63] Ángel Hernández-Gómez, Victor Ramirez, Damien Guilbert, and Belem Saldivar. Development of an adaptive static-dynamic electrical model based on input electrical energy for pem water electrolysis. *International Journal of Hydrogen Energy*, 45(38):18817–18830, 2020.

[64] Thomas G Wilson. The evolution of power electronics. *IEEE Transactions on Power electronics*, 15(3):439–446, 2000.

[65] Mengxing Chen, Shih-Feng Chou, Frede Blaabjerg, and Pooya Davari. Overview of power electronic converter topologies enabling large-scale hydrogen production via water electrolysis. *Applied Sciences*, 12(4):1906, 2022.

[66] Joonas Koponen, Anton Poluektov, Vesa Ruuskanen, Antti Kosonen, Markku Niemelä, and Jero Ahola. Comparison of thyristor and insulated-gate bipolar transistor-based power supply topologies in industrial water electrolysis applications. *Journal of Power Sources*, 491:229443, 2021.

[67] Julio José Caparrós Mancera, Francisca Segura Manzano, José Manuel Andújar, Francisco José Vivas, and Antonio José Calderón. An optimized balance of plant for a medium-size pem electrolyzer: design, control and physical implementation. *Electronics*, 9(5):871, 2020.

[68] Solar Energy Laboratory. *TRNSYS 17 - a TRaN sient S Ystem Simulation program - Volume 4 - Mathematical Reference*. University of Wisconsin-Madison, 2009.

[69] Rafael García-Valverde, Nieves Espinosa, and Antonio Urbina. Simple pem water electrolyser model and experimental validation. *international journal of hydrogen energy*, 37(2):1927–1938, 2012.

[70] ME Lebbal and Stéphane Lecœuche. Identification and monitoring of a pem electrolyser based on dynamical modelling. *International journal of hydrogen energy*, 34(14):5992–5999, 2009.

[71] H Ito, T Maeda, A Nakano, Y Hasegawa, N Yokoi, CM Hwang, M Ishida, A Kato, and T Yoshida. Effect of flow regime of circulating water on a proton exchange membrane electrolyzer. *International journal of hydrogen energy*, 35(18):9550–9560, 2010.

[72] Z Abdin, CJ Webb, and E MacA Gray. Modelling and simulation of a proton exchange membrane (pem) electrolyser cell. *International Journal of Hydrogen Energy*, 40(39):13243–13257, 2015.

[73] Kazuo Onda, Toshio Murakami, Takeshi Hikosaka, Misaki Kobayashi, and Kohei Ito. Performance analysis of polymer-electrolyte water electrolysis cell at a small-unit test cell and performance prediction of large stacked cell. *Journal of The Electrochemical Society*, 149(8):A1069, 2002.

[74] Huiyong Kim, Mikyoung Park, and Kwang Soon Lee. One-dimensional dynamic modeling of a high-pressure water electrolysis system for hydrogen production. *International Journal of Hydrogen Energy*, 38(6):2596–2609, 2013.

[75] Meng Ni, Michael KH Leung, and Dennis YC Leung. Energy and exergy analysis of hydrogen production by a proton exchange membrane (pem) electrolyzer plant. *Energy conversion and management*, 49(10):2748–2756, 2008.

[76] Zhiquan Wu, Shaoxiang Zhou, and Liansuo An. The second law (exergy) analysis of hydrogen. *Journal of Sustainable Development*, 4(1):260–263, 2011.

[77] Meng Ni, Michael KH Leung, and Dennis YC Leung. Energy and exergy analysis of hydrogen production by solid oxide steam electrolyzer plant. *International journal of hydrogen energy*, 32(18):4648–4660, 2007.

[78] Jingke Mo, Zhenye Kang, Gaoqiang Yang, Scott T Retterer, David A Cullen, Todd J Toops, Johney B Green Jr, and Feng-Yuan Zhang. Thin liquid/gas diffusion layers for high-efficiency hydrogen production from water splitting. *Applied energy*, 177:817–822, 2016.

[79] Zirong Yang, Qing Du, Sen Huo, and Kui Jiao. Effect of membrane electrode assembly design on the cold start process of proton exchange membrane fuel cells. *International Journal of Hydrogen Energy*, 42(40):25372–25387, 2017.

[80] Joonas Koponen, Antti Kosonen, Vesa Ruuskanen, Kimmo Huoman, Markku Niemelä, and Jero Ahola. Control and energy efficiency of pem water electrolyzers in renewable energy systems. *International journal of hydrogen energy*, 42(50):29648–29660, 2017.

[81] Denis THOMAS. State of play and developments of power-to-hydrogen technologies. `https://etipwind.eu/wp-content/uploads/A2-Hydrogenics_v2.pdf`, 2019.

[82] Denis THOMAS. Large scale pem electrolysis: technology status and upscaling strategies. `http://hybalance.eu/wp-content/uploads/2019/10/Large-scale-PEM-electrolysis.pdf`, 2019.

[83] Feras Alshehri, Víctor García Suárez, José L Rueda Torres, Arcadio Perilla, and MAMM van der Meijden. Modelling and evaluation of pem hydrogen technologies for frequency ancillary services in future multi-energy sustainable power systems. *Heliyon*, 5(4):e01396, 2019.

UNIVERSITÉ CATHOLIQUE DE LOUVAIN
École polytechnique de Louvain
Rue Archimède, 1 bte L6.11.01, 1348 Louvain-la-Neuve, Belgique | **www.uclouvain.be/epl**